약학박사 학위논문

Identification of a PET radioligand for metabotropic glutamate receptor subtype 1 (mGluR1) imaging in rat brain

랫트 두뇌의 제 1 형 대사성글루타메이트수용체 영상용 PET 방사성리간드 동정

2017 년 2 월

서울대학교 융합과학기술대학원

분자의학 및 바이오제약학과

이 보 은

Identification of a PET radioligand for metabotropic glutamate receptor subtype 1 (mGluR1) imaging in rat brain

지도교수 이 동 수 / 정 재 민

이 논문을 약학박사 학위논문으로 제출함

2016 년 10 월

서울대학교 융합과학기술대학원

분자의학 및 바이오제약학과

이 보 은

이보은의 박사학위논문을 인준함

2016 년 12 월

위 원 장 _____ (인)

부 위 원 장 _____ (인)

위 원 _____ (인)

위 원 _____ (인)

위 원 _____ (인)

Abstract

Identification of a PET radioligand for metabotropic glutamate receptor subtype 1 (mGluR1) imaging in rat brain

Lee, Boeun

Department of Molecular Medicine and Biopharmaceutical Sciences
The Graduate School of Convergence Science and Technology
Seoul National University

Introduction:

Glutamate is an important excitatory neurotransmitter in mammalian central nervous system. After it is released from the presynaptic vesicles, it binds to glutamate receptors to acts as the first messenger. Among the 8 subtypes metabotropic glutamate receptors, metabotropic glutamate receptor subtype 1 (mGluR1) is widely distributed in the brain, especially in the cerebellum. mGluR1 regulates the release of glutamate and γ-aminobutyric acid (GABA) in the postsynaptic region to control synaptic transmission, neuronal excitability and brain plasticity. Thus, mGluR1 is related with various neurological and

psychiatric diseases, such as anxiety, depression, epilepsy, Parkinson's disease, and neuropathic pain. Due to its important roles in central nervous system, mGluR1 is an important target for drug development and imaging, of course.

Hence, I synthesized fluorine-18 labeled quinoline radioligand (3-ethyl-2-fluoro-[^{18}F]quinolin-6-yl)((1*S*,4*S*)-4-methoxycyclohexyl) methanone ([^{18}F]**7a**) as a PET tracer for selective mGluR1 imaging and its trans- isomer (3-ethyl-2-fluoro-[^{18}F]quinolin-6-yl)((1*R*,4*R*)-4-methoxycyclohexyl)methanone ([^{18}F]**7b**), and evaluated their physico-chemical properties in rodents.

Methods:

A chloroquinoline precursor (**6**) and cold product (**7a** and **7b**) were synthesized, and the radioactive [^{18}F]**7a** and [^{18}F]**7b** were labeled by nucleophilic substitution reaction. The resulting radioactive compounds were purified using semi-preparative high performance liquid chromatography (HPLC). The radiolabeling efficiencies and radio-chemical purities of [^{18}F]**7a** and [^{18}F]**7b** were measured using radio-TLC and analytical HPLC.

In vitro experiments confirmed lipophilicity and stability of [^{18}F]**7a**. Biodistribution and metabolites analysis were performed on BALB/c

mice, and small animal PET and autoradiography studies were carried out to investigate the specific binding of [^{18}F]**7a** to mGluR1 in normal Sprague-Dawley rat brains.

Results:

[^{18}F]**7a** and [^{18}F]**7b** were obtained with high radiochemical purities (>99%) and specific activities (63-246 GBq/μmol for [^{18}F]**7a** and 30.5-93.2 GBq/μmol for [^{18}F]**7b**). The distribution coefficient value (Log $D_{7.4}$) of [^{18}F]**7a** was 3.24, and the initial brain uptake of [^{18}F]**7a** at 10 min was over 4% of injected dose per gram in BALB/c mice.

According to PET and *ex vivo* autoradiography studies in Sprague-Dawley rats, [^{18}F]**7a** showed wide distribution in the whole brain and the highest uptake in the cerebellum which is a mGluR1-rich region. Hippocampus, thalamus, and striatum also showed higher uptake of radioactivity than other brain regions. Pre-treatment of unlabeled **7a** and mGluR1-specific antagonist JNJ16259685 blocked the binding of [^{18}F]**7a** to mGluR1, homogeneous distribution of radioactivity throughout the whole brain showed nonspecific binding of [^{18}F]**7a**.

However, pre-treatment of mGluR5-specific antagonist ABP688 did not reduce the uptake of [^{18}F]**7a** in the rat brain. The trans isomer [^{18}F]**7b** which has low affinity to mGluR1 showed no specific

distribution in rat brain in all PET images, even if it also entered into rats' brain rapidly.

Conclusions:

[^{18}F]**7a** and [^{18}F]**7b** were successfully prepared using a chloro-derivative precursor and cyclotron produced ^{18}F anion, and formulated as an injection for animal study. *In vitro* and *in vivo* experiments using rodents showed [^{18}F]**7a** had specific binding to mGluR1 in the brain. However, [^{18}F]**7b** having trans configuration on cyclohexyl ring of quinoline derivative was nonspecific to mGluR1. Thus, it was proved that [^{18}F]**7a** is a promising PET radioligand for mGluR1 imaging.

---

keywords: Metabotropic glutamate receptor subtype 1 (mGluR1), radioligand, fluorination, automatic synthesis, metabolism, autoradiography, positron emission tomography (PET)

***Student Number*: 2009-31346**

Contents

List of Figures, Schemes and Tables

List of Abbreviations

mGluR	Metabotropic glutamate receptor
GABA	γ-Aminobutyric acid
HPLC	High performance liquid chromatography
CNS	Central nervous system
iGluR	Ionotropic glutamate receptors
NMDA	*N*-Methyl-D-aspartate
AMPA	α-Amino-3-hydroxy-5-methyl-4-isoxazole propionate
KA	Kainate
GPCRs	G-protein-coupled receptors
VFT	Venus flytrap
HD	Heptahelical domain
IP3	Inositol triphosphate
cAMP	Cyclic adenosine monophosphate

PKA	Protein kinase A
NAc	Nucleus accumbens
FDA	Food and Drug Administration
SNRI	Serotonin and norepinephrine reuptake inhibitor
BBB	Blood-brain barrier
PET	Positron emission tomography
IND	Investigational new drug
TLC	Thin layer chromatography
UV	Ultraviolet
$KMnO_4$	Potassium permanganate
NaOH	Sodium hydroxide
NMR	Nuclear magnetic resonance
TMS	tetramethylsilane
ESI	Electrospray ionization
MS	Mass spectroscopy

LC-MS	Liquid chromatography-mass spectroscopy
CDI	1,1'-Carbonyldiimidazole
CH_2Cl_2	Dichloromethane
$MgSO_4$	Magnesium sulfate
EtOAc	Ethyl acetate
Et_3N	Triethylamine
DMF	*N,N'*-Dimethylformamide
$POCl_3$	Phosphoryl chloride
n-BuLi	n-Butyl lithium
THF	Tetrahydrofuran
DMSO	Dimethyl sulfoxide
KF	Potassium fluoride
$KHCO_3$	Potassium bicarbonate
MeCN	Acetonitrile
EtOH	Ethanol (ethyl alcohol)

SD	Sprague-Dawley
OSEM	Ordered subsets expectation maximization
TAC	Time activity curve
Halex	Selective halogen exchange

I. Introduction

Glutamic acid (glutamate) is one of the most important excitatory neurotransmitters abundant in the central nervous system (CNS) of mammals. Glutamate biosynthesized from α-ketoglutaric acid is stored in presynaptic vesicles and released by calcium-dependent exocytosis. After being released from vesicle, it acts as the first messenger via membrane-bound glutamate receptors.

Glutamate receptors are categorized into ionotropic and metabotropic by their affinity to various ligands. Ionotropic glutamate receptors (iGluR) comprise *N*-methyl-D-aspartate (NMDA), α-amino-3-hydroxy-5-methyl-4-isoxazole propionate (AMPA), and kainate (KA) receptors (*1, 2*). iGluRs are ligand-gated ion channels, allowing cations permeation such as Na^+, K^+ and Ca^{2+} upon glutamate binding. The activation of iGluRs makes depolarization and postsynaptic current for fast excitatory signaling in the brain. NMDA receptors are activated by the binding of glutamate with co-agonist glycine and depolarization of postsynaptic neuron, simultaneously (*3*). AMPA receptors are responsible for most of fast excitatory neurotransmission in the brain, and are related to learning and memory (*4*). KA receptors modulate presynaptic release of neuro-transmitter, and regulate the strength of synaptic connections (*4*).

Whereas, metabotropic glutamate receptors (mGluR) comprise G-protein-coupled receptors (GPCRs) those are classified into eight subtypes (mGluR1-8) based on their pharmacology, signal transduction mechanism and sequence homology (*5*). The structure of mGluRs consists of three domains: the extracellular domain, the transmembrane domain, and the intracellular domain. The N-terminus extracellular domain consists of the venus flytrap (VFT) which is a binding site of glutamate, and a cysteine-rich region which connect the VFT to the transmembrane domain. The transmembrane region is the heptahelical domain (HD), and it connects the extracellular domain with intracellular domain where G-protein is coupled through the cell membrane (Figure 1) (*6*). Generally, mGluRs form dimers stabilized by disulfide bonds in the cysteine-rich region, and binding of glutamate causes a conformatio-nal change of receptors with more tightened dimeric structures for signaling activation (*6, 7*).

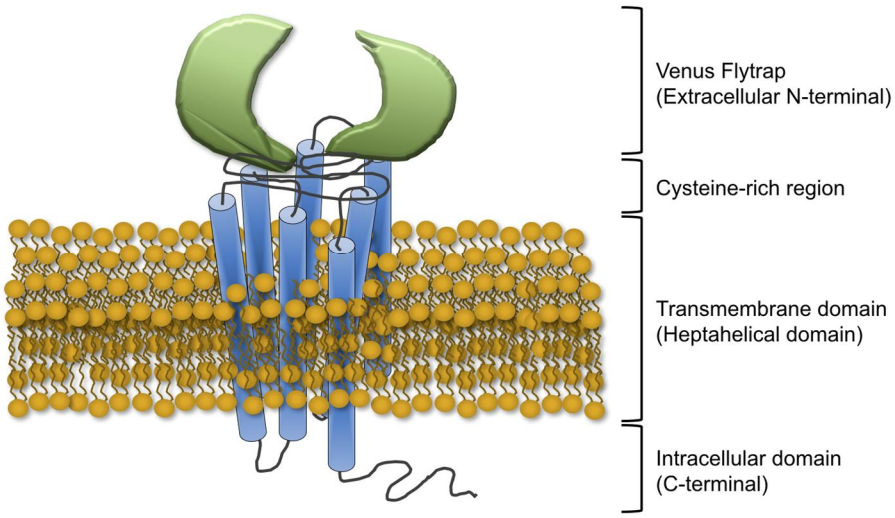

Figure 1. Schematic structure of metabotropic glutamate receptors.

Eight subtypes of mGluRs are divided into three groups: Group I, II and III (8). The amino acid sequence homology of mGluRs in a group is over 70%, but that between groups is only 45% (*7*).

Group I mGluRs include mGluR1 and mGluR5, and are located at peripheral portion of postsynaptic region in Purkinje cells (*9*) and hippo-campal CA1-3 neurons (*10, 11*). These receptors are coupled to Gq/11, which stimulates phospholipase C, an enzyme that hydrolyzes phospha-tidylinositol 4,5-bisphosphate to produce inositol triphosphate (IP3) and diacylglycerol. IP3 then binds to the IP3 receptors on the endoplasmic reticulum, triggering the release of Ca^{2+} from intracellular stores as the second messenger. The released Ca^{2+} and diacylglycerol activate protein kinase C. Meanwhile, group I receptors regulate K^{+} channels for negative modulation (Figure 2) (*1, 2, 5, 8, 12, 13*).

Group II (mGluR2 and mGluR3) and group III (mGluR4, mGluR6, mGluR7, and mGluR8) receptors are coupled to Gi protein. These receptors act for negative control of glutamate release at presynaptic regions in neuronal and glial cells (*14*). The activation of group II receptors inhibits adenylate cyclase to reduce intracellular concentration of cyclic adenosine monophosphate (cAMP) and protein kinase A (PKA) activity (*6, 8, 13, 15*). Group III inhibit the release of glutamate or γ-aminobutyric acid (GABA) (*8*) through the suppression of presynaptic voltage-dependent calcium channels (Figure 2) (*16*).

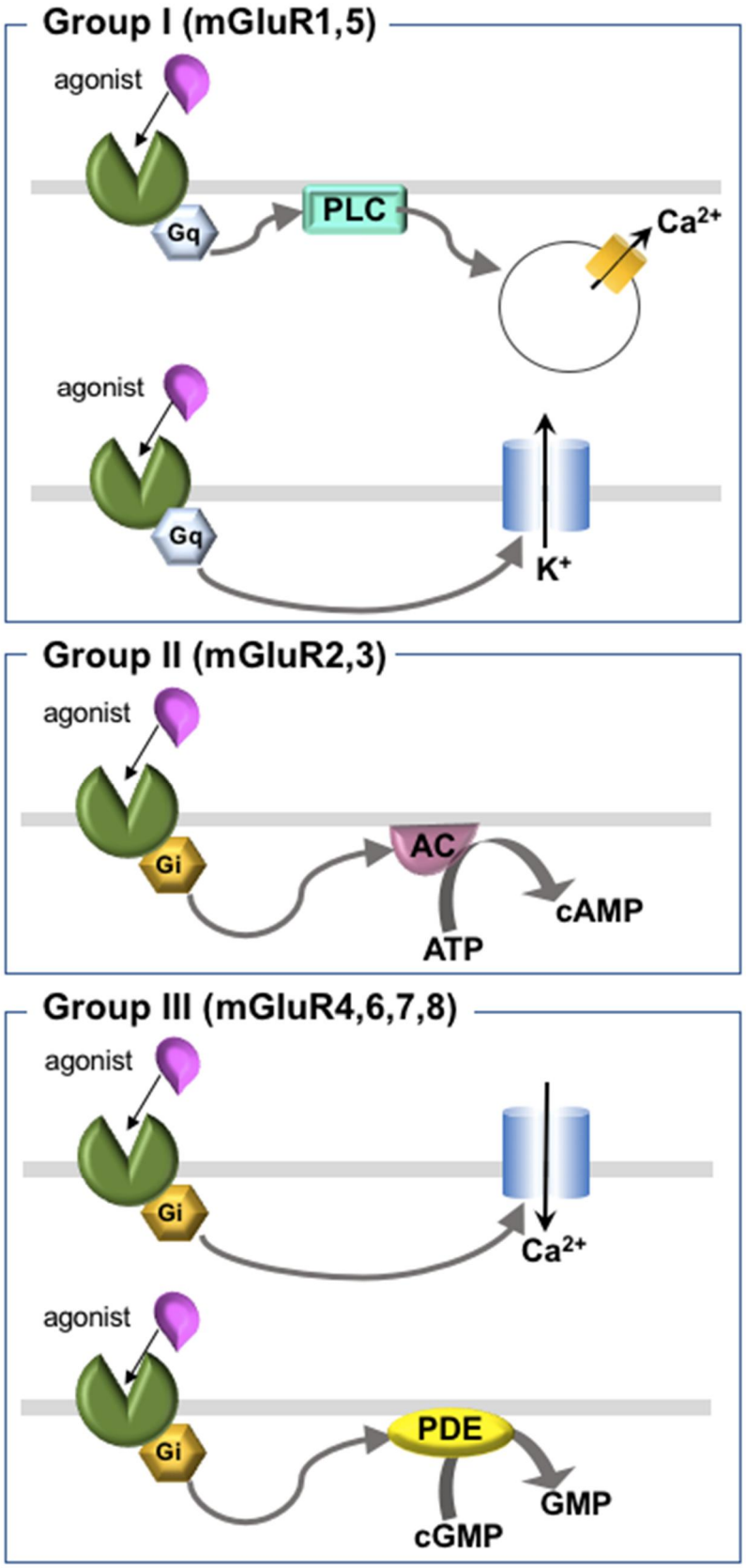
Group I (mGluR1,5)
agonist
Gq
PLC
Ca2+
agonist
Gq
K+
Group II (mGluR2,3)
agonist
Gi
AC
cAMP
ATP
Group III (mGluR4,6,7,8)
agonist
Gi
Ca2+
agonist
Gi
PDE
GMP
cGMP

Figure 2. Mechanisms of mGluRs signaling.

AC, adenylate cyclase; ATP, adenosine triphosphate; cAMP, cyclic ade-nosine monophosphate; cGMP, cyclic guanosine monophosphate; GMP, guanosine monophosphate; PDE, phosphodiesterase; PKC, protein kina-se C; PLC, phospholipase C.

The distributions of mGluRs are quite different depending on the receptor subtypes (Figure 3) (*13, 17*).

The two mGluRs of group I (mGluR1 and mGluR5) have complemen-tary distribution, but the reason is not clear yet. mGluR1 is widely distributed in CNS, cerebellum is the most mGluR1 abundant region in the brain. It also presents in hippocampus, thalamus and striatum but less than in the cerebellum (*18*). The other group I receptor, mGluR5 is mainly expressed in telencephalic regions including cerebral cortex, olfactory bulb, olfactory tubercle, hippocampus, and striatum. In the hippocampus where dendrites and cell bodies of neuron are located, both mGluR1 and mGluR5 are expressed.

Group II receptors are commonly found in presynaptic regions in the forebrain, perhaps for the inhibitory regulations of these receptors. mGluR2 has been mainly observed in the cerebellar cortex and accessory olfactory bulb. In the cerebellar cortex, mGluR2 expression is distin-guished with mGluR1 because mGluR2 is located in deeper layers than mGluR1. The most prominent expression of mGluR3 is in the Golgi cells of the cerebellar cortex, and in the thalamic reticular nucleus neurons.

Group III receptors are also located in presynaptic neurons like group II receptors, but are distributed in more restricted areas in the brain. The regions where mGluR4 is expressed are the cerebellum and

the olfactory bulb. mGluR7 is found in much wider brain regions, olfactory bulb, neo-cortex, piricortex and hippocampus. mGluR8 has lower density in the brain than other mGluRs, it is expressed in the cerebellum, olfactory bulb, and cortex. Meanwhile, mGluR6 is distributed in the retina, not in the brain.

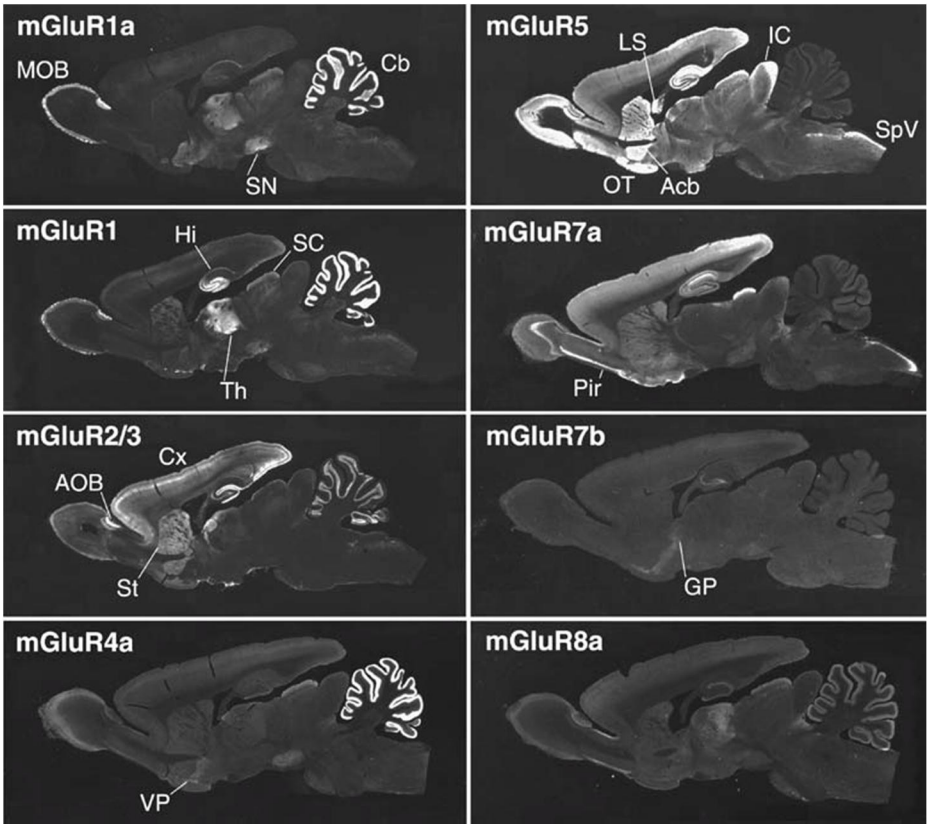

Figure 3. Distribution of mGluRs in adult rat brain.

AOB, accessory olfactory bulb; Acb, accumbens nucleus; Cb, cerebellum; Cx, neocortex; GP, globus pallidus; Hi, hippocampus; IC, inferior colliculus; LS, lateral septum; MOB, main olfactory bulb; OT, olfactory tubercle; Pir, piriform cortex; SC, superior colliculus; SN, substantia nigra; SpV, spinal vestibular nucleus; St, neoustriatum; Th, thalamus; VP, ventral pallidum.

mGluR1 controls postsynaptic release of glutamate and GABA via interactions with the NMDA receptors (*19*), it regulates synaptic transmission, neuronal excitability and brain plasticity. Due to its regulatory roles in the brain, mGluR1 is related to various neurological and psychiatric disorders, such as anxiety (*20, 21*), depression (*22-24*), schizoph-renia (*19, 25-27*), epilepsy (*28, 29*), Parkinson's disease (*30-32*), and neuropathic pain (*33-35*). Therefore, the development of mGluR1 target-ing drugs has been an attractive subject for decades (*36*).

For a safer and faster therapeutics of anxiety, mGluR1 antagonists were studied. mGluR1 antagonists block the activation of NMDA receptors, following inhibitory GABA system stimulation (*37*). It is better for medication than traditional anxiolytic drugs those of GABA modulators (e.g. benzodiazepines) since GABA modulators have lots of side effects such as drowsiness, sedation, confusion, amnesia, tolerance, dependence, psychomotor and cognitive impairment.

According to previous studies, NMDA receptor antagonists such as ketamine had antidepressant activity in animal models and in humans (*22, 38, 39*). It means mGluR1 also has the possibility of antidepressant effects, and suppression of mGluR1 contributes to antidepressant activity. In fact, a potent mGluR1 antagonist, JNJ16257083, has shown effective results in rats and mice behavioral assays (*22*).

Schizophrenia is a severe psychical disorder that manifests complicated clinical symptoms, and is associated with dysfunction of dopaminergic, glutamatergic and GABAergic neurotransmission. Dopa-mine hypothesis was suggested as an early physiopathological mecha-nism of schizophrenia. Presynaptic dopamine synthesis is increased in the schizophrenic brain, therefore, most of the early stage of schizoph-renia treatments were focused on dopamine D2 receptor blockade (*40*). The second hypothesis was established in the mid-nineties, the NMDA receptor hypofunction triggers the inhibition of GABAergic system with consequent hyperdopaminergic state (*41*). Group I mGluRs are func-tionally coupled with ionotropic NMDA receptors and are related with cognitive impairment in schizophrenia. Thus, recently, positive modulators of the group I mGluRs are attractive in the field of drug discovery for schizophrenia treatment *(25-27, 37*).

Addiction arose from several abusive drugs, including cocaine, heroin, nicotine, opiates, and alcohols, affecting changes of synaptic activity and plasticity due to the impairments of glutamate homeostasis and receptors (*42-48*). For example, in the nucleus accumbens (NAc) where cocaine craving region, increased AMPA receptor levels by cocaine-induced addiction are effectively repressed by mGluR1 activation using a positive allosteric modulator (*49*). Hence, mGluR1

has been suggested as a beneficial target for prevention of drug self-administration and relapse (*50*).

Neuropathic pain is caused by incorrect signals of damaged nerve fibers (*51*), and its characteristic symptoms are shooting and burning pain, tingling and numbness, allodynia, and hyperalgesia. This chronic pain is a kind of intractable neural disease, because it is difficult to respond to common or narcotic analgesics. Pregabalin (Lyrica®, Pfizer Inc.), duloxetine (Cymbalta®, Eli Lilly), Carbamazepine (Tegretol®, Novatis) and gabapentin (Neurotin®, Pfizer Inc.) are already approved medications for neuropathic pain from Food and Drug Administration (FDA) in U.S. Duloxetine is a serotonin and norepinephrine reuptake inhibitor (SNRI), and others are GABA modulator (*52*). These drugs have some deficiencies, such as drug interactions or low efficacy. Thus, ionotropic or metabotropic glutamate receptors are recent trends of study for neuropathic pain treatments. NMDA receptor antagonists have powerful therapeutic effects to neuropathic pain, but lead to severe adverse effects in CNS such as psychotic behavior (*53, 54*), cognitive impairment, drowsiness, and sedation. The relation of mGluRs to neuropathic pain is determined by several studies. mGluR1 antagonists have pain relief effect in the thalamus and amygdala *(42, 55*).

As a new target for various neurological disorders treatment drugs, development of noncompetitive antagonists of mGluR1 is very active. Noncompetitive antagonists trigger conformational change of receptor with binding to allosteric site in cysteine-rich region, so they are indepen-dent of agonist including endogenous ligand concentrations. Allosteric modulators with high selectivity are attractive for CNS drug discovery, and in general, conventional drugs of competitive agonists or antagonists have lack of receptor selectivity and undesirable side effects (*56*).

Over the past few years, selective antagonists for mGluR1 have been discovered. Some of the early developed compounds based on phenyl-alanine moiety such as (-)-CPCCOEt (*57, 58*), BAY36-7620 (*59*), LY-367385 (*60*), LY456236 (*61*), CPPG (*62*) and AIDA (*63*) were improper for mGluR1 targeting drugs due to their low potency (*K*i values were tens to hundreds of μM or more), low lipophilicity for blood-brain barrier (BBB) penetration, and/or low mGluR1 selectivity (Figure 4).

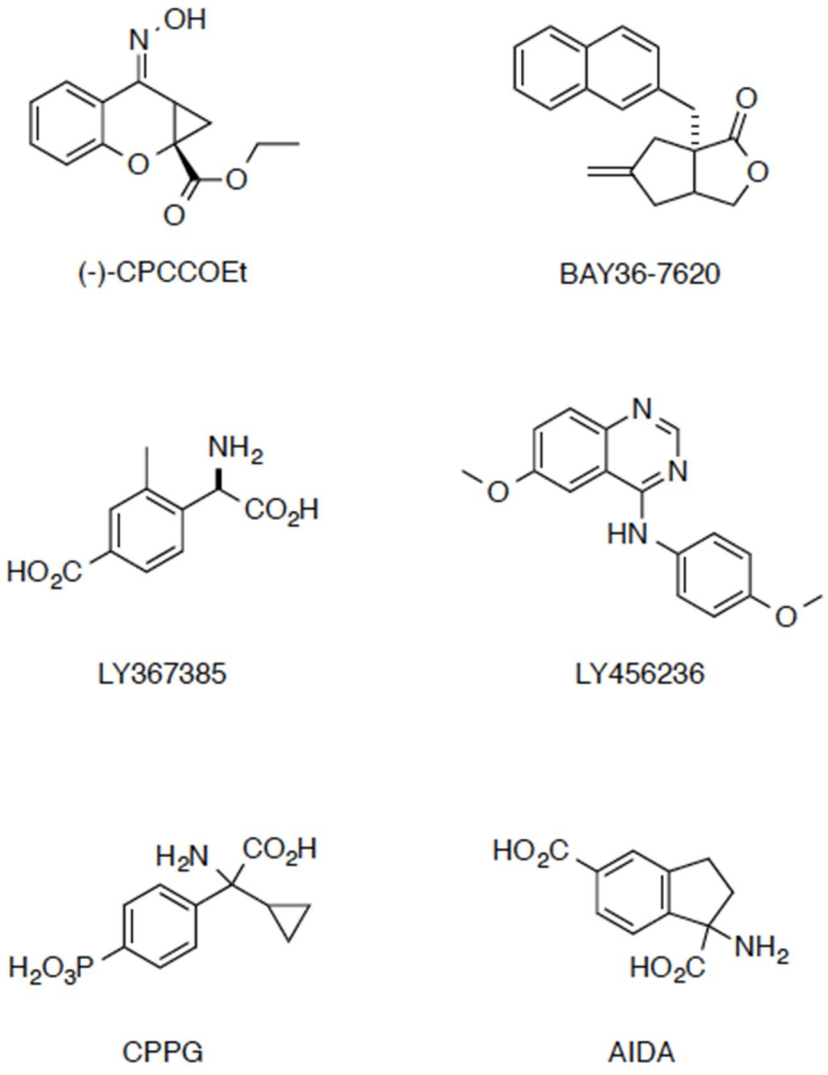

Figure 4. Structures of early developed mGluR1 antagonists.

Later, Mabrie et al. reported more than 500 quinoline derivatives as noncompetitive mGluR1 antagonists (Figure 5) (*64*). Among these com-pounds, JNJ16259685 showed the highest binding affinity and selec-tivity to mGluR1 in the rat and human brain. The reported values of IC_{50} in rat and human mGluR1 were 3 and 0.55 nM, respectively (*64*). Thus, JNJ16259685 has been used as a standard for measuring specific binding of new mGluR1 antagonist candidates (*65*). In addition, R214127 (*66*), YM-298198 (*67, 68*), YM-202074 (*69*), FTIDC (*70*) and CFMTI (*71*) were designed for mGluR1 antagonists with higher potency and selectivity than early-stage antagonists (Figure 5). Some of these antago-nists are competitive antagonists and others are noncompetitive antago-nists.

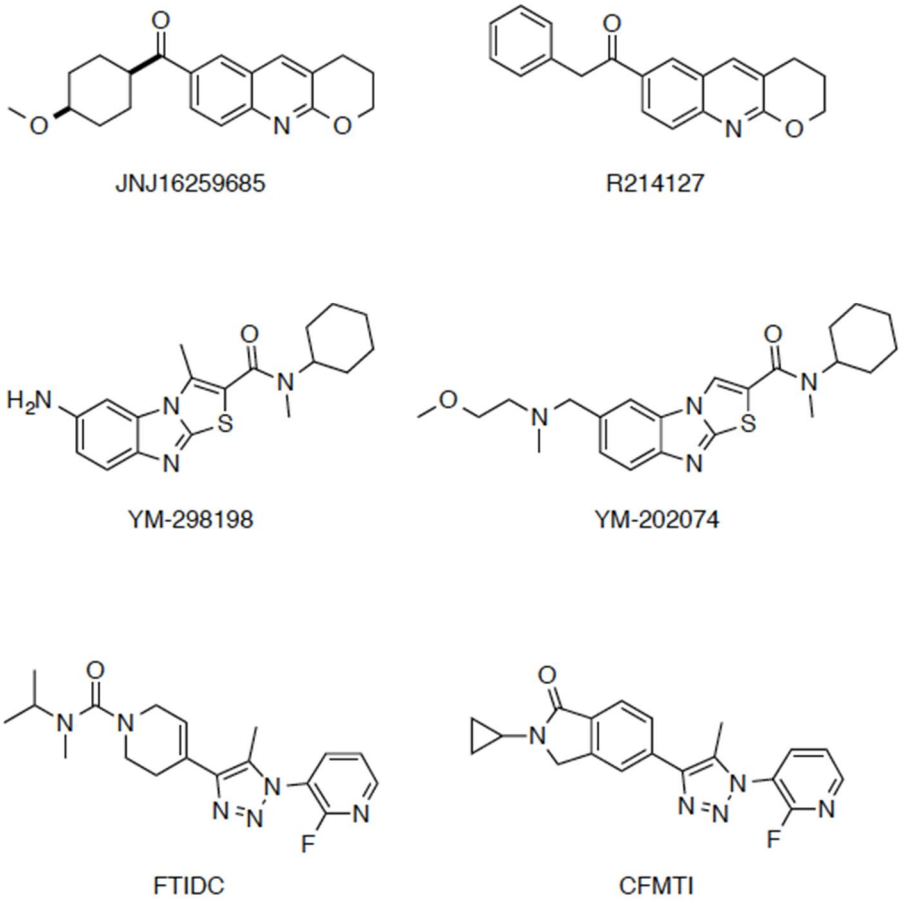

Figure 5. Structures of mGluR1 antagonists with high potency and selectivity.

Noninvasive molecular imaging technique is a cutting edge of medical and pharmaceutical industries. New drug discovery is an enormously expensive and time-consuming work. For one novel drug commerciali-zation, more than 5,000 of new drug candidates should be tested, and it takes about 10 years, costing US$ 2.6 billion (*72*). However, the use of positron emission tomography (PET) can make drug development more efficient by reducing research costs and times. There are several reasons why PET imaging is useful for drug developments. First, PET study provides lots of biological information of various diseases, since the images reflect functional change of organs and tissues on the molecular level. Based on this information, identification of target for new drugs is very effective. Second, PET images acquired with radiolabeled ligands enable picking out potential compounds among a large number of candidates for new drug. Generally, the doses of radioligands admini-stered to human for PET is trace amounts (pico-nano mole), so PET study is quite safe. Eventually, clinical studies using PET can be performed with simplified toxicological experiments and investigational new drug (IND) application procedures, it helps the shortening of time to market of remarkable drugs (*73, 74*).

A well optimized radioligand is necessary to acquire PET images for accurate data analysis. For this reason, many researchers are putting in

a great deal of efforts to develop novel radioligands for brain receptor imaging include mGluR1. The criteria for good radioligand for brain receptor imaging are labeling condition and ligand stability, lipophilicity for BBB penetration, high selectivity and specificity to target receptor, low nonspecific binding, appropriate pharmacokinetic and pharmaco-dynamic properties (*75*).

Based on the previous study of quinoline compounds for mGluR1 antagonists, Huang et al. developed ^{11}C-labeled PET ligand, [^{11}C]JNJ-16567083 (Figure 6) (*76, 77*). Nonradioactive JNJ16567083 showed high affinity to mGluR1, IC_{50} values were 3 and 8 nM in rat and human mGluR1, respectively. The K_i values were 4.41 nM for rat mGluR1 and 13.3 nM for human mGluR1. It is the first tracer labeled with positron emitter for mGluR1 imaging which showed high uptake in rat cerebellum-the mGluR1-abundant region.

However, [^{11}C]JNJ16567083 had several shortcomings. The ^{11}C-labeling reaction is not simple because tin precursor and palladium catalyst are used for labeling, and the reaction temperature is quite high (Scheme I) (*76*). The *in vitro* metabolic stability of JNJ16567083 in human liver microsomes was very low, only 8% of original compound was remained after 30 min incubation (*64*). Moreover, there were no further evaluations including clinical investigation have been reported.

Above this, ^{11}C-labeled ligands have some disadvantages for practical use due to a short half-life.

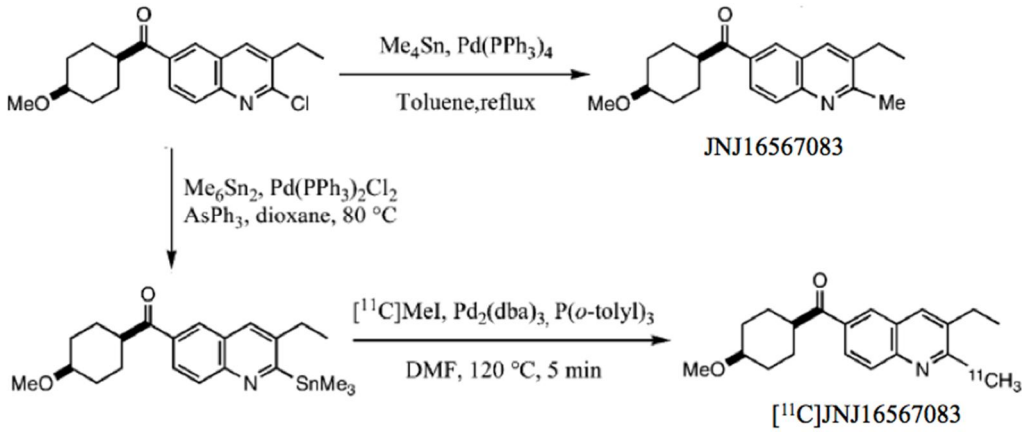

Scheme I. Previously reported synthetic scheme of [^{11}C]JNJ-16567083.

There are several radioligands for mGluR1 imaging (Figure 6). [^{11}C]YM-202074 had high affinity to mGluR1 (K_i = 4.8 nM for rat) *in vitro* study, but it showed low brain uptake due to lower lipophilicity than [^{11}C]JNJ16567083. The triazole-based compound [^{18}F]MK-1312 was the first ^{18}F-labeled radioligand for mGluR1 imaging. The ligand showed high selectivity for mGluR1 (K_i = 0.40 nM) and rapid uptake without de-fluorination in rhesus monkey brains (*78*). [^{18}F]FPIT (IC_{50} = 5.4 nM) (*79*) and [^{18}F]FTIDC (K_i = 3.9 nM) (*70*) are derivatives of MK-1312, they also indicated specific binding to mGluR1 in rat and monkey brains. The binding of [^{11}C]MMTP to mGluR1 was specified in the cerebellum of the baboon brain (K_i = 7.9 nM), but no other mGluR1 rich regions were detected (*80*). Compared with other ligands, [^{18}F]FITM was a potential ligand for mGluR1 (IC_{50} = 5.1 nM) with high metabolic stability (*81*). Approximately 95% of [^{18}F]FITM was retained in the rat brain for 120 min after injection. However, [^{18}F]FITM had a low synthetic yield (*81*), and its kinetics was too slow to measure its B_{max} and *Kd* values in the cerebellum (*82, 83*). [^{11}C]ITMM, [^{11}C]ITDM and [^{18}F]FIMX have similar molecule structures with [^{18}F]FITM, all of these ligands have a pyrimidinyl-thiazolyl-*N*-methyl-benzamide moiety. The first study in human of mGluR1 imaging was performed using [^{11}C]ITMM (K_i = 12.6 nM in rat brain) (*84, 85*), and there was no radioligand applied to human before

the [^{11}C]ITMM study. However, [^{11}C]ITMM could not clearly detect mGluR1 focal regions except the cerebellum, and showed inade-quate quantifications in the human brain. [^{11}C]ITDM (K_i = 13.6 nM (*86*)) had faster kinetics and higher regional distribution volume (V_T) value than [^{11}C]ITMM in the monkey brain (87, 88). Among ^{18}F-labeled tracers, [^{18}F]FIMX which had high affinity for mGuR1 (IC_{50} = 5.1 nM for human brain) (*89, 90*) has been studied clinically for the first time (*91*). [^{18}F]FIMX showed a well correlated mGluR1 density, but the analysis took over 170 min.

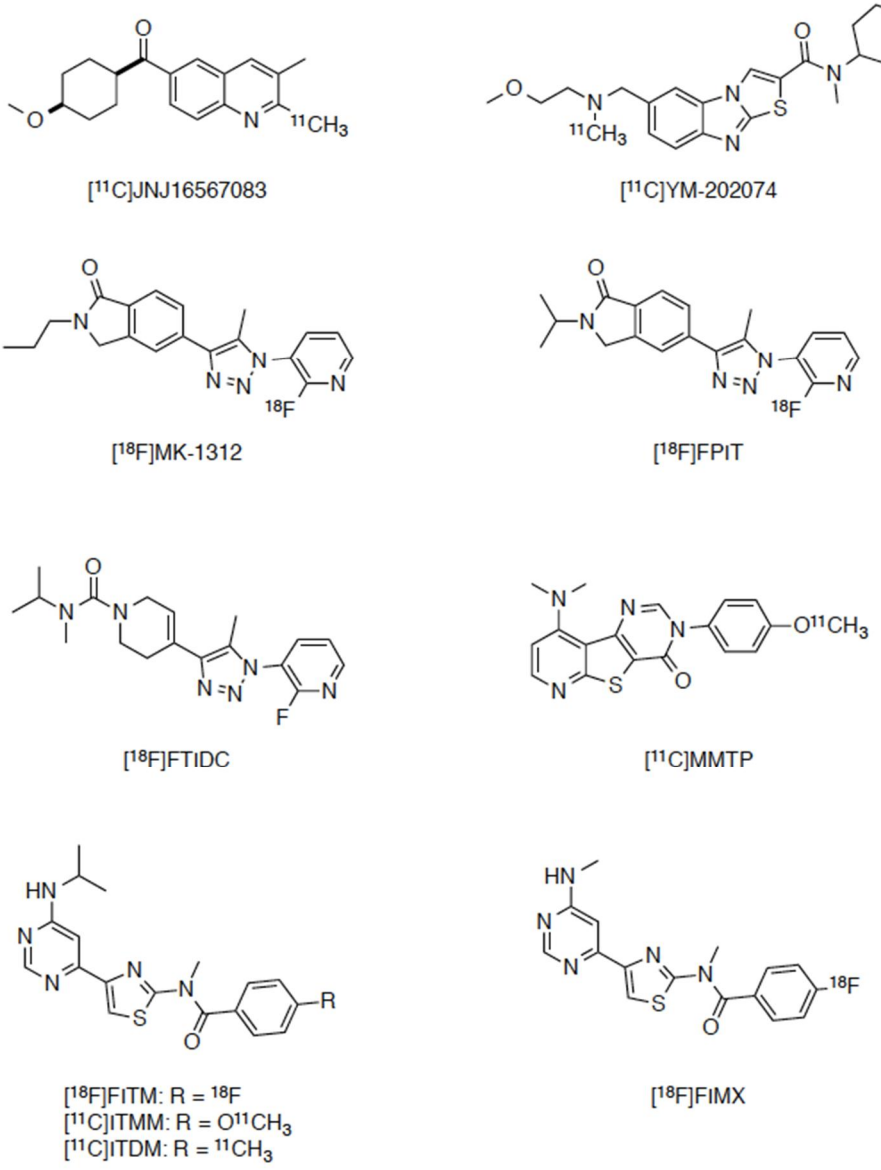

Figure 6. Structures of radioligands for mGluR1 imaging.

A fluorine containing quinoline derivative, (3-ethyl-2-fluoroquinolin-6-yl)((1*S*,4*S*)(4-methoxycyclohexyl)methanone (**7a**)) is a noncompetitive mGluR1 antagonist with high binding affinity for rat and human mGluR1 (Figure 7) (*64*). It can be developed as a radioligand for mGluR1 PET imaging, replacing fluorine-19 with radioactive one. Fluorine-18 (^{18}F) is the most widely used radioisotope for PET imaging. It is produced from ^{18}O-enriched water target by (p,n) reaction or from ^{20}Ne gas target by (d,α) reaction. ^{18}F has relatively long half-life compared to other positron emitters, and ^{18}F-labeled radiopharmaceuticals can be commercially distributed to elsewhere. It means that some institutes and hospitals can use ^{18}F-compounds without special facilities such as cyclotron and synthetic modules. Moreover, ^{18}F is preferred to other PET radioisotopes such as ^{11}C, ^{13}N, and ^{15}O to achive high resolution in PET images because of lower ß$^{+}$ energy (E_{max}: 0.635 MeV) and shorter linear range in water (2.4 mm) (Table I) (*92*). Thus, ^{18}F-labeled radioligand **7a** was prepared for mGluR1 imaging study.

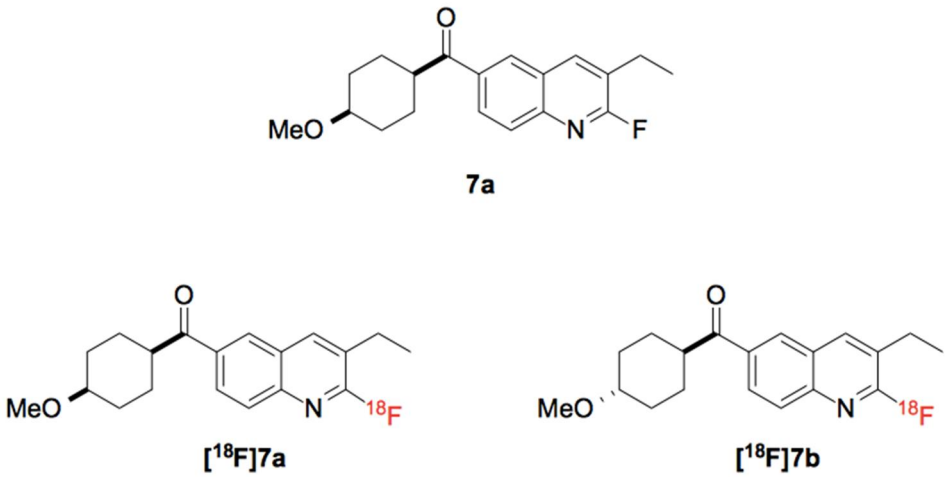

Figure 7. Structures of mGluR1 antagosists containing fluorine in quinoline moiety.

Table I. Radioisotpes for PET.

Isotopes	$T_{1/2}$ (min)	$ß^+$ Decay (%)	E_{max} ($ß^+$) (MeV)	Range in water (mm)
^{11}C	20.4	99.8	0.961	4.1
^{13}N	9.96	99.8	1.198	5.4
^{15}O	2.04	99.9	1.732	8.2
^{18}F	109.8	96.7	0.635	2.4

While this study was going on, [^{18}F]**7a** was reported by Huang et al, including *in vitro* and *in vivo* studies in rats and baboons (*77, 93*). However, brain images and radioactive metabolites of it have not been reported. In addition, the trans isomer [^{18}F]**7b** has not been evaluated using PET.

In the present study, [^{18}F]**7a** and [^{18}F]**7b** were further investigated including synthesis with automation, radiochemical properties, *in vivo* metabolism, PET and *ex vivo* autoradiography study in small animals.

II. Materials and Methods

General

Unlabeled mGluR1 antagonists, the precursor for ^{18}F-labeling, and ABP688 were prepared according to previously reported procedure (*64, 94)*. JNJ16259685 was purchased from Toronto Research Chemicals Inc. (Toronto, Canada). All reagents and solvents for synthesis were used commercially available products without further purification, which were purchased from Sigma-Aldrich Korea Ltd. (Yongin, Korea), Fluka (Buchs, Switzerland), or TCI (Tokyo, Japan). High performance liquid chromatography (HPLC)-grade solvents were purchased from Fisher. All non-aqueous reactions were performed under an inert atmosphere of dry argon. Nonradioactive reactions were monitored by thin layer chro-matography (TLC) analysis using Merck silica gel 60 F_{254} thin layer plates (Merck, Darmstadt, Germany). The spots were detected under ultraviolet (UV) light (254 nm and 356 nm) and stained using potassium permanganate ($KMnO_4$) solution (1.5 g $KMnO_4$, 10 g K_2CO_3, and 1.25 mL 10% NaOH in 200 mL water). Flash column chromatography was carried out on silica gel 60 (230-400 mesh) for non-radioactive compounds purification and all chromatographic solvents were HPLC grade. ^{1}H and ^{13}C nuclear magnetic resonance (NMR) spectra were recorded in δ units relative to deuterated solvent

($CDCl_3$) as an internal reference by 300- or 400- MHz NMR instrument (JEOL Ltd., Tokyo, Japan). ^1H chemical shifts are reported in parts per million (ppm) those were measured relative to tetramethylsilane (TMS). Electrospray ioni-zation mass spectra (ESI-MS) were acquired using a Waters 3100 liquid chromatography-mass spectroscopy (LC-MS) (Waters Corporation, MA, U.S.A.), ESI ion trap for positive and negative ions detection. The samples were diluted 1 to 100 with methanol and injected directly into the source.

[^{18}F]Fluoride was produced by the $^{18}O(p,n)^{18}F$ reaction using ^{18}O-enriched (98%) water and a 16.5-MeV proton beam generated by a PETtrace 10 cyclotron (GE Healthcare, Uppsala, Sweden). A HPLC system (Gilson Inc., WI, U.S.A.) equipped with a gamma radioactivity flow-through detector Gabi Star (Raytest GmbH, Straubenhardt, Germany) was used to confirm and purify the radiolabeled compounds. The radiochemical purities were checked by analytical HPLC (Gilson Inc., WI, U.S.A.) and radio-TLC scanning (AR-2000; Bioscan, Washing-ton, D.C., U.S.A.) of aluminum-backed silica gel 60 F_{254} TLC plates (Merck Co., Darmstadt, Germany). A dose calibrator (Atomlab 100; Bio-dex Medical Systems, Inc., New York, NY, U.S.A.) was used for mea-suring the levels of radioactivity.

All animal studies were carried out with the approval of Institutional Animal Care and Use Committee of Clinical Research Institute, Seoul

National University Hospital. This facility was accredited by the Associ-ation for the Assessment and Accreditation of Laboratory Animal Care International. In addition, National Research Council guidelines for the care and use of laboratory animals (revised in 1996) were observed throughout.

Two-tailed analysis of Student's t-test was used to confirm the statisti-cal significance of two group means.

Chemistry

***N*,4-Dimethoxy-*N*-methylcyclohexanecarboxamide (2).**

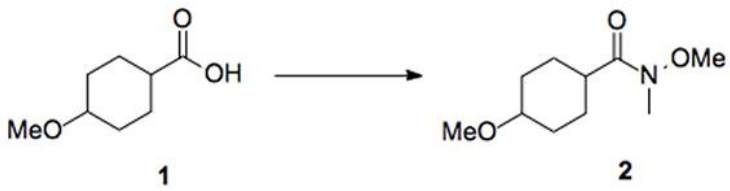

1,1'-Carbonyldiimidazole (CDI) (3.62 g, 22.32 mmol) was added por-tionwise to 4-methoxycyclohexanecarboxylic acid **1** (3 g, 18.96 mmol) solution in anhydrous dichloromethane (CH_2Cl_2) (40 mL). The mixture was stirred at room temperature for 1 h. Then *N,O*-dimethyl-hydroxyl-amine hydrochloride (2.15 g, 22.04 mmol) was added and stirred at room temperature for overnight. The resultant mixture was diluted with H_2O, and extracted with CH_2Cl_2. The combined organic layer was dried with over magnesium sulfate ($MgSO_4$) and evaporated. The crude product was purified by flash column chromatography on silica gel (hexane/ethyl acetate (EtOAc), 1:1.5) to give 5 (3.74 g, 18.58 mmol, 98%) as a light yellow liquid.: ^{1}H NMR ($CDCl_3$, 300 MHz) δ 1.16-1.62 (m, 4H), 1.79-1.93 (m, 2H), 1.98-2.18 (m, 2H), 2.61-2.75 (m, 1H), 3.18 (d, 3H), 3.33 (d, 3H), 3.44-3.48 (m, 1H), 3.71 (d, 3H).

***N*-(4-Bromophenyl)butyramide (4).**

3 4

4-Bromoaniline **3** (3.0 g, 17.4 mmol) and trimethylamine (Et_3N) (3.6 mL, 25 mmol) were dissolved in anhydrous CH_2Cl_2 (30 mL) and cooled to 0°C. A solution of butyryl chloride (2.0 mL, 19.7 mmol) in anhydrous CH_2Cl_2 (10 mL) was added dropwise. After the addition, the solution was stirred at room temperature for overnight. Water (40 mL) was then added, and the mixture was extracted with CH_2Cl_2, and the organic layer was washed with water (30 mL) and brine (30 mL). The organic layer was dried with over $MgSO_4$ and concentrated in vacuo to afford **4** (3.7g, 88%) as a white solid.: ^{1}H NMR ($CDCl_3$, 300 MHz) δ 1.01 (t, *J* = 6.0 Hz, 3H), 1.70-1.82 (m, 2H), 2.33 (t, *J* = 9.0 Hz, 2H), 7.43 (s, 3H).

6-Bromo-2-chloro-3-ethylquinoline (5).

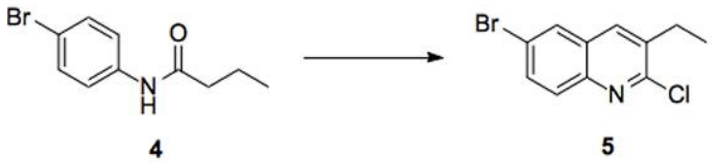

4 5

N,N'-Dimethylformamide (DMF) (1.5 mL, 19.4 mmol) was added dropwise to phosphoryl chloride ($POCl_3$) (3.0 mL, 33.2 mmol) at 0°C, and the solution was stirred at room temperature for 2 hr. After cooling of the solution to 0°C, compound **4** (2.3 g, 9.5 mmol) was added slowly. The reaction mixture was allowed to stir at 90°C for 5 hr and cooled to room temperature. The resultant solution was poured on iced H_2O and filtered. The filtrate was concentrated in vacuo. Purification of the residue by flash column chromatography on silica gel (hexane/EtOAc, 4:1) afforded the desired product **5** (1.8g, 70%) as a white solid.: ^{1}H NMR ($CDCl_3$, 300 MHz) δ 1.36 (t, J = 9.0 Hz, 3H), 2.92 (q, J = 15, 6 Hz, 2H), 7.74 (d, J = 9 Hz, 1H), 7.86 (d, J = 9 Hz, 2H), 7.94 (d, J = 3 Hz, 1H).

(2-Chloro-3-ethylquinolin-6-yl)(4-methoxycyclohexyl)methanone (6)

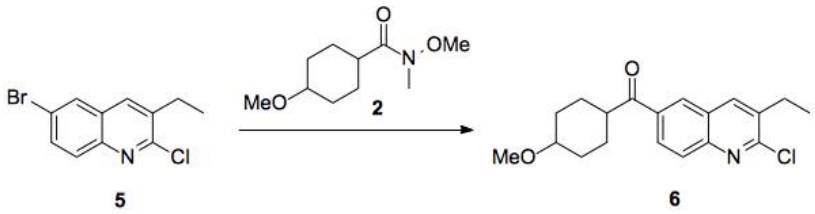

n-Butyl lithium (*n*-BuLi) (1.6 M) in hexane (2 mL, 3.2 mmol) was added dropwise to a solution of **2** (700 mg, 2.59 mmol) in distilled tetra-hydrofuran (THF) (5.5 mL) at -78°C, and stirred at -78°C for 1 h. Com-pound **5** (510 mg, 2.53 mmol) was dissolved in distilled THF (4 mL) and added dropwise to the stirred solution of **2**, and the reaction mixture was stirred at -78°C for 2 hr. The resultant mixture was warmed to 0°C, quenched by H_2O (5 mL), extracted with EtOAc and washed with brine. The organic layer was dried with over $MgSO_4$, filtered, and concentrated. The crude product was separated by flash column chromatography on silica gel (hexane/EtOAc, 4:1) to give pure *cis*-form **6a** (200 mg, 0.6 mmol, 23.4%), pure *trans*-form **6b** (22.2 mg, 0.07 mmol, 2.6%), and *cis-/trans*- mixture **6** (381 mg, 1.15 mmol, 44.4%) as light yellow solids, res-pectively.

(2-Chloro-3-ethylquinolin-6-yl)((1*S*,4*S*)-4-methoxycyclohexyl)methanone (6a).

^{1}H NMR ($CDCl_3$, 300 MHz) δ 1.39 (t, *J* = 6.0 Hz, 3H), 1.51-1.77 (m, 5H), 1.89-2.07 (m, 3H), 2.94 (q, *J* = 15, 9 Hz, 2H), 3.33 (s, 3H), 3.36-3.51 (m, 2H), 8.06 (app. t, *J* = 9 Hz, 2H), 8.18 (d, *J* = 9 Hz, 1H), 8.38 (s, 1H).

(2-Chloro-3-ethylquinolin-6-yl)((1*R*,4*R*)-4-methoxycyclohexyl)methanone (6b).

^{1}H NMR ($CDCl_3$, 300 MHz) δ 1.32-1.45 (m, 5H), 1.62(app. dddd, *J* = 24, 12, 3 Hz, 2H), 2.02-2.06 (m, 2H), 2.20-2.26 (m, 2H), 2.94 (app. q, *J* = 15, 6 Hz, 2H), 3.21 (app. tt, *J* = 12, 3 Hz, 1H), 3.37 (app. tt, *J* = 24, 3 Hz, 1H), 3.40 (s, 3H), 8.07 (app. t, *J* = 9 Hz, 2H), 8.20 (dd, *J* = 9, 3 Hz, 1H), 8.40 (d, *J* = 3 Hz, 1H).

(3-Ethyl-2-fluoroquinolin-6-yl)((1*S*,4*S*)-4-methoxycyclohexyl)methanone (7a) and (3-ethyl-2-fluoroquinolin-6-yl)((1*R*,4*R*)-4-methoxycyclohexyl)methanone (7b)

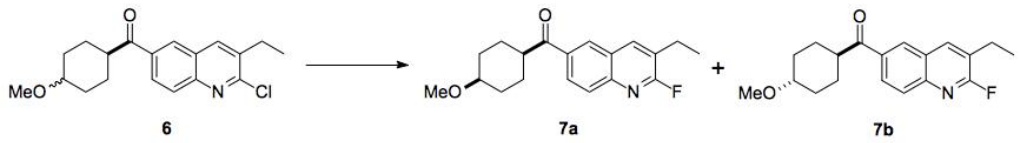

To a solution of **6** (70 mg, 0.21 mmol) in dimethyl sulfoxide (DMSO) (1.7 mL), potassium fluoride (KF) (120 mg, 2.1 mmol) was added and stirred at 120°C for 20 hr. After the reaction mixture was cooled to room temperature, water (30 mL) and EtOAc (30 mL) were added and the layers were separated. The aqueous layer was extracted with EtOAc (30 mL) again. The combined organic extracts were washed with brine, dried with over $MgSO_4$, and evaporated in vacuo. The crude product was purified by flash column chromatography on silica gel (hexane/EtOAc, 3:1) afforded the desired products **7a** and **7b** as light yellow solids.

(3-Ethyl-2-fluoroquinolin-6-yl)((1*S*,4*S*)-4-methoxycyclohexyl)methanone (7a).

^{1}H NMR ($CDCl_3$, 400 MHz) δ 1.37 (t, *J* = 8 Hz, 3H), 1.57-1.64 (m, 2H), 1.70-1.75 (m, 2H), 1.91-1.97 (m, 2H), 2.03-2.07 (m, 2H), 2.94 (q, *J* = 16, 8 Hz, 2H), 3.33 (s, 3H), 3.40 (app. tt, *J* = 12, 4 Hz, 1H), 3.51-3.54 (app. m, 1H), 7.97 (d, *J* = 8 Hz, 1H), 8.14 (d, *J* = 12 Hz, 1H), 8.17 (dd, *J* = 8.9, 1.8 Hz, 1H), 8.40 (d, *J* = 1.8 Hz, 1H).

(3-Ethyl-2-fluoroquinolin-6-yl)((1*R*,4*R*)-4-methoxycyclohexyl)methanone (7b).

^{1}H NMR ($CDCl_3$, 400 MHz) δ 1.37 (t, *J* = 8 Hz, 3H), 1.58-1.68 (m, 4H), 1.99-2.10 (m, 2H), 2.21-2.25 (m, 2H), 2.85 (q, *J* = 16, 8 Hz, 2H), 3.22 (app. tt, *J* = 12, 4 Hz, 1H), 3.32-3.38 (app. m, 1H), 3.40 (s, 3H), 7.97 (d, *J* = 8 Hz, 1H), 8.16 (d, *J* = 8 Hz, 1H), 8.20 (dd, *J* = 8.9, 1.8 Hz, 1H), 8.41 (d, *J* = 1.8 Hz, 1H).

Radiosynthesis

(3-Ethyl-2-fluoro-[^{18}F]quinolin-6-yl)((1*S*,4*S*)-4-methoxycyclohexyl) methanone ([^{18}F]7a) and (3-ethyl-2-fluoro-[^{18}F]quinolin-6-yl)((1*R*, 4*R*)-4-methoxycyclohexyl)methanone ([^{18}F]7b)

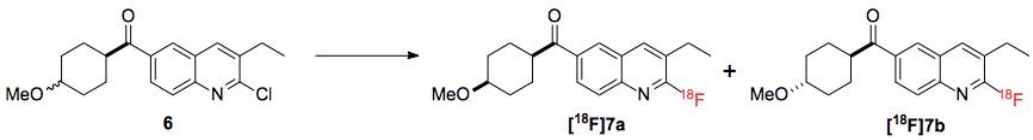

[^{18}F]Fluoride was produced by bombarding ^{18}O-enriched water with 16.5 MeV proton. The produced [^{18}F]fluoride was captured on a QMA light Sep-Pak cartridge (Waters) that had been preconditioned with 0.5 M potassium bicarbonate ($KHCO_3$) (5 mL) and washed with deionized water (10 mL). [^{18}F]Fluoride on the cartridge was eluted with a 1 mL solution of Kryptofix 2.2.2 (K2.2.2) (18.1 mg, 0.048 mmol)/K_2CO_3 (2.9 mg, 0.021 mmol) in acetonitrile (MeCN)/H_2O (50/50) (vol/vol). Azeotropic evaporation was performed twice at 100°C after adding MeCN (1 mL) under purging with nitrogen gas.

To the dried [^{18}F]fluoride, 1.5 mg of precursor **6** in DMSO (0.5 mL) was added and heated at 100°C for 5 min. The reaction mixture was loaded to a preparative HPLC (Xterra® preparative column RP18, 10 μm, 10×250 mm, Waters; 50% MeCN in H_2O, isocratic; flow rate, 5 mL/min). The retention times of [^{18}F]**7a** and [^{18}F]**7b** were 18.0 and 16.5 min, respectively, and collected separately.

A purified [^{18}F]**7a** or [^{18}F]**7b** fraction was diluted with 100 mL water, and passed through a Sep-Pak C18 light cartridge preconditioned with 5 mL of ethanol (EtOH) and 10 mL of deionized water. The adsorbed radioactive compounds were eluted with 0.8 mL EtOH, passed through a sterile Millex®-FG filter (Merck Millipore, Billerica, MA, U.S.A.), and collected in a sterile vial. The final products were diluted with normal saline to apply for *in vivo* system.

Radiochemical purity was checked using radio-TLC (aluminum-backed silica gel 60 F_{254} TLC plate; hexane/EtOAc, 75:25) and analytical HPLC (Xterra® analytical column RP18, 3.5 μm, 4.6×100 mm, Waters; 44%-50% MeCN gradient in H_2O from 0 to 15 min; flow rate, 1 mL/min). Specific activities were also determined using the same analytical HPLC system.

Automatic Radiosynthesis

Automatic synthesis of [^{18}F]**7a** or [^{18}F]**7b** was performed by using 3 mg of precursor in 0.7 mL of DMSO in a TRACERLab FX-FN module (GE medical Systems, Germany) (Figure 8). Reaction temperature and time were 110°C and 6 min, respectively. All other conditions were the same as in the manual synthesis.

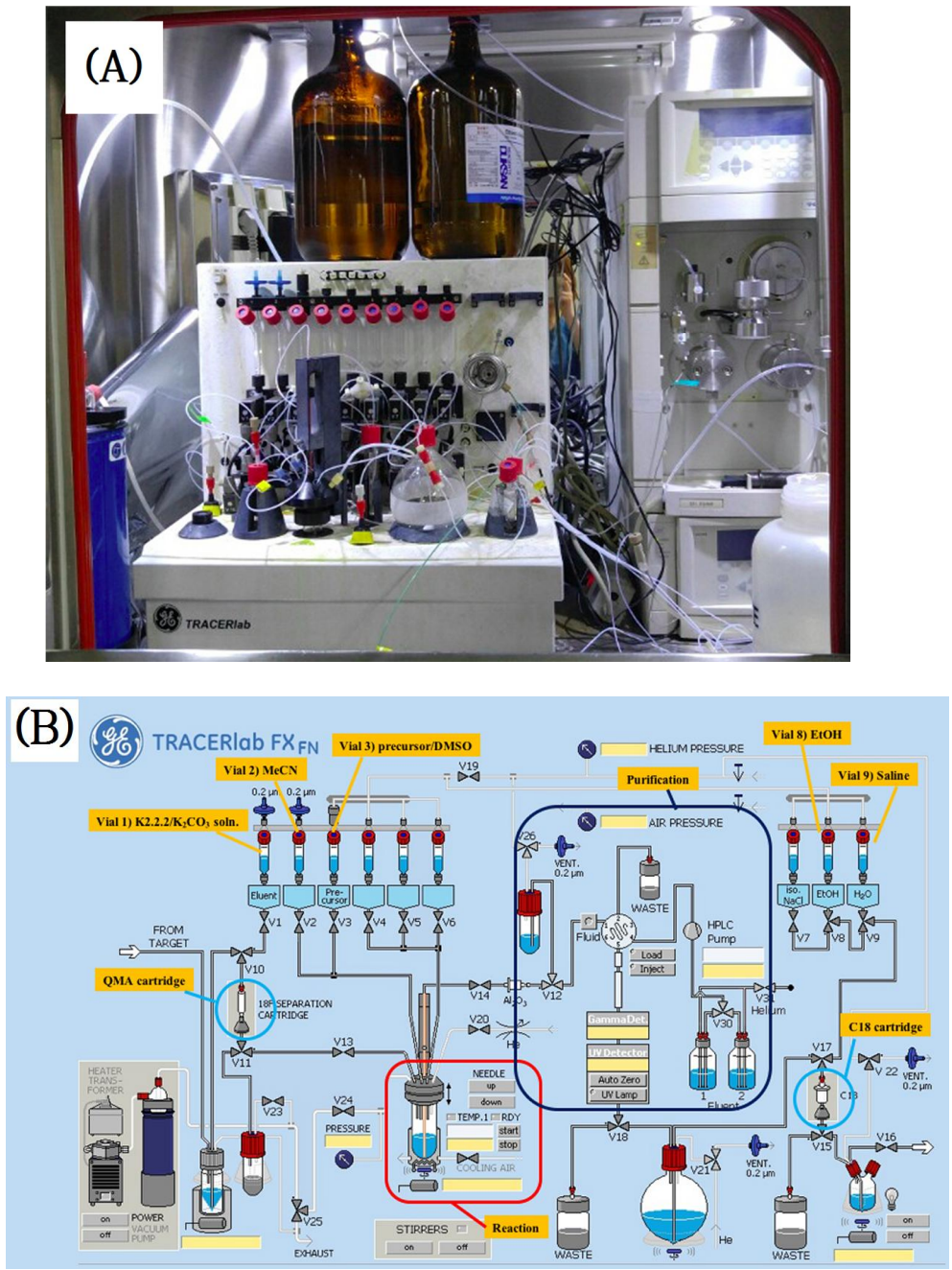

Figure 8. TRACERLab FX-FN module for automatic synthesis.

Module with preparative HPLC (A) and scheme for the automatic radio-synthesis of [^{18}F]7a and [^{18}F]7b (B).

Distribution coefficient (Log $D_{7.4}$)

The Log $D_{7.4}$ value of [^{18}F]**7a** was measured according to a slight modification of previous reported method (*95*). Briefly, a 10 μL EtOH solution containing [^{18}F]**7a** (radiochemical purity: 100%) was mixed with a mixture of 1-octanol (3.0 g) and 0.1 M phosphate buffer (3.0 g; pH 7.4), vortexed for 3 min at room temperature and followed by centrifugation at 3,000 rpm for 5 min. The samples from the organic and aqueous phases were weighted and counted using a gamma scintillation counter (DREAM r-10, Shinjin Medics Inc., Korea). An aliquot of organic layer (0.5 g) was re-partitioned until Log $D_{7.4}$ values were consis-tent. The Log $D_{7.4}$ was calculated as the ratio of radioactivity in the organic phase (cpm/g) and that in the aqueous phase (cpm/g) (Figure 9).

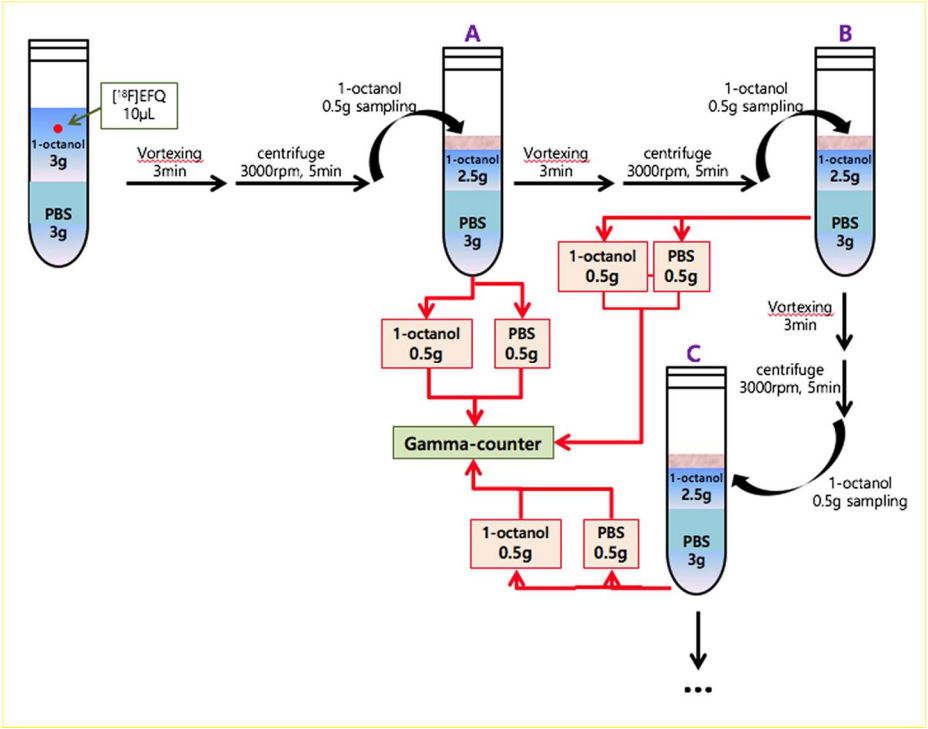

Figure 9. Octanol distribution method for Log $D_{7.4}$ measurement.

Stability test

The *in vitro* stabilities of [^{18}F]**7a** in the prepared medium (10% EtOH) at room temperature or in human serum at 37°C were measured. The purified [^{18}F]**7a** was stored at room temperature for 4 h and analyzed using radio-TLC and analytical HPLC. For stability test in human serum, the prepared [^{18}F]**7a** (25 μL) was mixed with human serum (325 μL) and incubated at 37°C for 4 hr. Absolute EtOH (775 μL) was added to the mixture to precipitate serum proteins, and centrifuged (3,000 rpm) for 5 min. The supernatant was also analyzed using radio-TLC and analytical HPLC.

Biodistribution study in mice

Male BALB/c mice (5 weeks old, n=4 per group, 23±1 g) were inject-ted with 148 kBq (187 pg) of [^{18}F]**7a** in 0.1 mL of 10% EtOH through the tail vein. For blind test, the injected mice were numbered randomly and sacrificed at 10, 60 or 120 min after injection by decapitation. 10 organs include brain and blood were rapidly separated, weighed and counted using a gamma scintillation counter. Results are expressed as percent injected dose per gram of tissue (% ID/g). Values are expressed as mean ± SD.

Metabolites analysis in mice

After intravenous injection of [^{18}F]**7a** (72.5 MBq/93.0 ng, 0.2 mL of 5% EtOH), male BALB/c mice (5 weeks old, n=1 per group, 23±1 g) were sacrificed by decapitation at 5, 15, 30 and 60 min. Urine, blood and the whole brain were removed and stored on ice. The urine sample (200 μL) was diluted with distilled water (200 μL) and filtered through a 0.22-μm filter. The blood sample was centrifuged at 3,300 rpm for 10 min at 4°C to separate the plasma. The plasma sample was mixed with MeCN (400 μL), vortexed for 15 s and centrifuged at 3,300 rpm for 10 min for deproteinization. The brain sample in ice-cooled MeCN (1.0 mL) was homogenized for 1 min using polytron homogenizer (Kinematica, West-bury, Canada). The homogenate was centrifuged at 3,300 rpm for 10 min at 4°C, and the supernatant was collected. To the brain precipitate, water (1.0 mL) was added. The mixture was re-homogenenized and re-centrifuged at 3,300 rpm for 10 min at 4°C. The collected supernatant was mixed with organic supernatant and centrifuged again at 3,300 rpm for 10 min at 4°C.

All samples obtained from the urine, plasma and brain homogenate were injected into the analytical HPLC (Xterra® analytical column RP18, 3.5 μm, 4.6×100 mm, Waters; 0%-45% MeCN gradient in H_2O from 0 to 6 min; 45% MeCN in H_2O, isocratic from 6 to 21 min; 100% MeCN, isocratic from 21 to 26 min; flow rate, 1 mL/min). The resultant

eluent was fractionized with time (0.33 min) and measured the fraction's radio-activities using a gamma scintillation counter.

PET study in rats

Male Sprague-Dawley (SD) rats (12 weeks old) were anesthetized with 2% (v/v) isoflurane at 1 L/min oxygen flow were positioned in the imaging chamber and were intravenously administrated with [^{18}F]**7a** (n=3 for [^{18}F]**7a**, 118.6 ng, 92.5 MBq) or [^{18}F]**7b** (n=1 for [^{18}F]**7b**, 312.9 ng, 92.5 MBq) prepared as described above. PET studies were performed with a dedicated small animal PET scanner (eXplore VISTA, GE Health-care, NJ, U.S.A.), and list-mode data were acquired for 60 min with an energy window of 400-700 keV. These list-mode data were framed into a dynamic sequence of 10 x 30 s, 5 x 60 s, 4 x 300 s, and 3 x 600 s frames. These images were reconstructed to temporally framed sinograms using Fourier rebinning and an ordered subsets expectation maximization (OSEM) reconstruction algorithm without attenuation correction. All images were analyzed using parametric mapping software (SPM2, University College of London, London, U.K.).

To confirm the selectivity and specificity of [^{18}F]**7a** for mGluR1, blocking studies were performed. SD Rats (n=1 per group) were pre-treated with the pure cold compound **7a**, the mGluR1 selective antagonist JNJ16259685 or the mGluR5 antagonist ABP688 (3 mg/kg each, iv) 10 min before the administration of radioligand [^{18}F]**7a**. After [^{18}F]**7a** injection, PET imaging studies were conducted as described above.

Ex vivo autoradiography in rats

A [^{18}F]**7a** (148 MBq, 190 ng, 0.5 mL) solution of 5% EtOH in saline was intravenously injected into a male SD rat (12 weeks old, n=1) through the tail vein. To confirm the specific binding, JNJ16259685 (3 mg/kg) was co-injected with [^{18}F]**7a** into a rat (12 weeks old, n=1). 10 min after the radioligand injection, the rats were sacrificed and the rats' brains were dissected. The brains were rapidly frozen at -80°C for 30 min. Brain sagittal sections of 20 μm thickness were cut using a cryostat microtome (Leica CM 1800, Leica Inc., Germany), and thaw-mounted on glass slides. The prepared brain sections were exposed to imaging plates, and autoradiograms were obtained using a BAS-2000 system (FLA-2000, FUJIFILM Inc., Japan)(96).

III. Results

Chemistry

The precursor **6**, nonradioactive **7a** and **7b** were synthesized according to the described methods (Scheme II). *N*-(4-Bromophenyl)butyramide (**4**) was prepared from commercially available 4-bromoaniline and butyryl chloride. The resulting anilide **4** was reacted with $POCl_3$ and DMF, Vilsmeier-Haack type reaction, to give a quinoline moiety (**5**). The compound **5** was lithiodebrominated using *n*-BuLi at -78°C, and foll-owed by addition of Weinreb amide *N*,4-Dimethoxy-*N*-methyl-cyclo-hexanecarboxamide (**2**) that was synthesized from 4-methoxy-cyclo-hexanecarboxylic acid (**1**) to afford the chloroquinoline precursor (**6**) for fluorination. The crude products were purified by silica gel column chro-matography. However, the *cis/trans*- mixture of precursor **6** was not separated since both **7a** and **7b** were produced even if only a purified *cis*- or *trans*- precursor was used due to the harsh reaction conditions (120°C, overnight) (Figure 10). In order to obtain the cold form of **7a** and **7b**, compound **6** was reacted with KF in DMSO at 120°C, and chromato-graphed on a silica gel column.

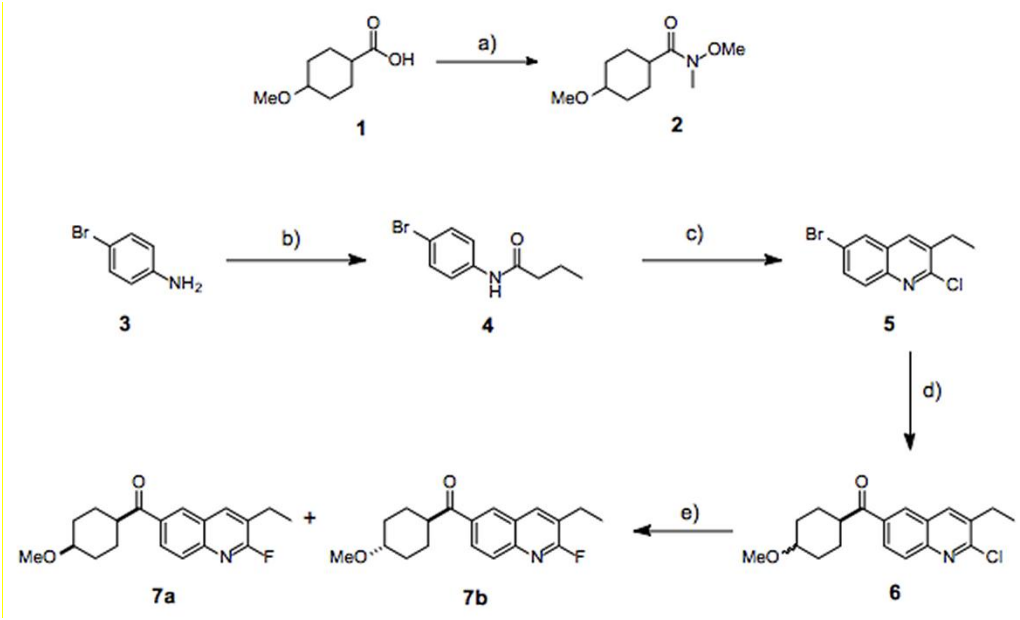

Scheme II. Synthesis of fluoroquinoline compounds for mGluR1 antagonist.

Reagents and conditions: (a) CDI, CH_2Cl_2, rt, 1 hr then $H_3CNHOCH_3 \cdot HCl$, rt, overnight; (b) $CH_3(CH_2)_2COCl$, Et_3N, CH_2Cl_2, rt, overnight; (c) $POCl_3$, DMF, rt, 2 hr then compound 4, 90°C, 5 hr; (d) compound **2**, *n*-BuLi, THF, -78°C, 1 hr then compound 5, -78°C, 2 hr; (e) KF, DMSO, 120°C, 20 hr.

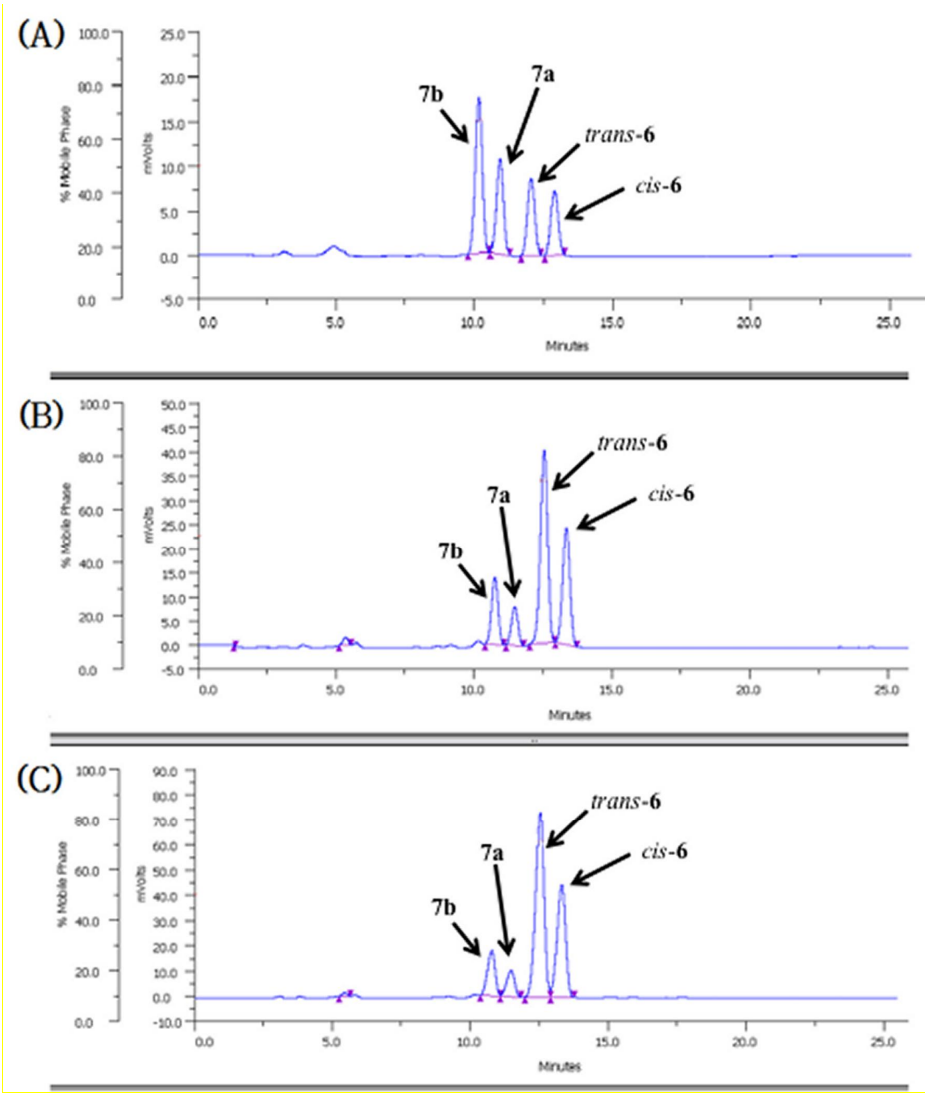

Figure 10. Isomerization in fluorination reaction.

HPLC chromatograms of reaction mixtures when pure *cis*-form **6a** (A), pure *trans*-form **6b** (B), or *cis*/*trans*- mixture **6** (C) was used for reaction.

Radiolabeling

The radiolabeling of [^{18}F]**7a** and [^{18}F]**7b** were performed beginning with the *cis/trans*- mixture of precursor **6** by the nucleophilic aromatic substitution reaction (Scheme III).

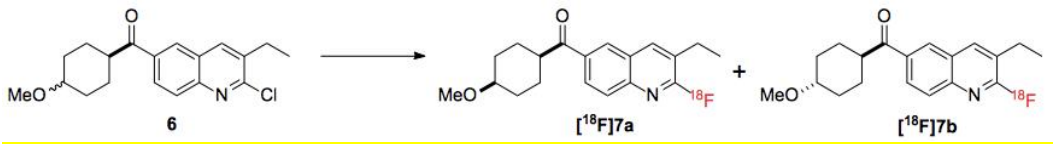

Scheme III. Radiolabeling of [^{18}F]7a and [^{18}F]7b.

Reagents and conditions: K2.2.2/K_2CO_3, DMSO, 100°C, 5 min.

The optimum precursor amount for rapid reaction times was found to be 1.5 mg. When 1 mg of precursor was used for labeling, it took over 10 min to obtain sufficient labeled compounds at 100°C. However, there was no significant difference between the 1.5 mg and 2.0 mg of precursor's labeling time. The labeled products were found to be very rapid after addition of precursor in both cases (Figure 11).

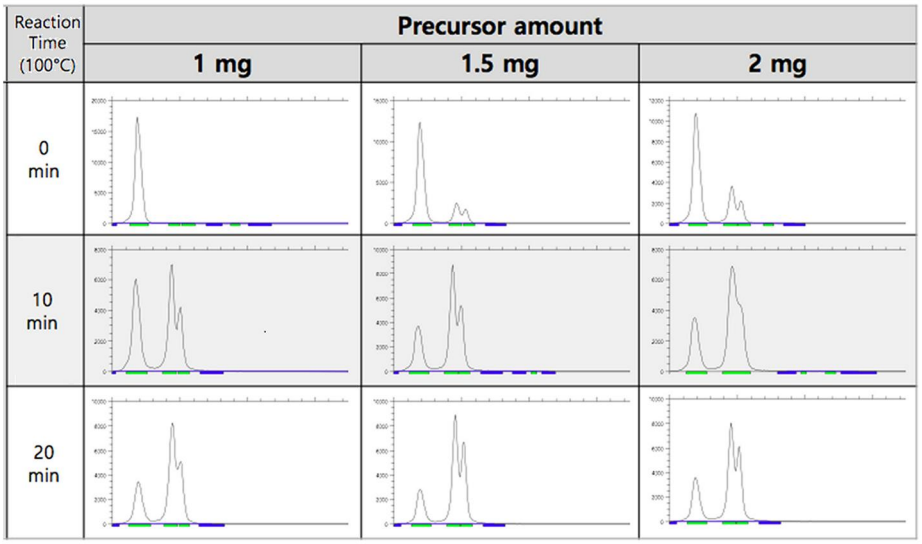

Figure 11. Relationship between precursor amount and reaction time.

Radio-TLC chromatograms of reaction mixture. R_f values of unreacted fluoride is 0, [^{18}F]**7b** is 0.3, and [^{18}F]**7a** is 0.4. (aluminum-backed silica gel 60 F_{254} TLC plate; hexane/EtOAc, 75:25)

Reaction temperature is another important option for labeling. When the reaction was carried out at high temperature (120°C), the labeled compounds were synthesized rapidly, but they decomposed quickly after 3 min of reaction. At 100°C, the highest labeling efficiency was achieved within 5 min after addition of the precursor, and the decomposition rate was not too fast (Figure 12). From these results, the reaction temperature and time, 100°C and 5 min were optimized.

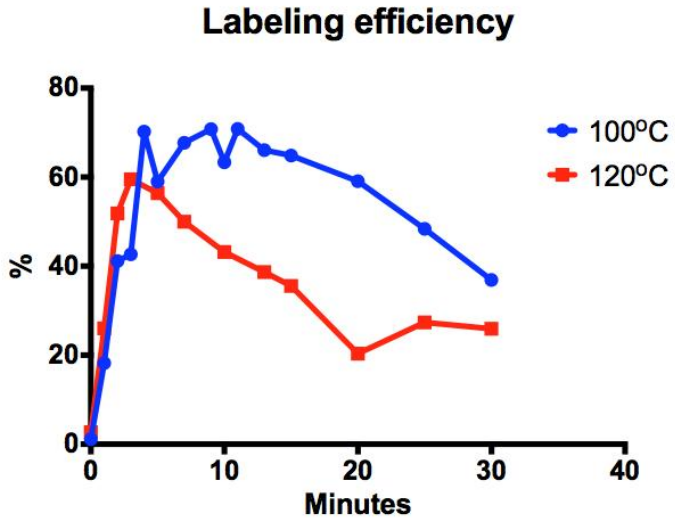

Figure 12. Labeling efficiency of *cis*-/*trans*- [^{18}F]7 at two different temperatures (100°C and 120°C).

The crude radioactive product was purified using semi-preparative HPLC. The retention times of [^{18}F]**7b** and [^{18}F]**7a** were 16.5 and 18.0 min, respectively (Figure 13). After removal of MeCN, the purified compounds were formulated with normal saline for intravenous injection. The radiolabeling efficiencies of [^{18}F]**7a** and [^{18}F]**7b** were 29% and 49% respectively. The total synthesis time from the starting reaction of precursor with [^{18}F]fluoride to the formulation was about 60 min. The purities and specific activities of [^{18}F]**7a** and [^{18}F]**7b** were measured using analytical HPLC. The retention times of [^{18}F]**7a** and [^{18}F]**7b** were 8.5 and 7.5 min, respectively (Figure 14). The radiochemical purities of those products were over 99%. The specific activity of [^{18}F]**7a** was 63-246 GBq/μmol and that of [^{18}F]**7b** was 30.5-93.2 GBq/μmol, respect-tively. The radio-TLC results also showed the high purities of these radiolabeled compounds.

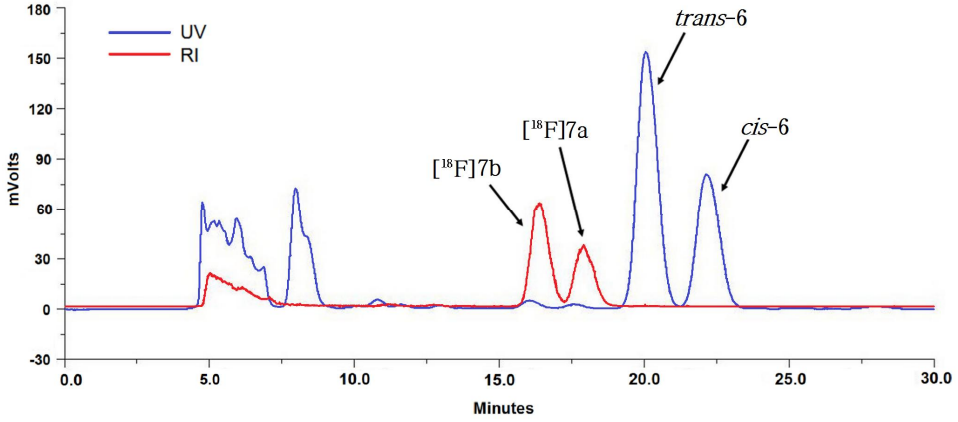

Figure 13. Preparative HPLC chromatogram.

The mixture of [^{18}F]**7a** and [^{18}F]**7b** for purification from precursor **6** after reaction.

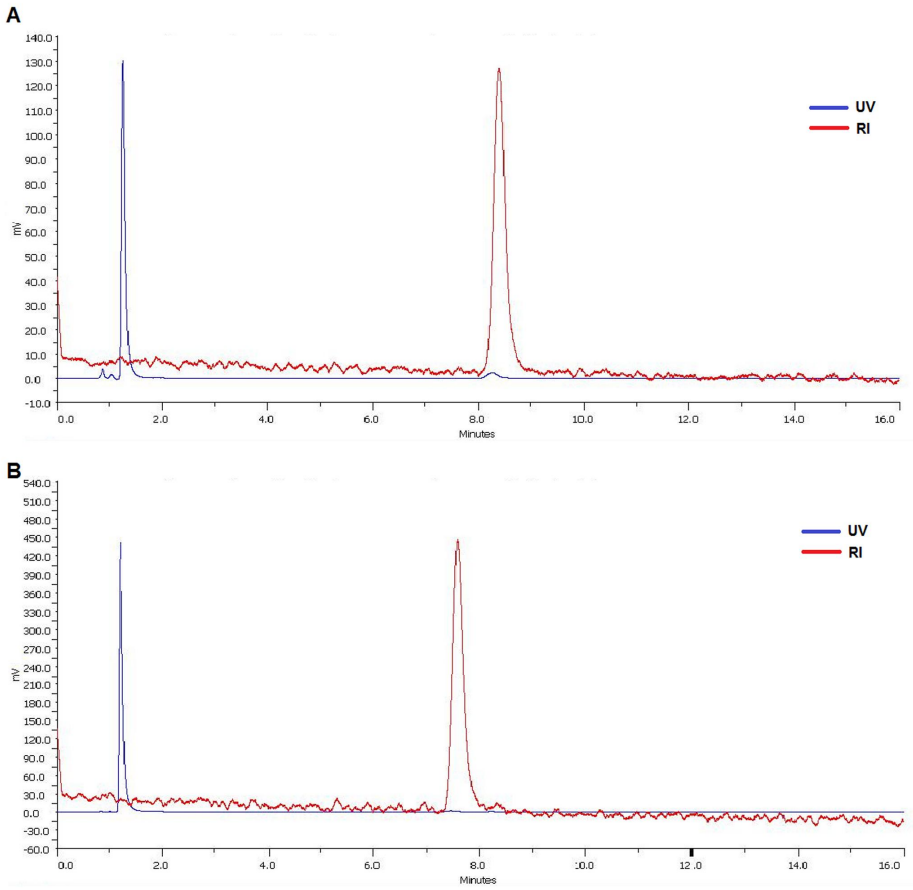

Figure 14. Analytical HPLC chromatograms.

Purified [^{18}F]**7a** (A) and [^{18}F]**7b** (B).

Automatic Radiosynthesis

When 1.5 mg of precursor was used for automatic synthesis, the final radioactive products were not enough for further animal or human study. This is because there are lots of tubes and vials in the module, which cause a loss of reagents and products during the process. The low yields of final products were recovered using increased quantities of precursor (3.0 mg) and solvent (0.7 mL DMSO).

Distribution coefficient (Log $D_{7.4}$)

The distribution coefficient of [^{18}F]**7a**, Log $D_{7.4}$ value was 3.24 ± 0.09 (n = 6), representing an adequate lipophilicity for penetration of the BBB.

Stability test

To confirm the stability of [^{18}F]**7a**, the labeled compound was incubated in 10% EtOH at room temperature or in human serum at 37°C for 4 hr. At room temperature, [^{18}F]**7a** did not show degradation over 4 hr. However, in human serum at 37°C, 1.2% of fluoride and 3.0% of radiometabolite were detected at 1 hr, which increased to 3.2% and 6.2% at 4 hr, respectively (Figure 15). The radioactive metabolite looked like *trans*- isomer [^{18}F]**7b**, but not. As the results of the metabolism study, it was confirmed that cis-trans isomerization did not occur in serum at human body temperature.

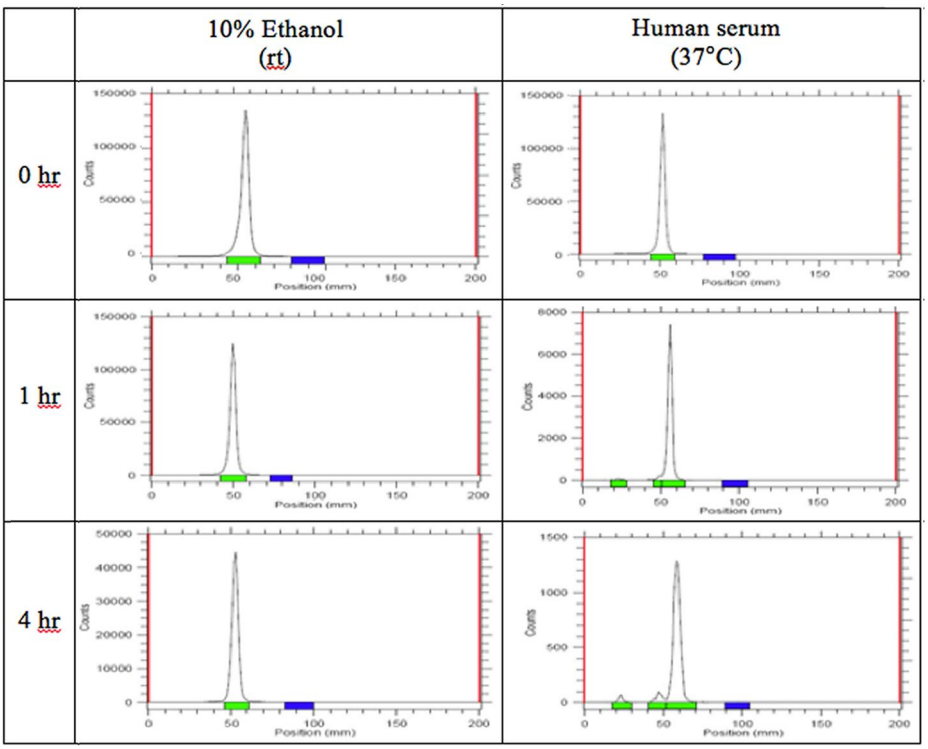

Figure 15. *In Vitro* Stability of [^{18}F]7a.

Stabilities in 10% ethanol at room temperature or in human serum at 37°C.

Biodistribution study in mice

The biodistribution of [^{18}F]**7a** was investigated with normal BALB/c mice at 10, 60, and 120 min (Table II, Figure 16). At 10 min after inject-tion, liver (16.77 ± 1.42% ID/g) showed the highest uptake level, and followed by the kidney (10.54 ± 0.78% ID/g). These radioactivities decreased over time, with increased intestinal uptake 16.94 ± 1.87 and 26.11 ± 1.64% ID/g at 60 and 120 min, respectively. It means hepato-biliary system is the main excretion route for [^{18}F]**7a**. The initial brain uptake was 4.42 ± 0.35% ID/g at 10 min, and the activity was decreased to 1.01 ± 0.11% ID/g at 60 min. Bone uptake was increased with time, from 2.39 ± 0.16% ID/g at 10 min to 15.43 ± 3.76% ID/g at 120 min. It means defluorination occurred *in vivo*.

Table II. Biodistribution of [^{18}F]7a in normal BALB/c mice.

(% ID/g Tissue: mean ± SD)

Tissue	10 min	60 min	120 min
Blood	2.51 ± 0.16	1.40 ± 0.07	0.71 ± 0.04
Muscle	2.76 ± 0.16	1.64 ± 0.17	1.32 ± 0.25
Brain	4.42 ± 0.35	1.01 ± 0.11	0.44 ± 0.04
Bone	2.39 ± 0.72	10.79 ± 0.39	15.43 ± 3.76
Heart	3.85 ± 0.23	1.76 ± 0.40	1.18 ± 0.46
Lung	6.61 ± 2.56	2.50 ± 0.15	1.08 ± 0.08
Liver	16.77 ± 1.42	12.98 ± 0.40	10.55 ± 1.39
Spleen	3.28 ± 0.42	2.43 ± 0.18	1.66 ± 0.16
Stomach	4.41 ± 0.92	21.14 ± 8.18	8.19 ± 3.88
Intestine	5.49 ± 0.58	16.94 ± 1.87	26.11 ± 1.64
Kidney	10.54 ± 0.78	7.68 ± 0.19	4.57 ± 0.33

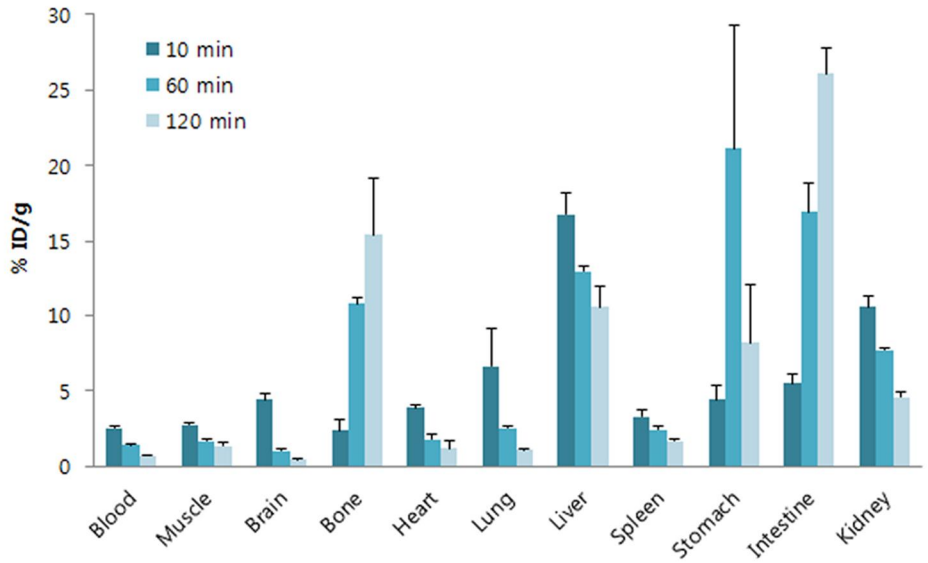

Figure 16. Biodistribution of [^{18}F]7a in normal BALB/c mice.

Metabolites analysis in mice

The radiometabolites of [^{18}F]**7a** in plasma, brain, and urine of normal BALB/c mice were analyzed by HPLC (Figure 17, Table III). The retention times of free [^{18}F]fluoride, [^{18}F]**7b**, and [^{18}F]**7a** were 1.4, 18.0, and 19.0 min, respectively. [^{18}F]**7a** showed six radiometabolites (metabolite 1-6) and free fluoride in plasma and brain homogenate samples. There was no *trans*- isomer [^{18}F]**7b** peak in all samples. It indi-cates cis-trans isomerization does not occur *in vivo*, due to insufficient temperature for the reaction. Metabolites 1-4 were not well separated from each other under the HPLC condition used. All radiometabolites showed faster retention times than the patent compound, indicating increased hydrophilicity after metabolism. The percentages of [^{18}F]**7a** in the brain were 88.9% and 59.5% at 5 and 30 min, respectively. The intact [^{18}F]**7a** in plasma was at 68.5% at 5 min, which decreased to 30.6% at 30 min. In the urine, there was no [^{18}F]**7a** and metabolite 6 at any time point. One the other hand, metabolite 1 was not found in the brain at any time.

Table III. Percentages of [^{18}F]7a and radiometabolites in the brain, plasma and urine of normal BALB/c mice.

	Rt (min)	plasma			brain			urine		
		5 min	15 min	30 min	5 min	15 min	30 min	5 min	15 min	30 min
[^{18}F]$^{-}$	1.4	4.2	19.0	16.8	0.2	1.6	4.6	9.5	52.4	11.3
Metabolite 1	6.7	0	6.6	11.1	0	0	0	4.0	4.1	5.9
Metabolite 2	7.3	4.8	10.6	16.6	0.2	1.3	5.2	26.1	17.7	11.3
Metabolite 3	8.4	9.3	11.5	14.0	1.5	3.3	5.5	23.1	18.9	15.4
Metabolite 4	9.0	2.1	5.5	4.0	0.8	2.7	4.4	4.6	1.0	7.1
Metabolite 5	10.9	9.9	11.5	13.1	5.6	14.9	20.0	2.5	3.0	0
Metabolite 6	13.2	1.0	0.6	0.4	1.4	1.1	0.8	0	0	0
[^{18}F]7a	19.0	68.5	36.7	30.6	88.9	74.8	59.5	0	0	0

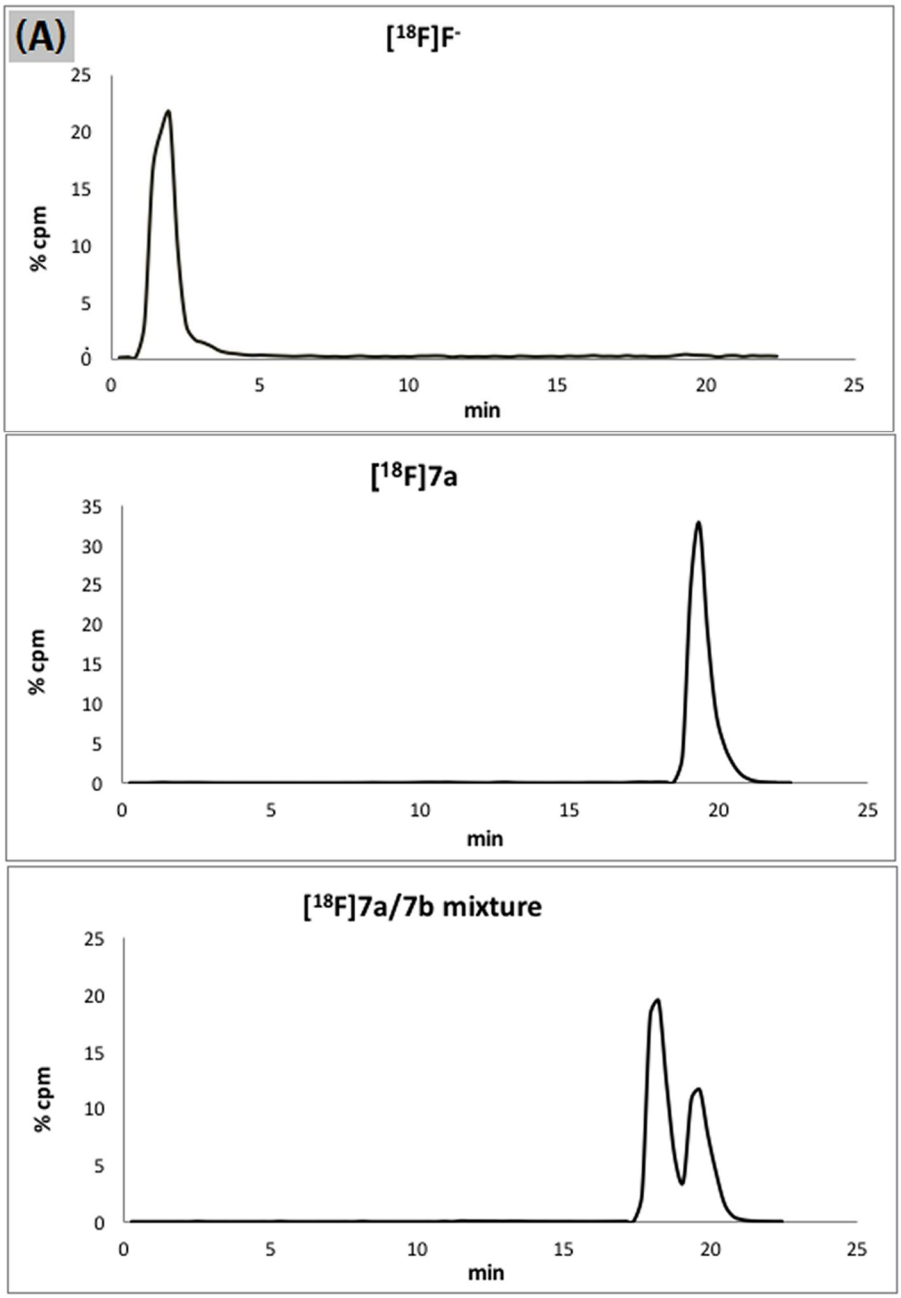
(A)
[18F]F-
% cpm
min
[18F]7a
% cpm
min
[18F]7a/7b mixture
% cpm
min

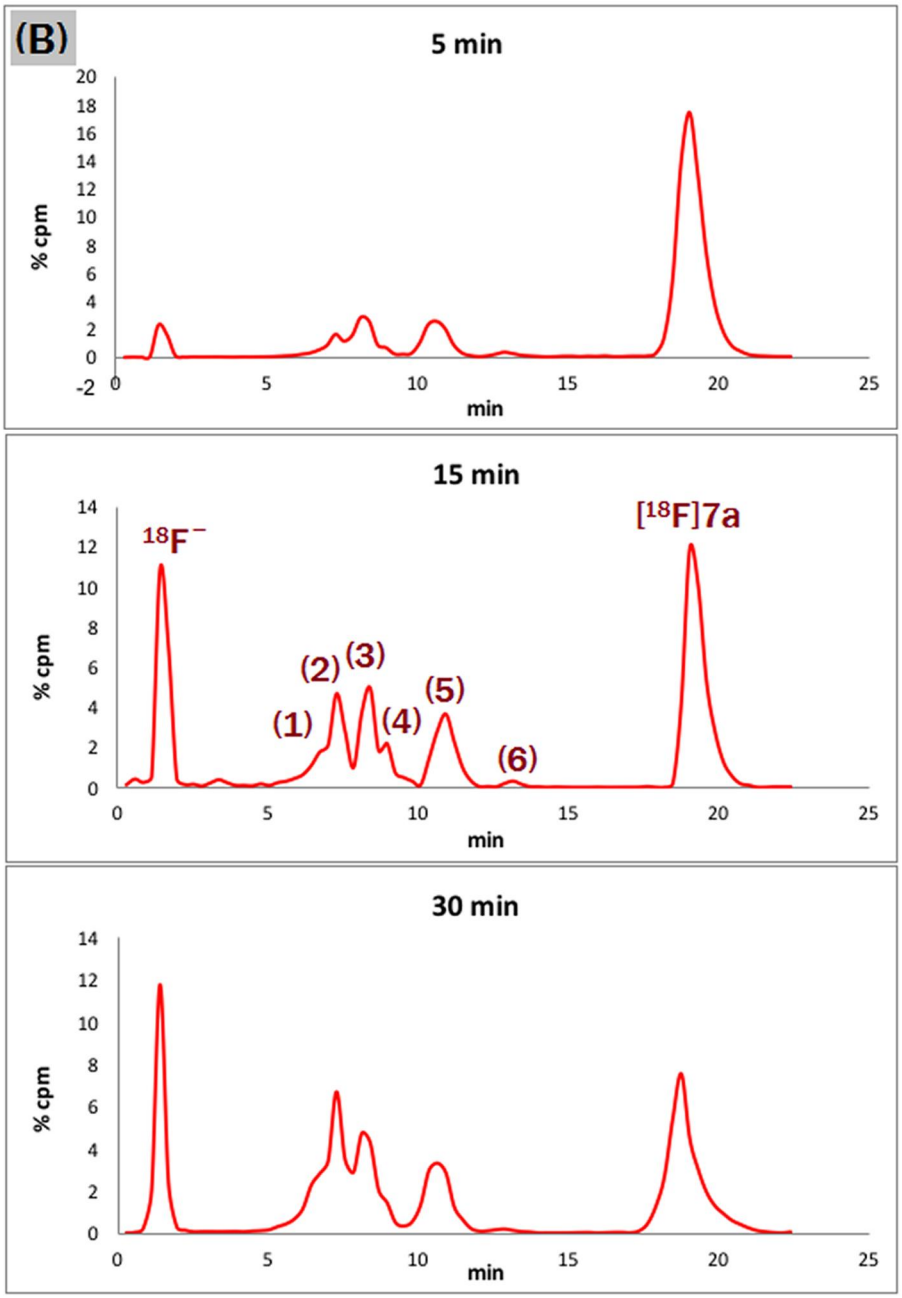
(B)
5 min
% cpm
min
15 min
$^{18}F^-$
[^{18}F]7a
(1)
(2)
(3)
(4)
(5)
(6)
30 min

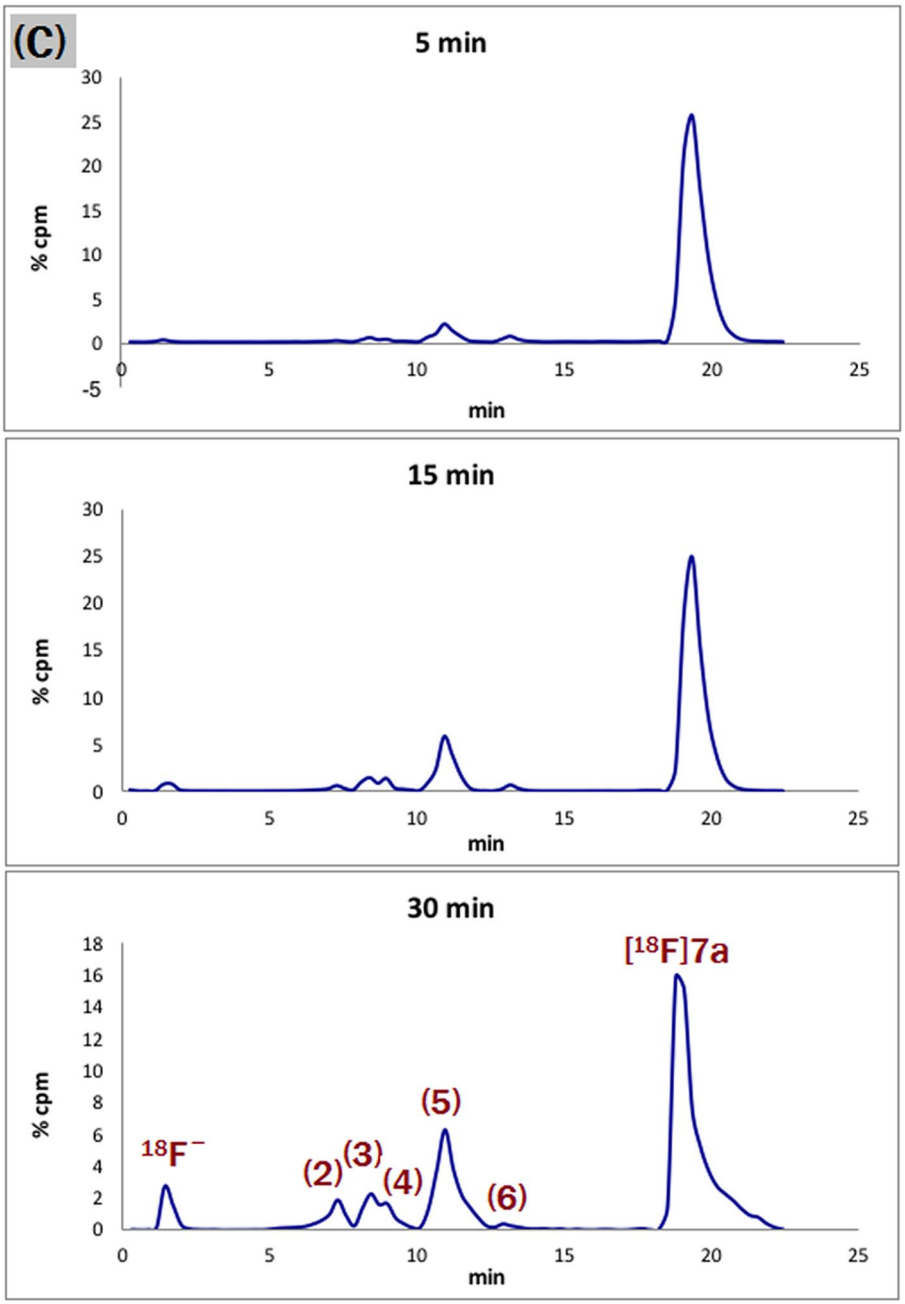
(C)
5 min
% cpm
min
15 min
% cpm
min
30 min
% cpm
min
$^{18}F^-$
(2)
(3)
(4)
(5)
(6)
[^{18}F]7a

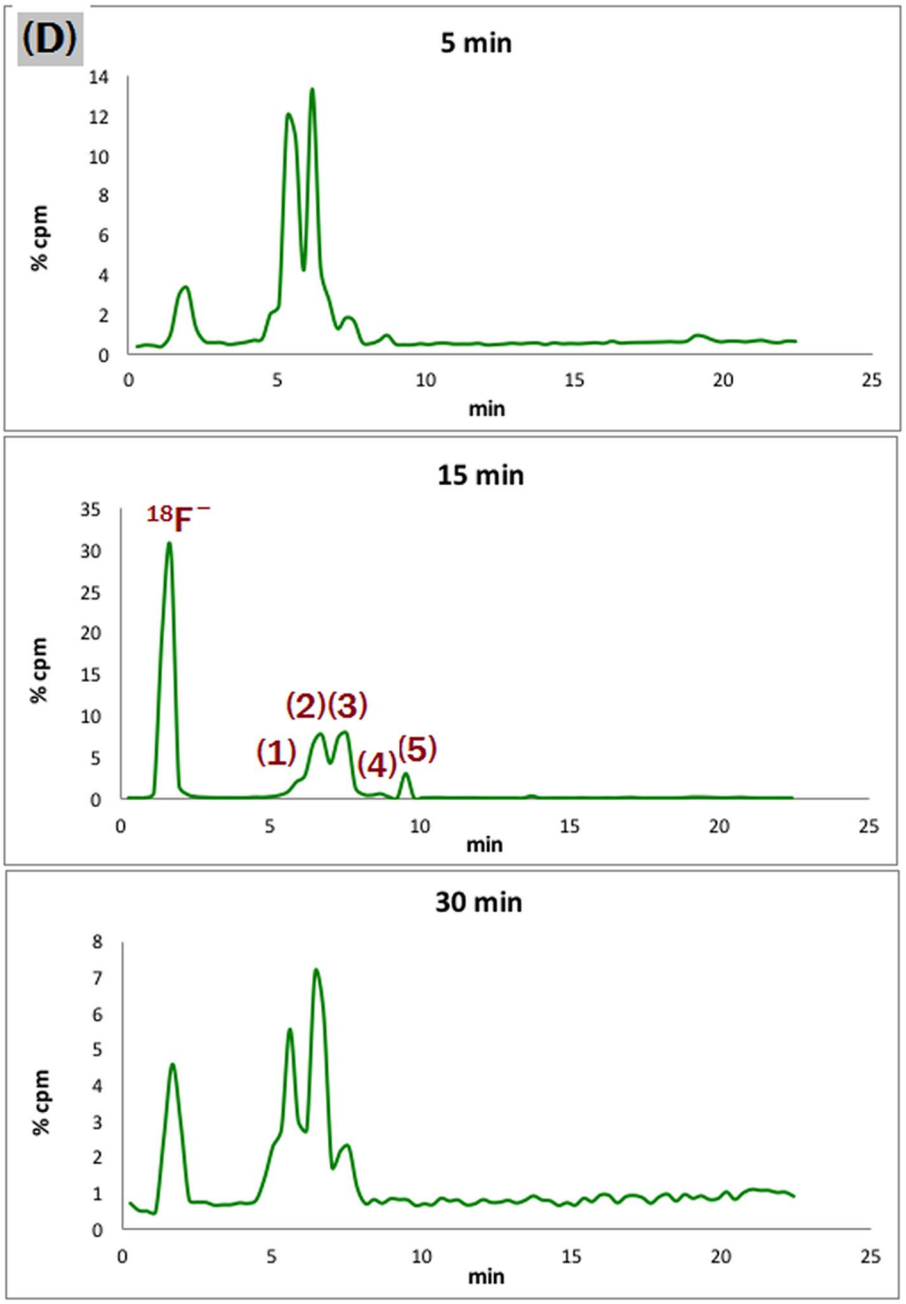

Figure 17. Metabolism of [^{18}F]7a in BALB/c mice at 5, 10, 30 min. HPLC chromatograms of radioactive standards (A) and radiometabolites in the plasma (B), in the brain (C), and in the urine (D).

PET study in rats

Dynamic animal PET imaging studies were performed in the rat brains after intravenous radioligands administration for 1 hr. [^{18}F]**7a** showed the highest uptake activity in the cerebellum, and slightly uptake in the hippocampus, thalamus, and striatum which are known as mGluR1-rich regions (Figure 18A). As shown in the time activity curves (TACs), radioactivity in the cerebellum increased rapidly after injection, peaked at 2 min and then decreased (Figure 18A). Although **7a** showed high affinity to mGluR1 (IC_{50} = 5 nM in rat (*64*)), [^{18}F]**7a** uptake in the brain decreased faster than expected.

The selectivity and specificity of [^{18}F]**7a** to mGluR1 were investigated by blocking test with using **7a**, JNJ16259685, and ABP688. JNJ1625-9685 and ABP688 have been already demonstrated as specific anta-gonists to mGluR1 and mGluR5, respectively. When rats were pretreated with **7a** or JNJ16259685 10 min before the injection of [^{18}F]**7a**, homo-geneous distributions of radioactivity in all brain regions were shown, indicating nonspecific uptake due to mGluR1 blockade (Figure 18B and 18C). However, preliminary injection of ABP688 did not affect the uptake pattern of [^{18}F]**7a** (Figure 18D).

The *trans*- isomer [^{18}F]**7b** did not show specific uptake in any brain region. This pattern was similar with nonspecific bindings of [^{18}F]**7a** in blocking studies with **7a** or JNJ16259685. The TAC showed that

[^{18}F]**7b** rapidly entered the brain along the bloodstream and quickly washed out without binding to the receptor (Figure 18E).

A

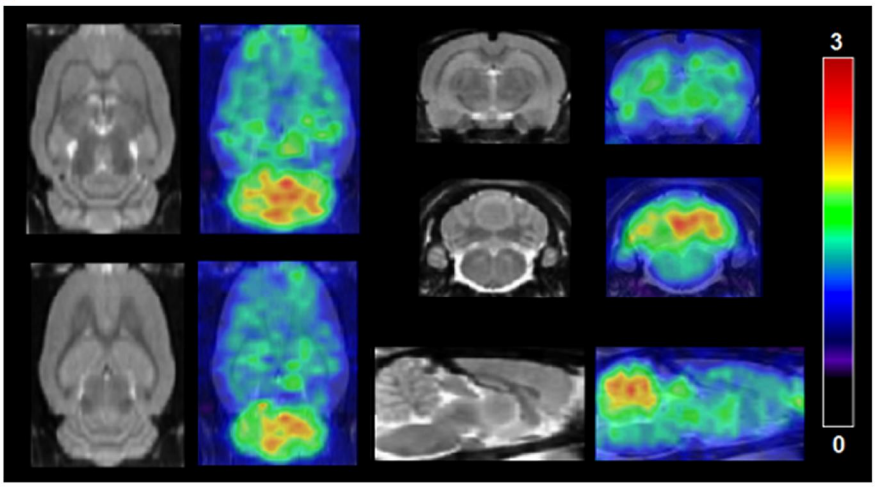
3
0

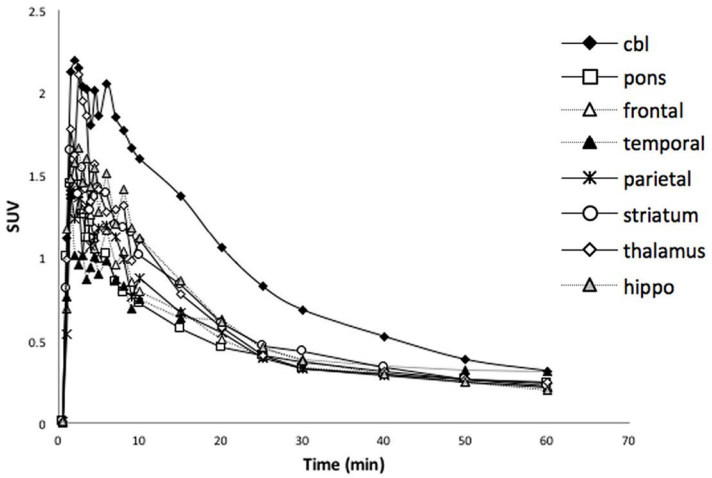
2.5
2
1.5
1
0.5
0
SUV
0
10
20
30
40
50
60
70
Time (min)
cbl
pons
frontal
temporal
parietal
striatum
thalamus
hippo

B

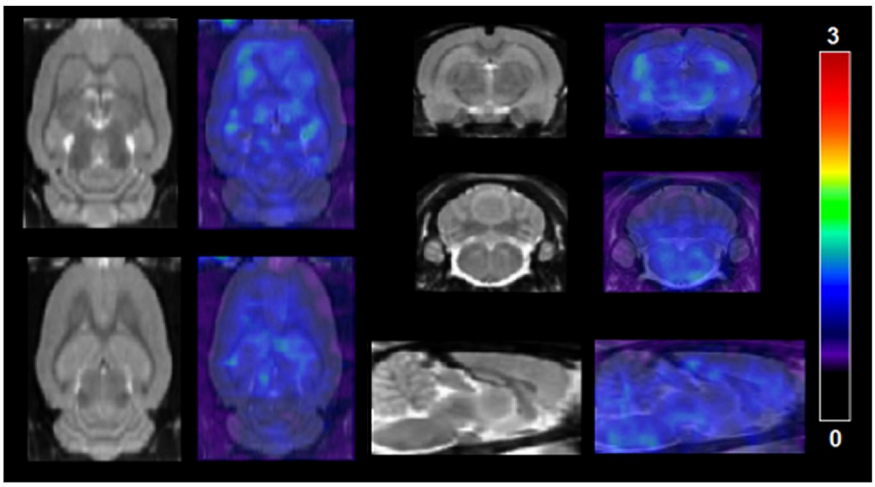
3
0

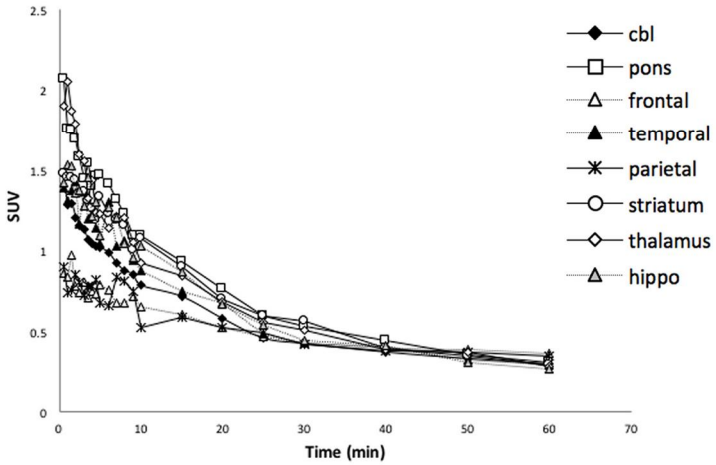
SUV
Time (min)
cbl
pons
frontal
temporal
parietal
striatum
thalamus
hippo

C

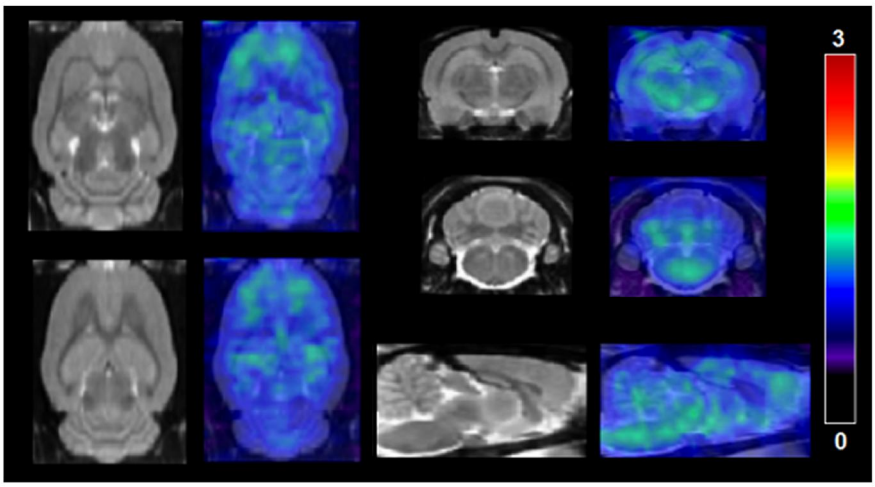
3
0

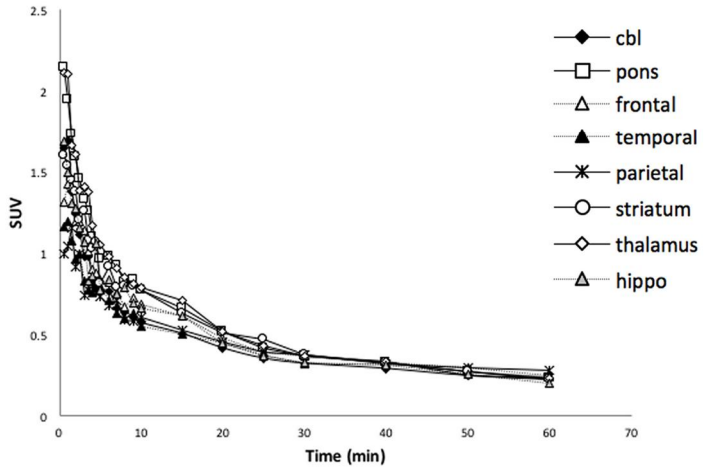
2.5
2
1.5
1
0.5
0
SUV
0
10
20
30
40
50
60
70
Time (min)
cbl
pons
frontal
temporal
parietal
striatum
thalamus
hippo

D

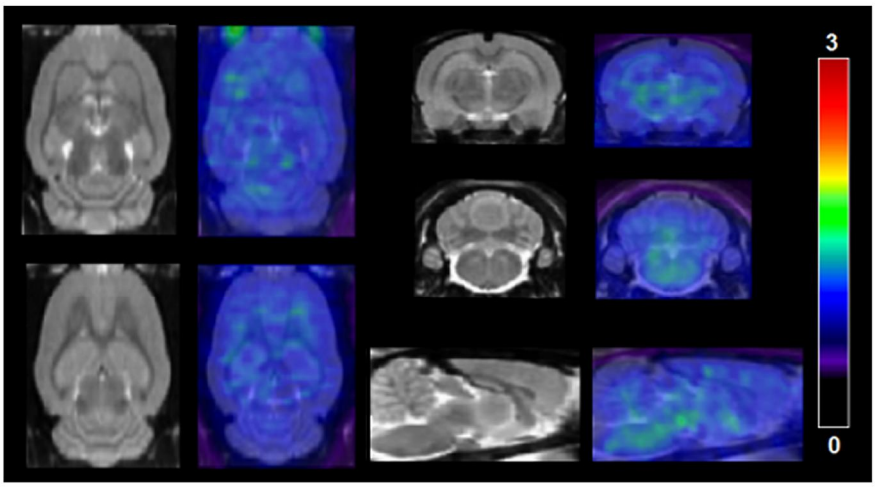
3
0

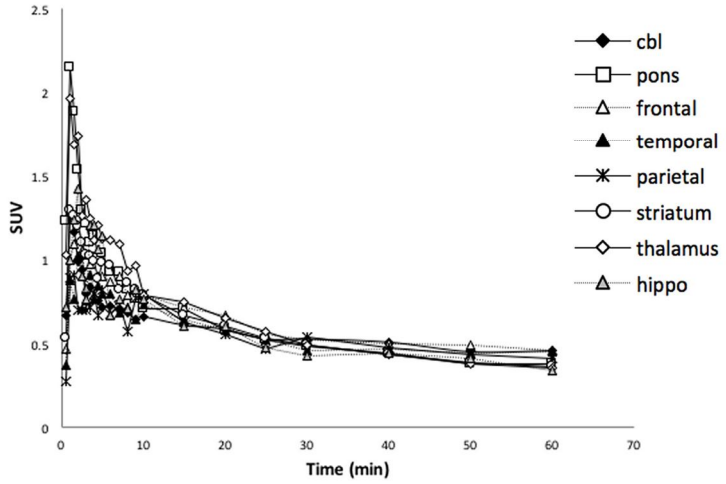
2.5
2
1.5
1
0.5
0
SUV
0
10
20
30
40
50
60
70
Time (min)
cbl
pons
frontal
temporal
parietal
striatum
thalamus
hippo

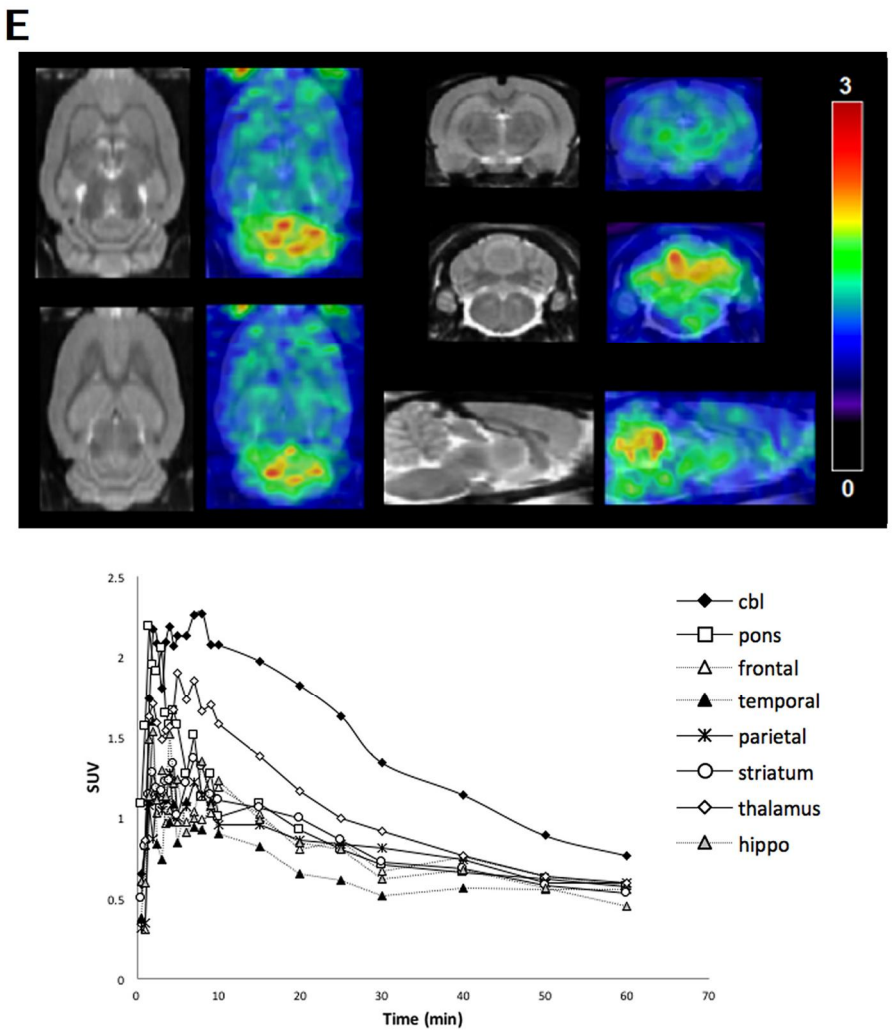

Figure 18. PET images and time-activity curves of [^{18}F]7a and [^{18}F]7b in normal SD rat brains.

[^{18}F]**7a** (A), [^{18}F]**7b** (B), [^{18}F]**7a** 10 min after pretreatment with 3 mg/kg **7a** (C), [^{18}F]**7a** 10 min after pretreatment with 3 mg/kg JNJ16259685 (D), and [^{18}F]**7a** 10 min after pretreatment with 3 mg/kg ABP688 (E). All PET images are 2-10 min sum images after injection.

Ex vivo autoradiography in rats

The specific binding of [^{18}F]**7a** in the rat brains was examined using *ex vivo* autoradiography (Figure 19). As the results of the PET studies, autoradiograms also showed wide distribution of radioactivity in almost all brain regions. The highest uptake was found in the cerebellum, followed by the thalamus, hippocampus, and striatum. Slightly increased radioactivity uptakes were also detected in the mGluR1 localized regions such as the olfactory tubercles and substantia nigra pars reticulate. [^{18}F]**7a** uptake in the rat brain was blocked by the presence of JNJ1625-9685 (Figure 19B), consistent with animal PET study.

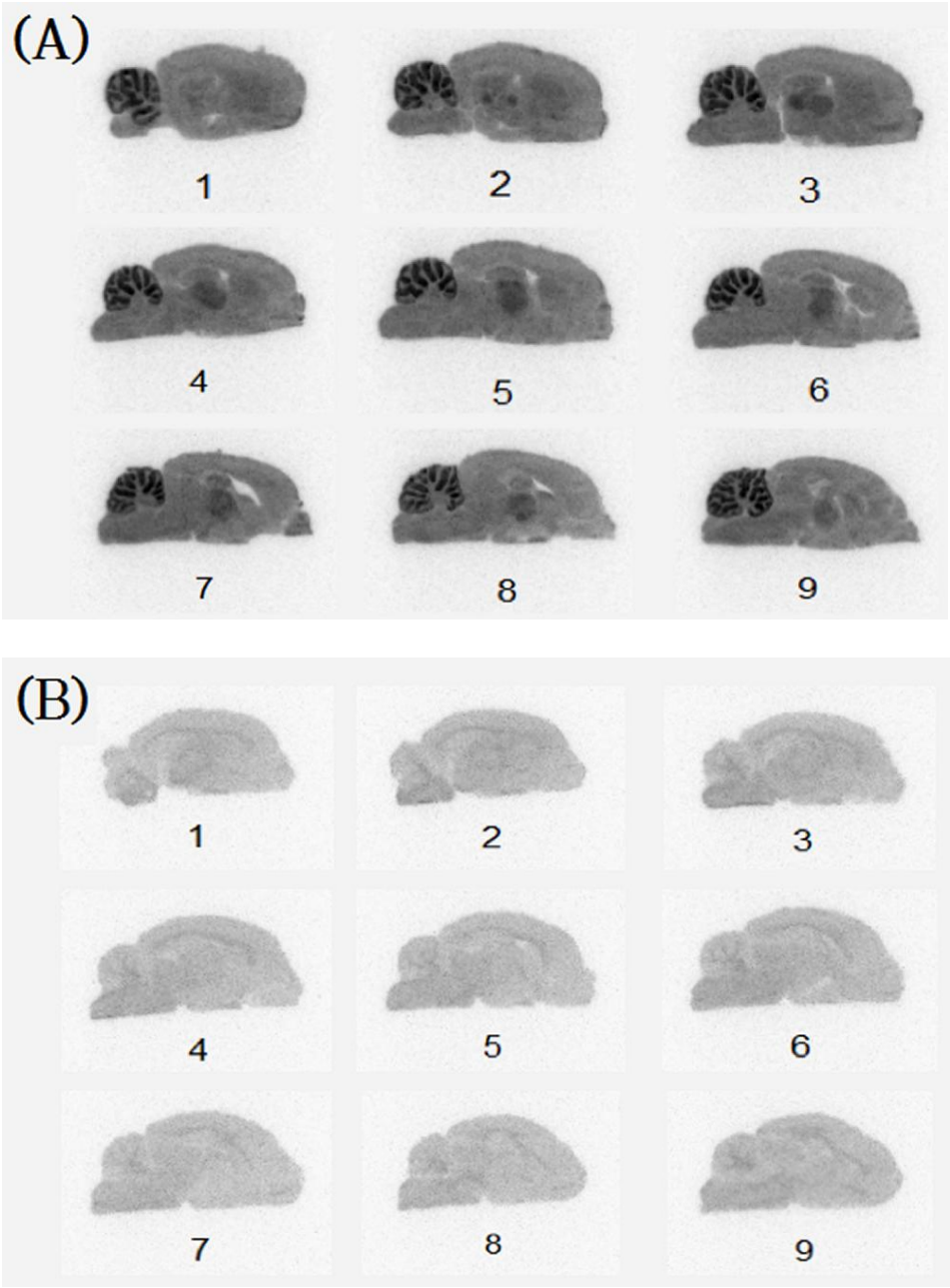

Figure 19. *Ex vivo* autoradiographic images of [^{18}F]7a in the SD rat brains.

[^{18}F]**7a** (A) and [^{18}F]**7a** with co-injection of JNJ16259685 (B).

IV. Discussion

Pharmacological modulation of mGluRs is a hot topic for the treatment of neuropsychiatric disorders associated with glutamatergic dysfunction (*42*). In recent trends in the development of mGuR targeting therapeutics, specific and selective receptor imaging ligands can be used as a highly-advanced tool for new drug discovery. Imaging studies of glutamatergic transmission in human have begun later than that of GABAergic system, but now, it is very active (*97*). Because mGluRs (especially mGluR1) are key modulators of various CNS functions, and mGluR-mediated drugs and non-drugs treatments are tried in neuro-logical disease. That is why a potential imaging radioligand is required to quantify mGluR1 and to evaluate the drug molecules targeting the receptor.

In this study, I synthesized [^{18}F]**7a** and [^{18}F]**7b** for imaging of mGluR1 in the brain and evaluated their physicochemical and biological proper-ties in rats and mice to confirm the potential of these compounds as mGluR1 imaging tracers.

[^{18}F]**7a** was labeled with ^{18}F by a selective halogen exchange (Halex) reaction (Figure 20) (*98, 99*). In the precursor molecule structure, the carbon positioned 2 on quinoline is positively charged due to the adjacent nitrogen, and chlorine have higher electronegativity than

carbon. Thus, fluoride can easily attack the carbon as a S_N2 reaction. The ^{18}F radio-labeling of [^{18}F]**7a** and [^{18}F]**7b** was quite simple and had high labeling efficiencies (29% of [^{18}F]**7a** and 49% of [^{18}F]**7b**) as expected.

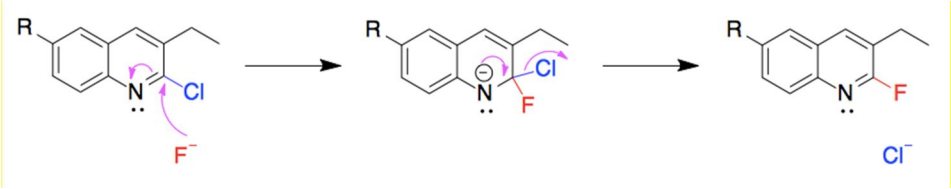

Figure 20. Mechanism of fluorination on quinoline ring.

In the fluorination condition (both radioactive and nonradioactive reactions), **7a** and **7b** were produced whenever pure *cis*- or pure *trans*-form precursor (**6a** or **6b**) was used. The ratio of produced [^{18}F]**7a** to [^{18}F]**7b** was about 2:3, because the *trans*- product was thermodynamically more stable than the *cis*- product (Figure 13). Unfortunately, *trans*- isomer [^{18}F]**7b** is a radioactive impurity that is inactive to mGluR1. Thus, due to the resultant [^{18}F]**7b** should be completely separated from [^{18}F]**7a**, the final [^{18}F]**7a** product obtained has a high labeling efficiency, but not much amount.

It has been reported that trans configuration on cyclohexyl ring of quinoline derivatives is less active or inactive to mGluR1, but *cis*- form chloroquinoline compound used as a precursor of [^{18}F]**7a** labeling has high potency in rat (IC_{50} = 5 nM) and human (IC_{50} = 4 nM) mGluR1 (*64*). For these reasons, perfect HPLC separation of [^{18}F]**7a** from [^{18}F]**7b** and precursor compounds was necessary for further studies. It caused a great loss in [^{18}F]**7a** production despite of its high radiolabeling efficiency.

Log $D_{7.4}$ value of [^{18}F]**7a** is the ratio of the total concentrations of [^{18}F]**7a** (both of ionized form and neutral form) in aqueous phase at pH 7.4 and that in organic phase. In this study, Log $D_{7.4}$ was measured using phosphate buffer solution for the aqueous phase and 1-octanol for

the organic phase at physiological pH. High Log *D* means high lipophilicity of the compound. For brain receptor imaging ligands, high lipophilicity is critical to penetrat BBB; nevertheless, too high lipophilicity might increase nonspecific binding to albumin or other tissues. The optimal range for Log $D_{7.4}$ values for brain targeting is 2.0-3.5 (*100*). [^{18}F]**7a** had suitable lipophilicity (Log $D_{7.4}$ = 3.24) for brain entry, thus it showed high initial brain uptake (4.24% ID/g) at 10 min after injection (Figure 16, Table II). However, the Log *P* value of [^{18}F]**7a** was measured to be about 3.54 in a previous study by Y. Huang et al., which is more lipophi-lic than the present result of this study, and it was concluded that the range of lipophilicity was not optimal for brain imaging (*77*). The relatively high lipophilicity of the brain imaging agent results in low free fraction and nonspecific binding.

In vitro stability tests were performed in the 10% ethanol solution and in human serum. In the ethanol solution at room temperature, the labeled compound was not degraded, but in human serum at 37°C it was decomposed into free ^{18}F and other radioactive metabolites over time. The peak of the decomposed radioactive metabolite seemed like [^{18}F]**7b** on radio-TLC. The isomerization of [^{18}F]**7a** *in vivo* is an important factor because it can make undesirable effects for brain PET imaging. Fortunat-ely, the radioactive isomer was not founded in

metabolite analysis studies using HPLC at any time points (Figure 17, Table III). Perhaps on radio-TLC condition, it was difficult to distinguish between trans isomer and other metabolites of [^{18}F]**7a** due to its low resolution.

The metabolic pathways of mGluR1 antagonists having a quinoline structure are oxidation in the quinoline ring, *O*-demethylation of the methoxy group on the cyclohexyl ring, carbonyl reduction, and combination of some of these pathways (*64*). There are several possible metabolic routes, [^{18}F]**7a** had 6 different radiometabolites and free fluoride *in vivo* system. Defluorination of [^{18}F]**7a** occurred in plasma (16.8% at 30 min), because of increased temperature and enzymes in serum. Free fluoride decomposed from [^{18}F]**7a** demonstrated increase of radioactivity in the bone with time (Figure 16,17 and Table II,III). Generally, higher levels of defluorination are found in mice than in humans (*101, 102*). Most of quinoline derivatives for mGluR1 antagonist had low metabolic stability. [^{11}C]JNJ16567083 showed good activity in mGluR1 (IC_{50} values in rat and human mGluR1 were 3 and 8 nM, respectively), but only 8% of parent compound was remained after 30 min incubation in human liver microsomes (*64*). Compared to JNJ1656-7083, **7a** had similar binding affinity to mGluR1 (IC_{50} = 4 and 9 nM in rat and human mGluR1, respectively.), but had better stability

(25% of the parent compound remained in human liver microsomes after 30 min) in same experimental condition. So, fluorinated compound **7a** is better for the quantification of mGluR1 than [^{11}C]JNJ16567083.

Radiometabolites in the brain are problematic for PET imaging because it is not possible to ascertain which chemical is the source of the detected radioactivity (*103*). The metabolism rate of [^{18}F]**7a** in the brain was considerably slower than that in plasma, and almost 90% of intact compound was detected in the brain at 5 min after injection (Figure 17, Table III). In spite of small amounts of radioactive metabolites including free fluoride in the brain homogenate samples, the specific binding of [^{18}F]**7a** to mGluR1 was determined because the main radioactivity was due to the parent [^{18}F]**7a**. Although ^{18}F remained in the brain, noticeable skull uptake was not visualized in the PET images for 1 hr. If the PET image is aquired within 10 min, the radioactivity originated from the intact compound (more than 80%). Thus, [^{18}F]**7a** can overcome rapid metabolism rate *in vivo* and estimate mGluR1 in the brain. The exact structures and lipophilicities of metabolites were not confirmed in this study. To analyze the structures of metabolites, more advanced techni-ques such as LC-MS/MS can be used. But in here, it is no matter what the metabolites are for imaging study. If the radiometabolites in blood stream have high lipophilicities enough for

BBB penetration, they will make more complex pharmacokinetic properties for quantitative analysis (*75*). It is important to remove radiometabolites which disturb the image evaluations in the brain.

The biodistribution study showed rapid uptake and wash out of [^{18}F]**7a** into and out of the brain. According to the results, brain PET images sh-ould be obtained in mice within 10 min. For clinical imaging, additionnal PET time-activity curve (TAC) studies might be required to obtain the highest quality image. The major excretion route was found as hepato-biliary tract according to biodistribution study. Increased radioactivity in the bone over time represents the *in vivo* defluorination of [^{18}F]**7a** in mice.

PET images and TACs of rats treated with [^{18}F]**7a** showed the distribu-tion of mGluR1 in the brain (Figure 18A). As expected, the highest and distinct radioactivity uptake was in the cerebellum, and slightly detect-able radioactivities were in the thalamus, hippocampus and striatum. In normal rat brain, the concentration of mGluR1 in the cerebellum was over 9 times higher than in the cortex and about 8 times higher than in the hippocampus and striatum (*18, 66, 77, 104*). Thus, the uptakes of [^{18}F]**7a** in other mGluR1 abundant regions except cerebellum were just detectable in PET and autoradiographic images. Perhaps, almost mGluR-1 PET images using [^{18}F]**7a** or other tracers

will have lower resolution in the human brain than in the rat brain because of the lower receptor density. The concentrations of mGluR1 (B_{max}) in rats were 47.1 ± 6.8 nM and 430.2 ± 204.2 nM in the cortex and cerebellum, respectively (*66*). Whereas, B_{max} values of human mGluR1 determined by [^{18}F]MK-1312 were 26 nM and 82 nM in the cortex and cerebellum, respectively (*78*). The human brain has lower mGluR1 density than the rat brain. The diff-errences in species may give different results in study.

The pretreatment with unlabeled **7a** or mGluR1 selective antagonist JNJ16259685 brought remarkable decrease of radioactivity in the whole brain compared to [^{18}F]**7a** baseline images. Excessive specific antago-nists already occupy the receptors and hinder the binding of radioactive compound to the receptors. However, pretreatment with the mGluR5 selective antagonist ABP688 had no influence on [^{18}F]**7a** binding. These results confirmed the specificity and selectivity of [^{18}F]**7a** as a PET tracer for mGluR1 imaging *in vivo*. Although bone uptake arose from defluori-nation was demonstrated in the biodistribution study, but there was no skull uptake in the 10-min PET image. The expression pattern of mGluR-1 in autoradiographic study was more similar but clearer than in PET images, and mGluR1 antagonist blocking images showed the same results with PET (Figure 19).

From the TACs in PET study, it was determined that [^{18}F]**7a** had rapid kinetics, rapid brain uptake and wash-out. Previously reported radio-ligands [^{11}C]ITMM and [^{11}C]ITDM have considerably long kinetics, it takes a long time for quantification of receptor density. For that, ^{11}C radioisotope has too short half-life. In addition, almost 3 hours for receptor quantification of [^{18}F]FIMX is a drawback for clinical use despite the enough long half-life of ^{18}F. Thus, fast kinetics is an advantage of radioligand for receptor imaging.

The low signal in the brain with [^{18}F]**7b** is a natural corollary of PET study because of its low affinity to mGluR1. The result was predictable before PET study judging by the previous study of Mabire et al (*64*). More to the point in here, PET has received much attention as a state-of-the-art technology for drug development. Using radiolabeled drug candi-dates and PET, it is possible to estimate the suitability of new drug molecules *in vivo* intuitionally and quantitatively without sacrificing animals in preclinical studies. It is a cost-benefit technique and minimize the risk of drug development (*105*).

Huang et al. verified the binding affinity of [^{18}F]**7a** to mGluR1 in rodent and non-human primates in previous study (*77*). The affinity of [^{18}F]**7a** changed with temperature, and the affinity at body temperature was lower than that measured at low temperature. The binding affinity

of [^{18}F]**7a** to mGluR1 also differed on species. Generally, lower affinity was found for cloned human mGluR1 than for rat mGluR1. Furthermore, non-human primates and humans have a relatively low mGluR1 density than rodents (*77, 78, 104*). Although the discrepancy between receptor density, binding affinity, and metabolism by species is a barrier to clinical application of [^{18}F]**7a** (*93*), this PET ligand is still useful in preclinical studies. The well-known selective mGluR1 antagonist, JNJ16259685, is the most widely used standard compound of mGluR1 targeting new drug discovery. Thus, [^{18}F]**7a** also can be used to evaluate new drug candi-dates with PET, because it has more similar binding affinities and meta-bolic stability with JNJ16259685 than [^{11}C]JNJ16567083. The necessi-ties of mGluR1 imaging radioligand will greatly expand along with in-depth studies of mGluR1-related neurological and psychiatric disorders.

To make [^{18}F]**7a** more useful, further studies of the ligand are needed. One of the additional studies is kinetics of the tracer. Commonly, receptor binding tracers are fitted to 3-compartmental model (*75*). However, in some cases the ligands exhibit more complex kinetics. For accurate quantitation of the receptor, a suitable kinetic model for the ligand should be found. The application of [^{18}F]**7a** to human is another further study. Although [^{18}F]**7a** showed a low binding affinity to

mGluR1 in baboon, nobody knows what will happen to human. Optimization of the synthetic condition is helpful for the production of [^{18}F]**7a**, and selective [^{18}F]**7a** production will lead beneficial effects with high labeling yields.

In addition, other structures of quinoline derivatives for PET ligand can be considered (Figure 21). These compounds are expected to have high affinity to mGluR1 due to structural similarity with JNJ16259685, but have not been studied yet.

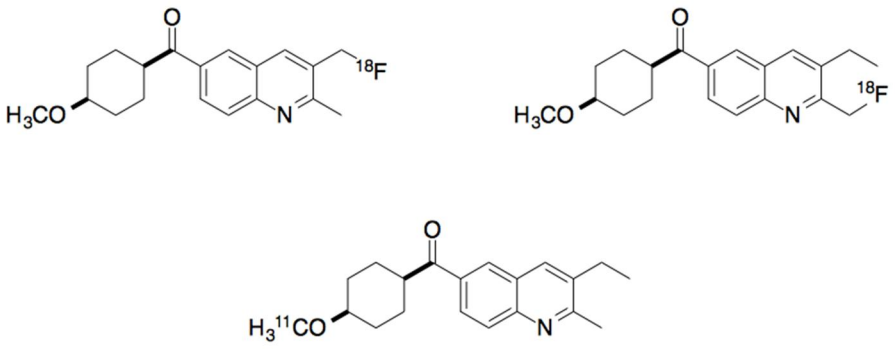

Figure 21. Structures of candidates for mGluR1 imaging radio-ligands with qunioline moiety.

V. Conclusion

In this study, a fluorinated quinoline compound [^{18}F]**7a** was developed as a selective mGluR1 imaging radioligand for brain PET studies. The chloro-derivative precursor, nonradioactive **7a** and **7b** compounds were successfully synthesized, and [^{18}F]**7a** and [^{18}F]**7b** were labeled both manually and automatically using synthetic module. These products had high specific activities and radiochemical purities with a short prepara-tion time. [^{18}F]**7a** had proper lipophilicity for brain receptor imaging tracer and showed rapid initial brain uptake and clearance from the results of biodistribution and time-activity curves from PET images. From the PET and autoradiography studies in the rat brains, [^{18}F]**7a** was demonstrated as a specific and selective mGluR1 binding radiotracer, whereas *trans*- isomer [^{18}F]**7b** was not due to its low binding affinity. In conclusion, [^{18}F]**7a** can be considered a potential PET radioligand for mGluR1 imaging in rats, even if there are some drawbacks, including that radiometabolites are contained in the brain and that the binding affinity is changed by species.

VI. References

1. Monaghan DT, Bridges RJ, Cotman CW. The excitatory amino-acid receptors - their classes, pharmacology, and distinct properties in the function of the central nervous-system. *Annu Rev Pharmacol*. **1989**;*29*:365-402.

2. Hollmann M, Heinemann S. Cloned glutamate receptors. *Annu Rev Neurosci.* **1994**;*17*:31-108.

3. Blanke ML, VanDongen. AMJ. Activation mechanisms of the NMDA receptor. In: *Biology of the NMDA receptor.* Boca Raton: CRC Press; **2009**. Chapter 13.

4. Madden DR. The structure and function of glutamate receptor ion channels. *Nat Rev Neurosci.* **2002**;*3*:91-101.

5. Schoepp DD. Unveiling the functions of presynaptic metabotropic glutamate receptors in the central nervous system. *J Pharmacol Exp Ther.* **2001**;*299*:12-20.

6. Pin JP, Acher F. The metabotropic glutamate receptors: structure, activation mechanism and pharmacology. *Curr Drug Targets CNS Neurol Disord.* **2002**;*1*:297-317.

7. Willard SS, Koochekpour S. Glutamate, glutamate receptors, and downstream signaling pathways. *Int J Biol Sci.* **2013**;*9*:948-959.

8. Bruno V, Battaglia G, Copani A, D'Onofrio M, Di Iorio P, De Blasi A, Melchiorri D, Flor PJ, Nicoletti F. Metabotropic glutamate receptor subtypes as targets for neuroprotective drugs. *J Cerebr Blood F Met.* **2001**;*21*:1013-1033.

9. Yuzaki M, Mikoshiba K. Pharmacological and immunocytochemi-cal characterization of metabotropic glutamate receptors in cul-tured Purkinje-cells. *J Neurosci.* **1992**;*12*:4253-4263.

10. Frenguelli BG, Potier B, Slater NT, Alford S, Collingridge GL. Metabotropic glutamate receptors and calcium signaling in den-drites of hippocampal CA1 neurons. *Neuropharmacol*. **1993**;*32*: 1229-1237.

11. Fotuhi M, Standaert DG, Testa CM, Penney JB, Jr., Young AB. Differential expression of metabotropic glutamate receptors in the hippocampus and entorhinal cortex of the rat. *Mol Brain Res.* **1994**; *21*:283-292.

12. Kano M, Hashimoto K, Tabata T. Type-1 metabotropic glutamate receptor in cerebellar Purkinje cells: a key molecule responsible

for long-term depression, endocannabinoid signalling and synapse elimination. P*hilos Trans R Soc Lond B Biol Sci.* **2008**;*363*:2173-2186.

13. Ferraguti F, Shigemoto R. Metabotropic glutamate receptors. *Cell Tissue Res.* **2006**;*326*:483-504.

14. Prezeau L, Carrette J, Helpap B, Curry K, Pin JP, Bockaert J. Pharmacological characterization of metabotropic glutamate receptors in several types of brain-cells in primary cultures. *Mol Pharmacol.* **1994**;*45*:570-577.

15. Layton ME. Subtype-selective noncompetitive modulators of metabotropic glutamate receptor subtype 1 (mGluR1). *Curr Top Med Chem.* **2005**;*5*:859-867.

16. Takahashi T, Forsythe ID, Tsujimoto T, BarnesDavies M, Onodera K. Presynaptic calcium current modulation by a metabotropic glu-tamate receptor. *Science*. **1996**;*274*:594-597.

17. Abe S, Suzuki T, Ito T, Yamaguchi M, Baba A, Hori T, Kurita H, Shiraishi H, Okado N. Effects of single and repeated phencyclidine administration on the expression of metabotropic glutamate receptor subtype mRNAs in rat brain. *Neuropsychopharmacol*. **2001**;*25*:173-84.

18. Lavreysen H, Pereira SN, Leysen JE, Langlois X, Lesage ASJ. Metabotropic glutamate 1 receptor distribution and occupancy in the rat brain: a quantitative autoradiographic study using [^{3}H]R-214127. *Neuropharmacology*. **2004**;*46*:609-619.

19. Lipina TV, Roder JC. Drug Discovery for Schizophrenia: Royal Society of Chemistry; **2015**.

20. Steckler T, Lavreysen H, Oliveira AM, Aerts N, Van Craenendonck H, Prickaerts J, Megens A, Lesage AS. Effects of mGlu1 receptor blockade on anxiety-related behaviour in the rat lick suppression test. *Psychopharmacology*. **2005**;*179*:198-206.

21. Swanson CJ, Bures M, Johnson MP, Linden AM, Monn JA, Scho-epp DD. Metabotropic glutamate receptors as novel targets for anxiety and stress disorders. *Nat Rev Drug Discov.* **2005**;*4*:131-144.

22. Belozertseva IV, Kos T, Popik P, Danysz W, Bespalov AY. Antidepressant-like effects of mGluR1 and mGluR5 antagonists in the rat forced swim and the mouse tail suspension tests. *Eur Neuropsychopharmacol*. **2007**;*17*:172-179.

23. Luscher C, Huber KM. Group 1 mGluR-dependent synaptic long-term depression: mechanisms and implications for circuitry and

disease. *Neuron*. **2010**;*65*:445-459.

24. Kang SJ, Liu MG, Chen T, Ko HG, Baek GC, Lee HR, Lee K, Collingridge GL, Kaang BK, Zhuo M. Plasticity of metabotropic glutamate receptor-dependent long-term depression in the anterior cingulate cortex after amputation. *J Neurosci*. **2012**;*32*: 11318-11329.

25. Bordi F, Ugolini A. Group I metabotropic glutamate receptors: implications for brain diseases. *Prog Neurobiol*. **1999**;*59*:55-79.

26. Moghaddam B. Targeting metabotropic glutamate receptors for treatment of the cognitive symptoms of schizophrenia. *Psychopharmacology*. **2004**;*174*:39-44.

27. Chaki S, Hikichi H. Targeting of metabotropic glutamate receptors for the treatment of schizophrenia. *Curr Pharm Des*. **2011**;*17*:94-102.

28. Tang FR, Lee WL, Yeo TT. Expression of the group I metabotropic glutamate receptor in the hippocampus of patients with mesial temporal lobe epilepsy. *J Neurocytol*. **2001**;*30*:403-411.

29. Moldrich RX, Chapman AG, De Sarro G, Meldrum BS.

Glutamate metabotropic receptors as targets for drug therapy in epilepsy. *Eur J Pharmacol*. **2003**;*476*:3-16.

30. Senkowska A, Ossowska K. Role of metabotropic glutamate receptors in animal models of Parkinson's disease. *Pol J Pharmacol.* **2003**;*55*:935-950.

31. Ossowska K, Wardas J, Pietraszek M, Konieczny J, Wolfarth S. The striopallidal pathway is involved in antiparkinsonian-like effects of the blockade of group I metabotropic glutamate receptors in rats. *Neurosci Lett.* **2003**;*342*:21-24.

32. Hodgson RA, Hyde LA, Guthrie DH, Cohen-Williams ME, Leach PT, Kazdoba TM, Bleickardt CJ, Lu SX, Parker EM, Varty GB. Characterization of the selective mGluR1 antagonist, JNJ1625-9685, in rodent models of movement and coordination. *Pharmacol Biochem Behav.* **2011**;*98*:181-187.

33. Wu WL, Burnett DA, Domalski M, Greenlee WJ, Li C, Bertorelli R, Fredduzzi S, Lozza G, Veltri A, Reggiani A. Discovery of orally efficacious tetracyclic metabotropic glutamate receptor 1 (mGluR1) antagonists for the treatment of chronic pain. *J Med Chem.* **2007**;*50*: 5550-5553.

34. Schkeryantz JM, Kingston AE, Johnson MP. Prospects for

metabo-tropic glutamate 1 receptor antagonists in the treatment of neuro-pathic pain. *J Med Chem.* **2007**;*50*:2563-2568.

35. Tappe-Theodor A, Fu Y, Kuner R, Neugebauer V. Homer1a signal-ing in the amygdala counteracts pain-related synaptic plasticity, mGluR1 function and pain behaviors. *Mol Pain*. **2011**;*7*:38.

36. Owen DR. Recent advances in the medicinal chemistry of the metabotropic glutamate receptor 1 (mGlu1). *ACS Chem Neurosci.* **2011**;*2*:394-401.

37. Lesage A, Steckler T. Metabotropic glutamate mGlu1 receptor stimulation and blockade: therapeutic opportunities in psychiatric illness. *Eur J Pharmacol*. **2010**;*639*:2-16.

38. Trullas R, Skolnick P. Functional antagonists at the NMDA receptor complex exhibit antidepressant actions. *Eur J Pharmacol.* **1990**; *185*:1-10.

39. Zarate CA, Singh JB, Carlson PJ, Brutsche NE, Ameli R, Lucken-baugh DA, Charney DS, Manji HK. A randomized trial of an *N*-methyl-*D*-aspartate antagonist in treatment-resistant major depre-ssion. *Arch Gen Psychiatry.* **2006**;*63*:856-864.

40. Howes OD, Kapur S. The dopamine hypothesis of schizophrenia: version III-the final common pathway. *Schizophr Bull.* **2009**;*35*: 549-562.

41. Olney JW, Farber NB. Glutamate receptor dysfunction and schizo-phrenia. *Arch Gen Psychiatry.* **1995**;*52*:998-1007.

42. Hovelso N, Sotty F, Montezinho LP, Pinheiro PS, Herrik KF, Mork A. Therapeutic potential of metabotropic glutamate receptor modulators. *Curr Neuropharmacol*. **2012**;*10*:12-48.

43. Lominac KD, Kapasova Z, Hannun RA, Patterson C, Middaugh LD, Szumlinski KK. Behavioral and neurochemical interactions between Group 1 mGluR antagonists and ethanol: Potential insight into their anti-addictive properties. *Drug Alcohol Depen.* **2006**;*85*: 142-156.

44. Dravolina OA, Danysz W, Bespalov AY. Effects of group I metabotropic glutamate receptor antagonists on the behavioral sensitization to motor effects of cocaine in rats. *Psychopharmacology*. **2006**;*187*:397-404.

45. Kotlinska J, Bochenski M. Pretreatment with group I metabotropic glutamate receptors antagonists attenuates lethality induced by acute cocaine overdose and expression of

sensitization to hyper-locomotor effect of cocaine in mice. *Neurotox Res*. **2011**;*19*: 23-30.

46. Xie XH, Ramirez DR, Lasseter HC, Fuchs RA. Effects of mGluR1 antagonism in the dorsal hippocampus on drug context-induced reinstatement of cocaine-seeking behavior in rats. *Psychopharma-cology*. **2010**;*208*:1-11.

47. Dravolina OA, Zakharova ES, Shekunova EV, Zvartau EE, Danysz W, Bespalov AY. mGlu1 receptor blockade attenuates cue- and nicotine-induced reinstatement of extinguished nicotine self-admi-nistration behavior in rats. *Neuropharmacology*. **2007**;*52*: 263-269.

48. Kotlinska J, Bochenski M. Comparison of the effects of mGluR1 and mGluR5 antagonists on the expression of behavioral sensiti-zation to the locomotor effect of morphine and the morphine with-drawal jumping in mice. *Eur J Pharmacol*. **2007**;*558*:113-118.

49. Loweth JA, Tseng KY, Wolf ME. Using metabotropic glutamate receptors to modulate cocaine's synaptic and behavioral effects: mGluR1 finds a niche. *Curr Opin Neurobiol*. **2013**;*23*:500-506.

50. Olive MF. Metabotropic glutamate receptor ligands as potential

therapeutics for addiction. *Curr Drug Abuse Rev.* **2009**;*2*:83-98.

51. Neugebauer V, Lucke T, Schaible HG. Requirement of metabotropic glutamate receptors for the generation of inflammation-evoked hyperexcitability in rat spinal cord neurons. *Eur J Neurosci*. **1994**;*6*:1179-1186.

52. O'Connor AB, Dworkin RH. Treatment of neuropathic pain: an overview of recent guidelines. *Am J Med*. **2009**;*122*:S22-32.

53. Collins S, Sigtermans MJ, Dahan A, Zuurmond WW, Perez RS. NMDA receptor antagonists for the treatment of neuropathic pain. *Pain Med*. **2010**;*11*:1726-1742.

54. Vorobeychik Y, Willoughby CD, Mao J. NMDA Receptor antagonists in the treatment of pain. In: *Comprehensive treatment of chronic pain by medical, interventional, and intergrative approaches*: Springer; **2015**. 61-67.

55. Ren W, Neugebauer V. Pain-related increase of excitatory transmission and decrease of inhibitory transmission in the central nucleus of the amygdala are mediated by mGluR1. *Mol Pain*. **2010**;*6*:93.

56. Epping-Jordan M, Le Poul E, Rocher J-P. Allosteric modulation:

a novel approach to drug discovery. *Innovations Pharm Technol.* **2007**;*24*:24-26.

57. Annoura H, Fukunaga A, Uesugi M, Tatsuoka T, Horikawa Y. A novel class of antagonists for metabotropic glutamate receptors, 7-(hydroxyimino)cyclopropa[b]chromen-1α-carboxylates. *Bioorg Med Chem Lett*. **1996**;*6*:763-766.

58. Litschig S, Gasparini F, Rueegg D, Stoehr N, Flor PJ, Vranesic I, Prézeau L, Pin JP, Thomsen C, Kuhn R. CPCCOEt, a noncompeti-tive metabotropic glutamate receptor 1 antagonist, inhibits receptor signaling without affecting glutamate binding. *Mol Pharmacol.* **1999**;*55*:453-461.

59. Carroll FY, Stolle A, Beart PM, Voerste A, Brabet I, Mauler F, Joly C, Antonicek H, Bockaert J, Müller T, Pin JP, Prézeau L. BAY36-7620: a potent non-competitive mGlu1 receptor antagonist with inverse agonist activity. *Mol Pharmacol.* **2001**;*59*:965-973.

60. Clark BP, Baker SR, Goldsworthy J, Harris JR, Kingston AE. (+)-2-methyl-4-carboxyphenylglycine (LY367385) selectively antago-nises metabotropic glutamate mGluR1 receptors. *Bioorg Med Chem Lett*. **1997**;*7*:2777-2780.

61. Varty GB, Grilli M, Forlani A, Fredduzzi S, Grzelak ME, Guthrie DH, Hodgson RA, Lu SX, Nicolussi E, Pond AJ, Parker EM, Hunter JC, Higgins GA, Reggiani A, Bertorelli R. The anti-nociceptive and anxiolytic-like effects of the metabotropic glutamate receptor 5 (mGluR5) antagonists, MPEP and MTEP, and the mGluR1 antagonist, LY456236, in rodents: a comparison of efficacy and side-effect profiles. *Psychopharmacology*. **2005**;*179*: 207-217.

62. Toms NJ, Jane DE, Kemp MC, Bedingfield JS, Roberts PJ. The effects of (RS)-***α***-cyclopropyl-4-phosphonophenylglycine ((RS)-CPPG), a potent and selective metabotropic glutamate receptor antagonist. *Brit J Pharmacol*. **1996**;*119*:851-854.

63. Moroni F, Lombardi G, Thomsen C, Leonardi P, Attucci S, Peruginelli F, Torregrossa SA, Pellegrini-Giampietro DE, Luneia R, Pellicciari R. Pharmacological characterization of 1-amino-indan-1,5-dicarboxylic acid, a potent mGluR1 antagonist. *J Pharmacol Exp Ther*. **1997**;*281*:721-729.

64. Mabire D, Coupa S, Adelinet C, Poncelet A, Simonnet Y, Venet M, Wouters R, Lesage AS, Van Beijsterveldt L, Bischoff F. Synthesis, structure-activity relationship, and receptor pharmacology of a new series of quinoline derivatives acting as

selective, non-competitive mGlu1 antagonists. *J Med Chem*. **2005**;*48*:2134-2153.

65. Lavreysen H, Wouters R, Bischoff F, Nobrega Pereira S, Langlois X, Blokland S, Somers M, Dillen L, Lesage AS. JNJ16259685, a highly potent, selective and systemically active mGlu1 receptor antagonist. *Neuropharmacology*. **2004**;*47*:961-972.

66. Lavreysen H, Janssen C, Bischoff F, Langlois X, Leysen JE, Lesage AS. [^{3}H]R214127: a novel high-affinity radioligand for the mGlu1 receptor reveals a common binding site shared by multiple allosteric antagonists. *Mol Pharmacol*. **2003**;*63*:1082-1093.

67. Kohara A, Toya T, Tamura S, Watabiki T, Nagakura Y, Shitaka Y, Hayashibe S, Kawabata S, Okada M. Radioligand binding properties and pharmacological characterization of 6-amino-*N*-cyclohexyl-*N*,3-dimethylthiazolo[3,2-***α***]benzimidazole-2-carbox-amide (YM-298198), a high-affinity, selective, and noncompetitive antagonist of metabotropic glutamate receptor type 1. *J Phar-macol Exp Ther*. **2005**;*315*:163-169.

68. Fukuda J, Suzuki G, Kimura T, Nagatomi Y, Ito S, Kawamoto H, Ozaki S, Ohta H. Identification of a novel transmembrane domain

involved in the negative modulation of mGluR1 using a newly discovered allosteric mGluR1 antagonist, 3-cyclohexyl-5-fluoro-6-methyl-7-(2-morpholin-4-ylethoxy)-4H-chromen-4-one. *Neuropharmacology*. **2009**;*57*:438-445.

69. Kohara A, Takahashi M, Yatsugi S, Tamura S, Shitaka Y, Hayashibe S, Kawabata S, Okada M. Neuroprotective effects of the selective type 1 metabotropic glutamate receptor antagonist YM-202074 in rat stroke models. *Brain Res.* **2008**;*1191*:168-179.

70. Suzuki G, Kimura T, Satow A, Kaneko N, Fukuda J, Hikichi H, Sakai N, Maehara S, Kawagoe-Takaki H, Hata M, Azuma T, Ito S, Kawamoto H, Ohta H. Pharmacological characterization of a new, orally active and potent allosteric metabotropic glutamate receptor 1 antagonist, 4-[1-(2-fluoropyridin-3-yl)-5-methyl-1H-1,2,3-triazol-4-yl]-*N*-isopropyl-*N*-methyl-3,6-dihydropyridine-1(2H)-carboxamide (FTIDC). *J Pharmacol Exp Ther*. **2007**;*321*: 1144-1153.

71. Satow A, Suzuki G, Maehara S, Hikichi H, Murai T, Murai T, Kawagoe-Takaki H, Hata M, Ito S, Ozaki S, Kawamoto H, Ohta H. Unique antipsychotic activities of the selective metabotropic glutamate receptor 1 allosteric antagonist 2-cyclopropyl-5-[1-(2-fluoro-3-pyridinyl)-5-methyl-1H-1,2,3-triazol-4-yl]-2,3-dihydro-

1H-isoindol-1-one. *J Pharmacol Exp Ther.* **2009**;*330*:179-190.

72. Mullard A. New drugs cost US$ 2.6 billion to develop. *Nat Rev Drug Discov*. **2014**;*13*:877.

73. Matthews PM, Rabiner EA, Passchier J, Gunn RN. Positron emission tomography molecular imaging for drug development. *Brit J Clin Pharmaco*. **2012**;*73*:175-86.

74. Cunha L, Szigeti K, Mathe D, Metello LF. The role of molecular imaging in modern drug development. *Drug Discov Today.* **2014**; *19*:936-948.

75. Heiss WD, Herholz K. Brain receptor imaging. *J Nucl Med.* **2006**; *47*:302-312.

76. Huang Y, Narendran R, Bischoff F, Guo N, Zhu Z, Bae SA, Lesage AS, Laruelle M. A positron emission tomography radioligand for the *in vivo* labeling of metabotropic glutamate 1 receptor: (3-ethyl-2-[^{11}C]methyl-6-quinolinyl)(*cis*-4-methoxycyclohexyl)methanone. *J Med Chem*. **2005**;*48*:5096-5099.

77. Huang Y, Narendran R, Bischoff F, Guo N, Bae SA, Hwang DR, Lesage AS, Laruelle M. Synthesis and characterization of two

PET radioligands for the metabotropic glutamate 1 (mGlu1) receptor. *Synapse*. **2012**;*66*:1002-1014.

78. Hostetler ED, Eng W, Joshi AD, Sanabria-Bohorquez S, Kawamoto H, Ito S, O'Malley S, Krause S, Ryan C, Patel S, Williams M, Riffel K, Suzuki G, Ozaki S, Ohta H, Cook J, Burns HD, Hargreaves R. Synthesis, characterization, and monkey PET studies of [^{18}F]MK-1312, a PET tracer for quantification of mGlu-R1 receptor occupancy by MK-5435. *Synapse*. **2011**;*65*:125-135.

79. Fujinaga M, Maeda J, Yui J, Hatori A, Yamasaki T, Kawamura K, Kumata K, Yoshida Y, Nagai Y, Higuchi M, Suhara T, Fukumura T, Zhang MR. Characterization of 1-(2-[^{18}F] fluoro-3-pyridyl)-4-(2-isopropyl-1-oxo-isoindoline-5-yl)-5-methyl-1H-1,2,3-triazole, a PET ligand for imaging the metabotropic glutamate receptor type 1 in rat and monkey brains. *J Neurochem.* **2012**;*121*:115-124.

80. Prabhakaran J, Majo VJ, Milak MS, Kassir SA, Palner M, Savenkova L, Pratap M, Arango V, Mann JJ, Parsey RV, Kumar JS. Synthesis, in vitro and in vivo evaluation of [^{11}C]MMTP: a poten-tial PET ligand for mGluR1 receptors. *Bioorg Med Chem Lett*. **2010**;*20*:3499-3501.

81. Yamasaki T, Fujinaga M, Yoshida Y, Kumata K, Yui J, Kawamura K, Yui J, Kawamura K, Hatori A, Fukumura T, Zhang MR. Radiosynthesis and preliminary evaluation of 4-[^{18}F]fluoro-*N*-[4-[6-(isopropylamino)pyrimidin-4-yl]-1,3-thiazol-2-yl]-*N*-methylb enzamide as a new positron emission tomography ligand for meta-botropic glutamate receptor subtype 1. *Bioorg Med Chem Lett*. **2011**;*21*:2998-3001.

82. Yamasaki T, Fujinaga M, Kawamura K, Yui J, Hatori A, Ohya T, Xie L, Wakizaka H, Yoshida Y, Fukumura T, Zhang MR. In vivo measurement of the affinity and density of metabotropic glutamate receptor subtype 1 in rat brain using ^{18}F-FITM in small-animal PET. *J Nucl Med.* **2012**;*53*:1601-1607.

83. Yamasaki T, Fujinaga M, Maeda J, Kawamura K, Yui J, Hatori A, Yoshida Y, Nagai Y, Tokunaga M, Higuchi M, Suhara T, Fukumura T, Zhang MR. Imaging for metabotropic glutamate receptor subtype 1 in rat and monkey brains using PET with [^{18}F]FITM. *Eur J Nucl Med Mol Imaging.* **2012**;*39*:632-641.

84. Fujinaga M, Yamasaki T, Yui J, Hatori A, Xie L, Kawamura K, Asagawa C, Kumata K, Yoshida Y, Ogawa M, Nengaki N, Fukumura T, Zhang MR. Synthesis and evaluation of novel radioligands for positron emission tomography imaging of

metabotropic gluta-mate receptor subtype 1 (mGluR1) in rodent brain. *J Med Chem*. **2012**;*55*:2342-2352.

85. Toyohara J, Sakata M, Oda K, Ishii K, Ito K, Hiura M, Fujinaga M, Yamasaki T, Zhang MR, Ishiwata K. Initial human PET studies of metabotropic glutamate receptor type 1 ligand ^{11}C-ITMM. *J Nucl Med.* **2013**;*54*:1302-1307.

86. Fujinaga M, Yamasaki T, Maeda J, Yui J, Xie L, Nagai Y, Hatori A, Yui J, Xie L, Nengaki N, Zhang MR. Development of *N*-[4-[6-(isopropylamino)pyrimidin-4-yl]-1,3-thiazol-2-yl]-*N*-methyl-4-[^{11}C]methyl benzamide for positron emission tomography imaging of metabotropic glutamate 1 receptor in monkey brain. *J Med Chem*. **2012**;*55*:11042-11051.

87. Yamasaki T, Maeda J, Fujinaga M, Nagai Y, Hatori A, Yui J, Xie L, Nengaki N, Zhang MR. PET brain kinetics studies of ^{11}C-ITMM and ^{11}C-ITDM, radioprobes for metabotropic glutamate receptor type 1, in a nonhuman primate. *Am J Nucl Med Mol Imaging*. **2014**; *4*:260-269.

88. Yamasaki T, Fujinaga M, Yui J, Ikoma Y, Hatori A, Xie L, Wakizaka H, Kumata K, Nengaki N, Kawamura K, Zhang MR. Noninvasive quantification of metabotropic glutamate receptor

type 1 with [^{11}C]ITDM: a small-animal PET study. *J Cereb Blood Flow Metab*. **2014**;*34*:606-612.

89. Satoh A, Nagatomi Y, Hirata Y, Ito S, Suzuki G, Kimura T, Maehara S, Hikichi H, Satow A, Hata M, Ohta H, Kawamoto H. Discovery and in vitro and in vivo profiles of 4-fluoro-*N*-[4-[6-(isopropylamino)pyrimidin-4-yl]-1,3-thiazol-2-yl]-*N*-methylbenz-amide as novel class of an orally active metabotropic glutamate receptor 1 (mGluR1) antagonist. *Bioorg Med Chem Lett.* **2009**;*19*: 5464-5468.

90. Xu R, Zanotti-Fregonara P, Zoghbi SS, Gladding RL, Woock AE, Innis RB, Pike VW. Synthesis and evaluation in monkey of [^{18}F]4-fluoro-*N*-methyl-*N*-(4-(6-(methylamino)pyrimidin-4-yl)thiazol-2-yl)benzami de ([^{18}F]FIMX): a promising radioligand for PET imaging of brain metabotropic glutamate receptor 1 (mGluR1). *J Med Chem.* **2013**;*56*:9146-9155.

91. Zanotti-Fregonara P, Xu R, Zoghbi SS, Liow JS, Fujita M, Veronese M, Gladding RL, Rallis-Frutos D, Hong J, Pike VW, Innis RB. The PET radioligand ^{18}F-FIMX images and quantifies metabotropic glutamate receptor 1 in proportion to the regional density of its gene transcript in human brain. *J Nucl Med*. **2016**;*57*: 242-247.

92. Jacobson O, Chen X. PET designated flouride-18 production and chemistry. *Curr Top Med Chem*. **2010**;*10*:1048-1059.

93. Li S, Huang Y. In vivo imaging of the metabotropic glutamate receptor 1 (mGluR1) with positron emission tomography: recent advance and perspective. *Curr Med Chem.* **2014**;*21*:113-123.

94. Hintermann S, Vranesic I, Allgeier H, Brulisauer A, Hoyer D, Lemaire M, Moenius T, Urwyler S, Whitebread S, Gasparini F, Auberson YP. ABP688, a novel selective and high affinity ligand for the labeling of mGlu5 receptors: identification, in vitro pharma-cology, pharmacokinetic and biodistribution studies. *Bioorg Med Chem*. **2007**;*15*:903-914.

95. Chang YS, Jeong JM, Lee YS, Kim HW, Ganesha RB, Kim YJ, Lee DS, Chung JK, Lee MC. Synthesis and evaluation of benzo-thiophene derivatives as ligands for imaging beta-amyloid plaques in Alzheimer's disease. *Nucl Med Biol.* **2006**;*33*:811-820.

96. Chang YS, Jeong JM, Yoon YH, Kang WJ, Lee SJ, Lee DS, Chung JK, Lee MC. Biological properties of 2'-[^{18}F]fluoroflumazenil for central benzodiazepine receptor imaging. *Nucl Med Biol.* **2005**;*32*: 263-268.

97. Fuchigami T, Nakayama M, Yoshida S. Development of PET and

SPECT probes for glutamate receptors. *Sci World J.* **2015**;*2015*: 716514.

98. Sun H, DiMagno SG. Room-temperature nucleophilic aromatic fluorination: experimental and theoretical studies. *Angew Chem Int Ed Engl*. **2006**;*45*:2720-2725.

99. Liang T, Neumann CN, Ritter T. Introduction of fluorine and fluorine-containing functional groups. *Angew Chem Int Ed Engl.* **2013**;*52*:8214-8264.

100. Waterhouse RN. Determination of lipophilicity and its use as a predictor of blood-brain barrier penetration of molecular imaging agents. *Mol Imaging Biol.* **2003**;*5*:376-389.

101. Ouyang Y, Tinianow JN, Cherry SR, Marik J. Evaluation of 2-[^{18}F]fluoroacetate kinetics in rodent models of cerebral hypoxia-ischemia. *J Cereb Blood Flow Metab.* **2014**;*34*:836-844.

102. Ponde DE, Dence CS, Oyama N, Kim J, Tai YC, Laforest R, Siegel BA, Welch MJ. ^{18}F-fluoroacetate: a potential acetate analog for prostate tumor imaging-in vivo evaluation of ^{18}F-fluoroacetate versus ^{11}C-acetate. *J Nucl Med.* **2007**;*48*:420-428.

103. Pike VW. PET radiotracers: crossing the blood-brain barrier and

surviving metabolism. *Trends Pharmacol Sci.* **2009**;*30*:431-440.

104. Mutel V, Ellis GJ, Adam G, Chaboz S, Nilly A, Messer J, Bleuel Z, Metzler V, Malherbe P, Schlaeger EJ, Roughley BS, Faull RL, Richards JG. Characterization of [^{3}H]quisqualate binding to recombinant rat metabotropic glutamate 1a and 5a receptors and to rat and human brain sections. *J Neurochem.* **2000**;*75*:2590-2601.

105. Wang J, Maurer L. Positron emission tomography: applications in drug discovery and drug development. *Curr Top Med Chem.* **2005**; *5*:1053-1075.

VII. Spectrum data

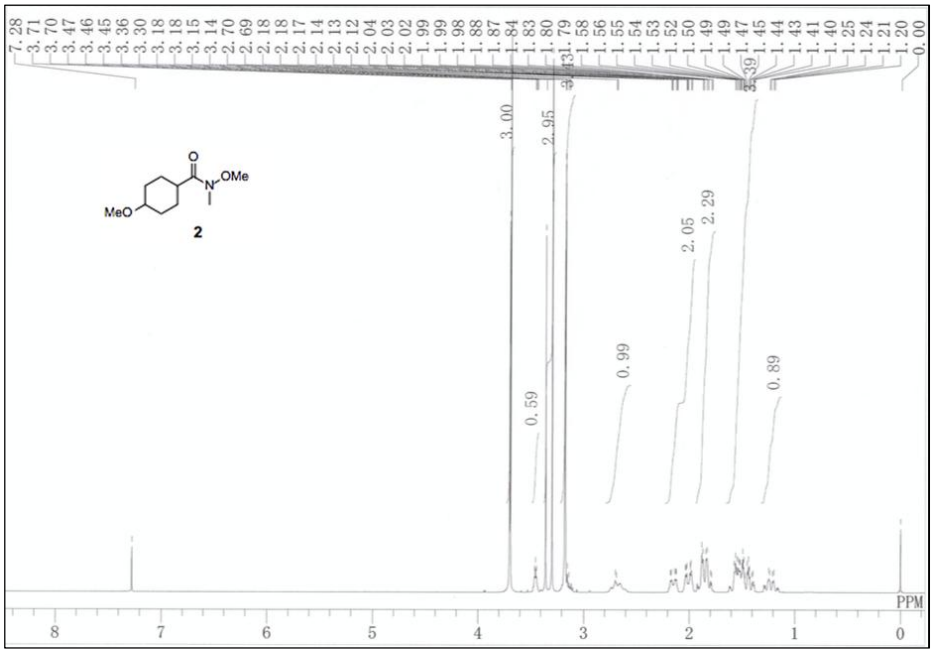

^{1}H-NMR spectrum of **2** (300 MHz)

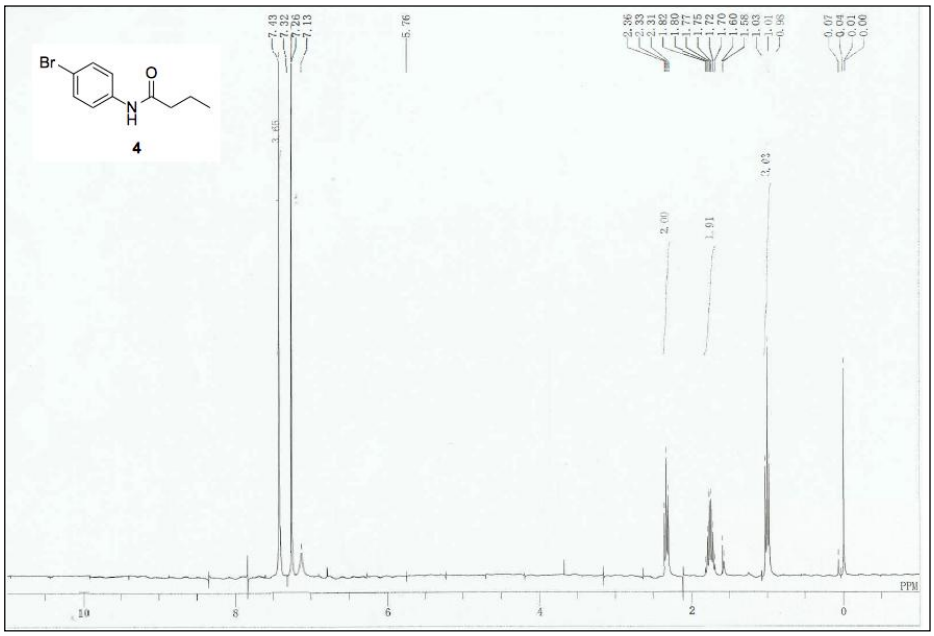

^{1}H-NMR spectrum of **4** (300 MHz)

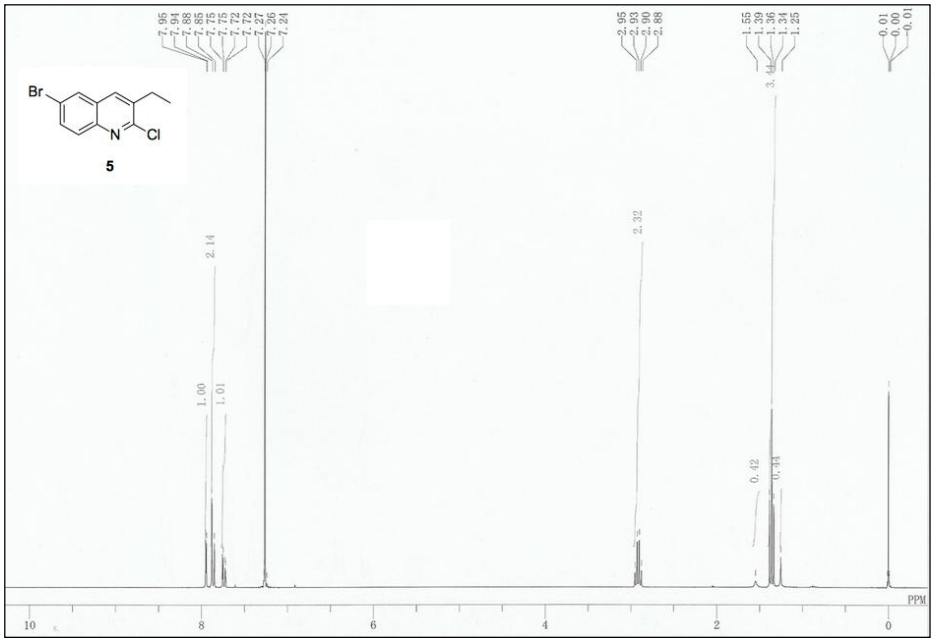

^{1}H-NMR spectrum of **5** (300 MHz)

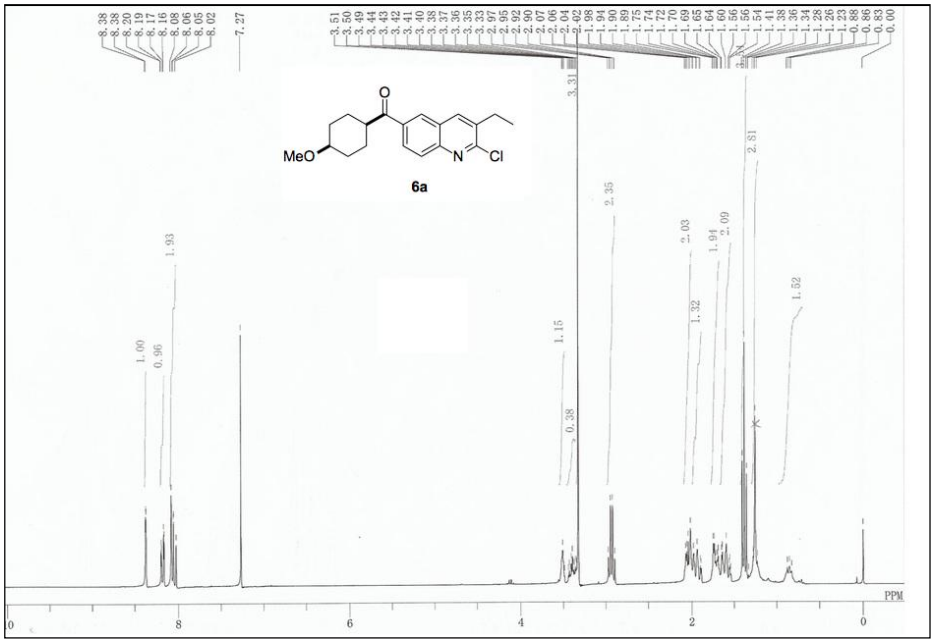

^{1}H-NMR spectrum of **6a** (300 MHz)

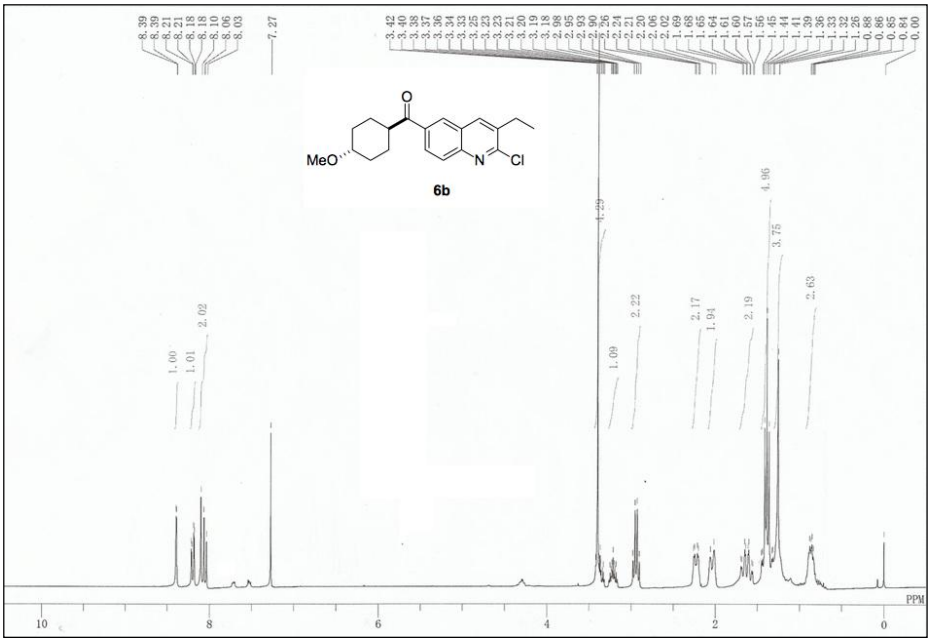

^{1}H-NMR spectrum of **6b** (300 MHz)

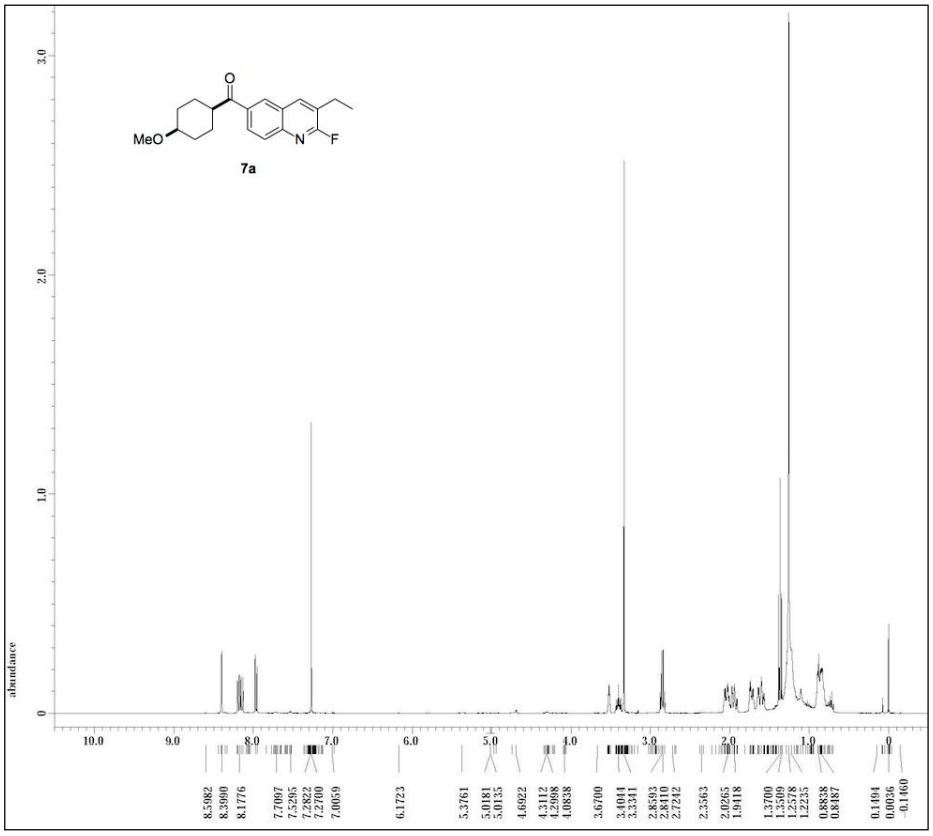

^{1}H-NMR spectrum of **7a** (400 MHz)

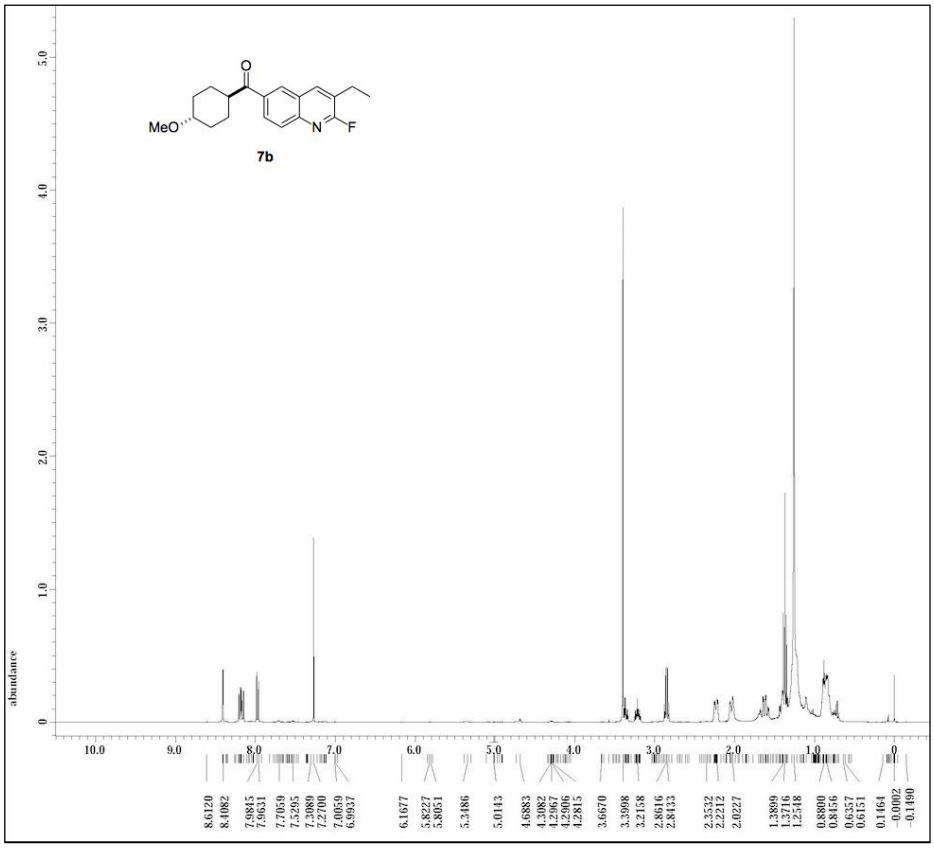

^{1}H-NMR spectrum of **7b** (400 MHz)

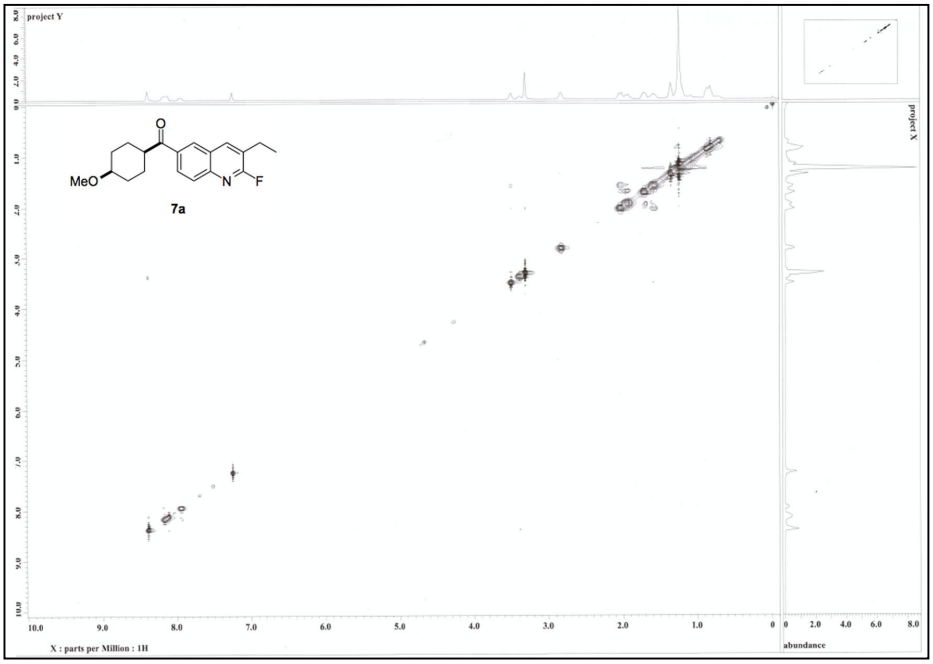

^{1}H-NOESY spectrum of **7a** (400 MHz)

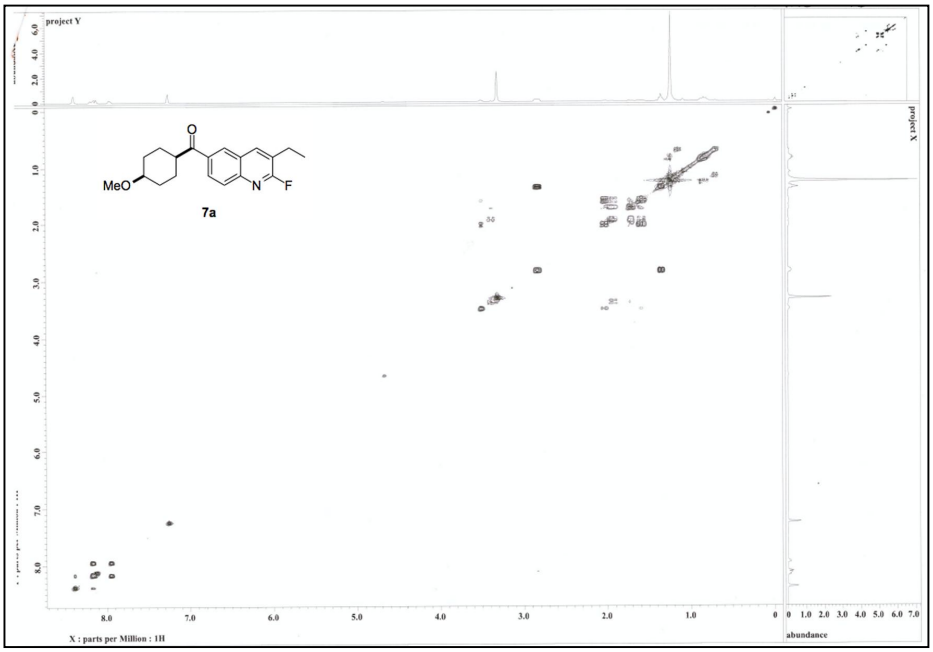

^{1}H-COSY spectrum of **7a** (400 MHz)

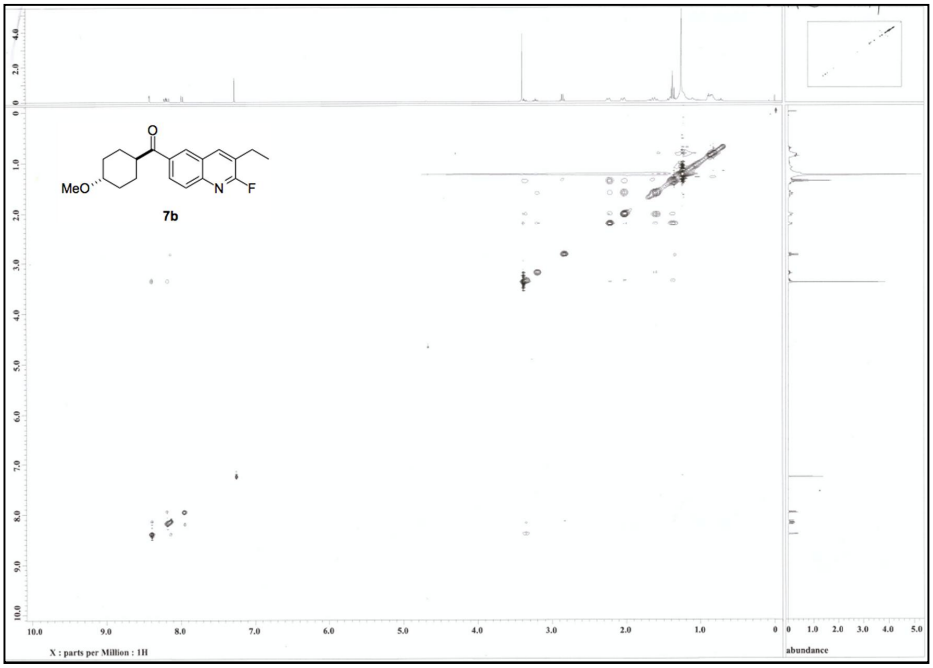

^{1}H-NOESY spectrum of **7b** (400 MHz)

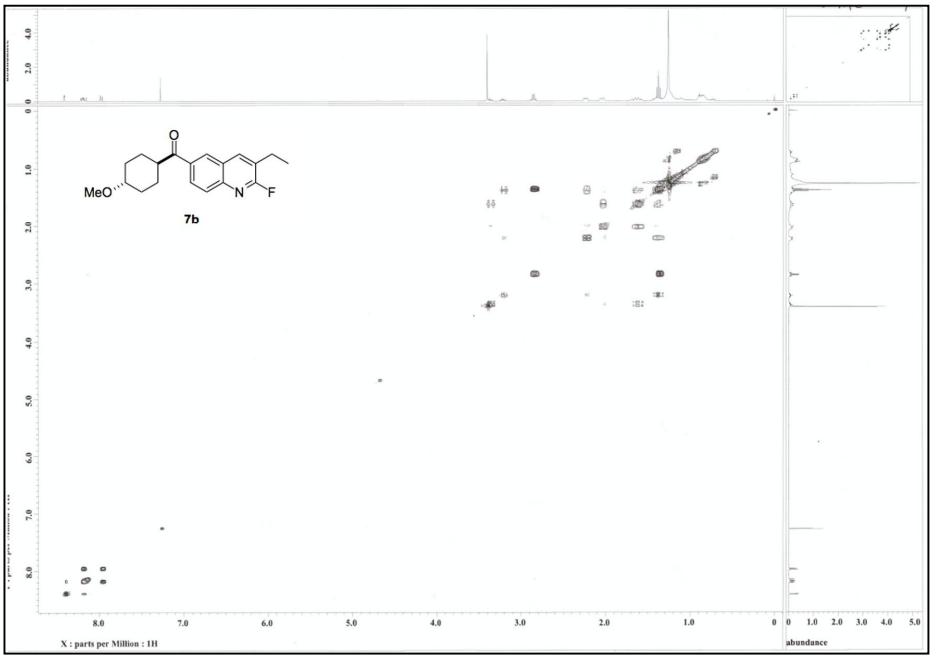

^{1}H-COSY spectrum of **7b** (400 MHz)

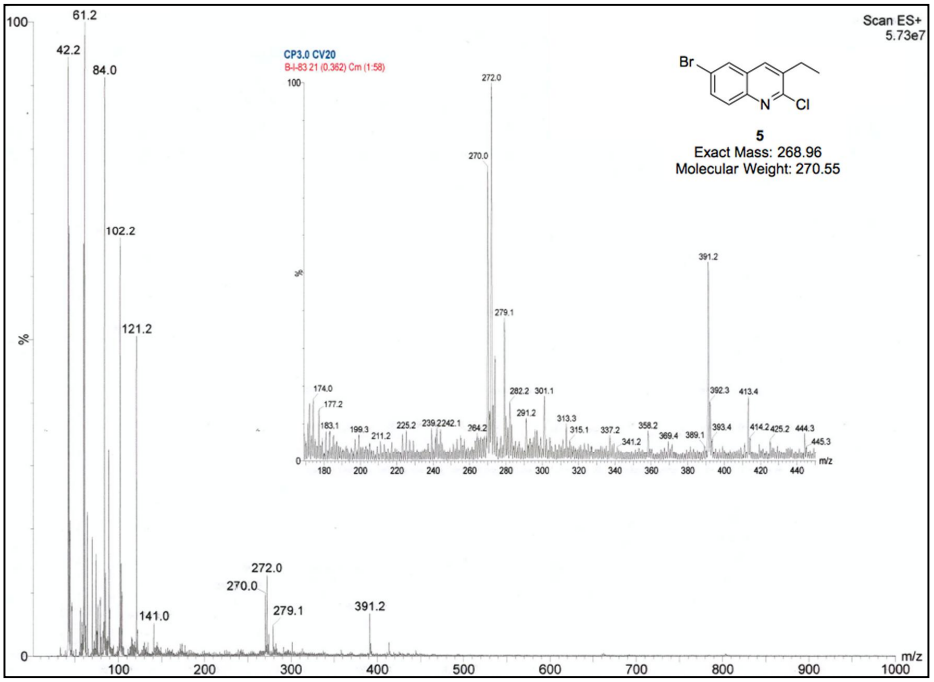

Mass spectrum of **5**

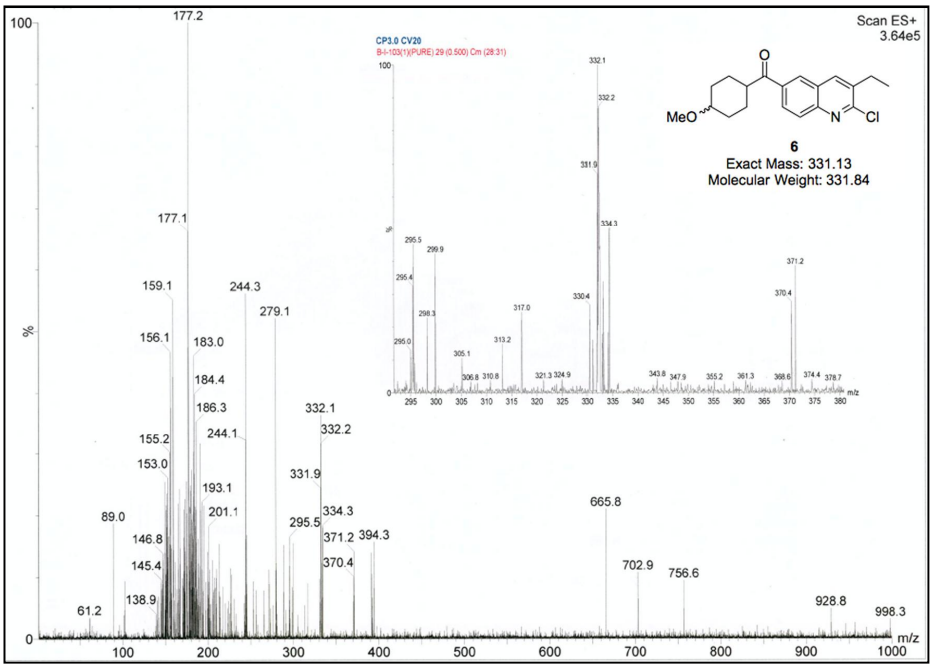

Mass spectrum of **6**

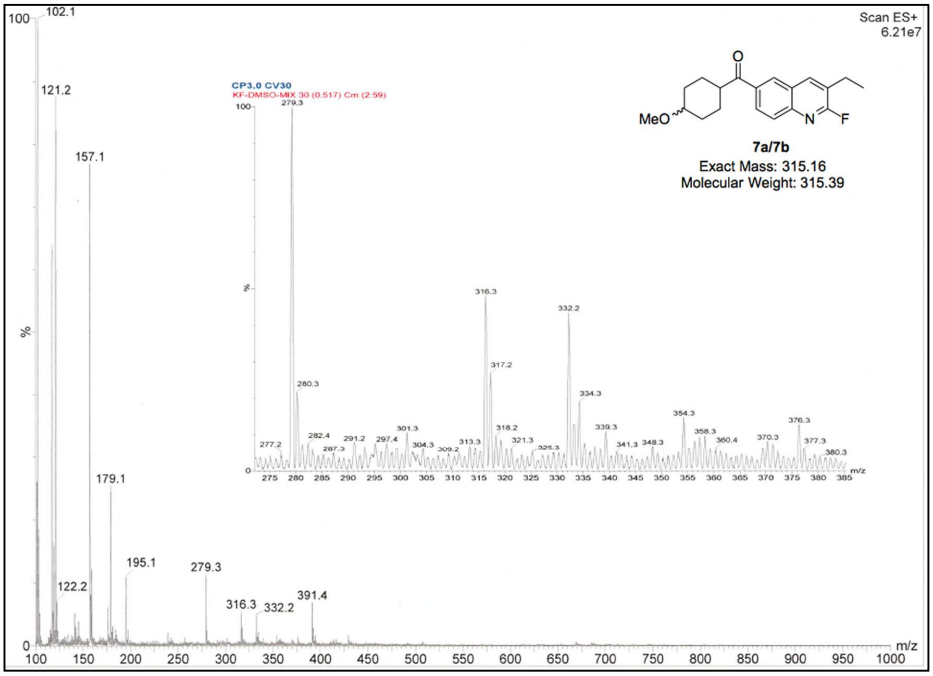

Mass spectrum of **7a** and **7b** mixture

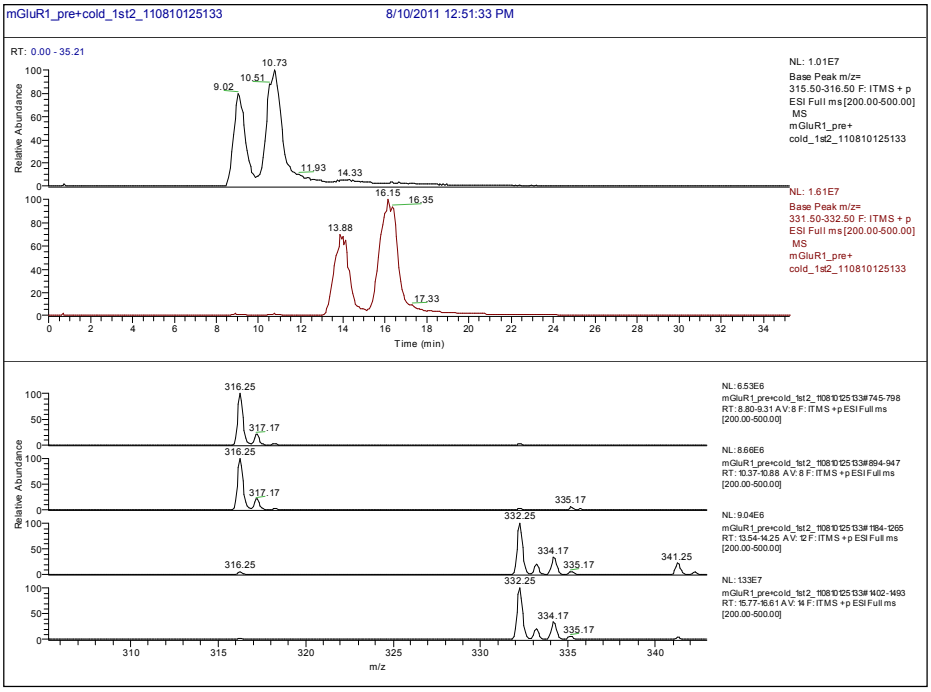

LC-MS spectrum of **6** and **7** mixture

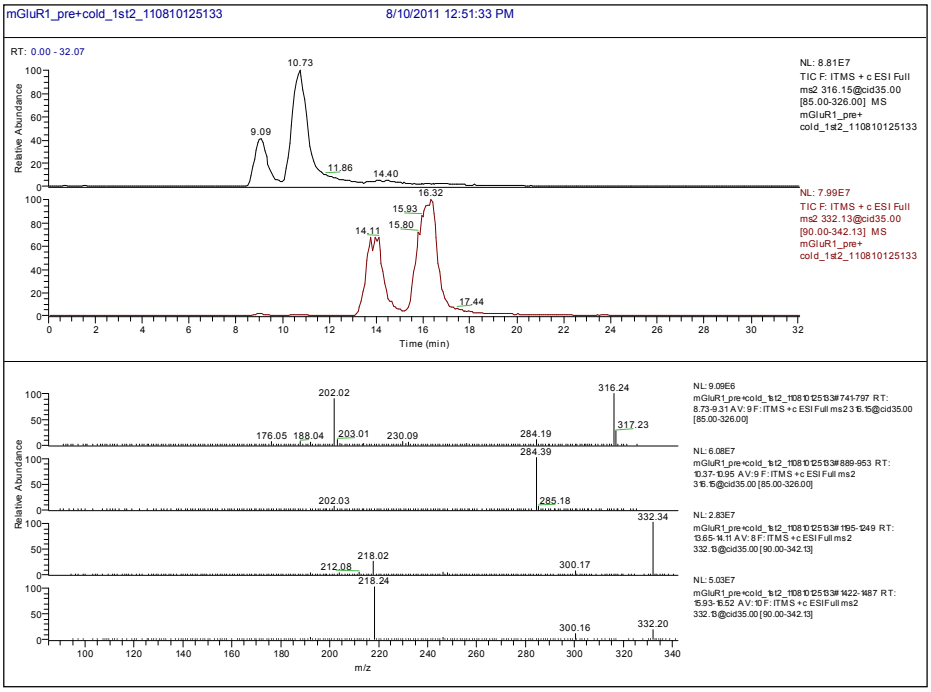

MS/MS spectrum of **6** and **7** mixture

요약 (국문초록)

목적:

글루타메이트는 포유류 중추신경계에 존재하는 중요한 흥분성 신경전달물질로서, 시냅스전 뉴런 내의 소포 속에 저장되어 있다가 외포작용(exocytosis)에 의해 방출된 뒤, 글루타메이트 수용체에 결합하여 신경전달 기능을 한다. 글루타메이트 수용체 중 제 1 형 대사성글루타메이트수용체(mGluR1)는 시냅스후 뉴런에서 발견되며, 시냅스 전달과 신경흥분성을 증대시키고 뇌가소성을 조절하는 역할을 한다. 최근에는 mGluR1 이 불안, 우울증, 간질, 파킨슨병, 신경성동통 등 다양한 신경정신과적 질환과 연관이 있음이 밝혀지고 있으며, 치료용 신약 개발에 있어 주요 수용체로 표적이 되고 있다. mGluR1 의 비상경적 길항제로서 quinoline 유도체가 개발되었는데, 이 중 불소 원자를 함유하는 (3-ethyl-2-fluoroquinolin-6-yl)((1*S*,4*S*)-4-methoxycyclohexyl)methanone (**7a**)는 불소-18 (^{18}F)로 표지하여 뇌 내의 수용체를 영상화하는 방사성리간드로 개발이 가능한 화합물이다. 따라서 본 연구에서는 불소-18 을 표지한 방사성리간드 [^{18}F]**7a** 와 trans 이성체인 [^{18}F]**7b** 를 합성하고, 설치류에서 물리화학적/생물학적 특성을 분석하여 선택적 mGluR1 영상용 PET 방사성 리간드로서의 활용 가능성을 평가하였다.

방법 및 결과:

[^{18}F]**7a** 와 [^{18}F]**7b** 화합물은 chloro-quinoline 전구체와 불소-18 음이온 ([^{18}F]F)을 가지고 친핵성 치환반응으로 표지하고, 분리용 고성능 크로마토그래프를 사용하여 정제하였다. 정제한 ^{18}F]**7a** 와 [^{18}F]**7b** 화합물의 방사화학적 순도는 모두 99% 이상이었으며, 비방사능은 [^{18}F]**7a** 가 63-246 GBq/μmol, [^{18}F]**7b** 가 30.5-93.2 GBq/μmol 이었다. [^{18}F]**7a** 의 Log $D_{7.4}$ 값은 3.24 로 뇌영상용 화합물에 적합한 친지질성을 가지고 있어, BALB/c 마우스를 사용한 체내분포실험에서 10 분 내에 4% 이상이 뇌로 섭취되는 것을 확인하였다. 랫트를 가지고 양전자단층촬영(positron emission tomography, PET)과 방사선 사진법(autoradiography)으로 뇌 영상을 얻었을 때, [^{18}F]**7a** 는 뇌에서 mGluR1 이 가장 많이 분포하는 것으로 알려진 소뇌 영역에 가장 많이 섭취되었으며, 소뇌 외에도 mGluR1 분포 영역으로 알려져 있는 해마, 시상, 그리고 선조체에 약간의 섭취가 있었다. 비방사성의 **7a** 와 mGluR1 의 선택적 길항제인 JNJ1259685 를 미리 투여한 경우에는 [^{18}F]**7a** 의 섭취가 뇌 전반에 걸쳐 감소하였고 특이적인 결합을 보이지 않았으나, mGluR5 선택적 길항제 ABP688 을 미리 투여한 쥐에서는 [^{18}F]**7a** 의 뇌섭취 경향에 영향이 없었다. 이로써 [^{18}F]**7a** 가 선택적으로 mGluR1 과 결합한다는 것을 확인할 수 있었다. 한편, trans 이성체인 [^{18}F]**7b** 를 랫트에 투여하고 뇌영상을 찍었을 때, [^{18}F]**7b** 는 [^{18}F]**7a** 와 마찬가지로 지질성이 커서 투여 즉시 뇌 속으로 빠르게 들어가지만 mGluR1 과 특이적 결합을 하지 않고 바로 빠져 나왔다.

결론:

본 연구에서는 뇌 내 mGluR1 영상용 방사성리간드로서 ^{18}F 이 표지된 퀴놀린 유도체 [^{18}F]**7a** 과 trans 이성체 [^{18}F]**7b** 를 성공적으로 합성하였고, 그 특성을 분석하였다. PET 와 자동사진법 실험으로 [^{18}F]**7a** 가 랫트 뇌의 mGluR1 과 선택적, 특이적으로 결합하여 mGluR1 의 분포 영역을 잘 영상화함을 확인하였으며, 이를 통해 [^{18}F]**7a** 가 PET 영상을 이용한 mGluR1 연구에 유용하게 사용할 수 있는 방사성리간드임을 증명하였다.

주요어 : 제 1 형 대사성글루타메이트수용체, 방사성리간드, 플루오린 화반응, 자동합성, 대사, 방사선사진법, 양전자단층촬영

학 번 : 2009-31346